

NORTHWESTERN UNIVERSITY

Model Independent Explorations of Majorana Neutrino Mass Origins

A DISSERTATION

SUBMITTED TO THE GRADUATE SCHOOL
IN PARTIAL FULFILLMENT OF THE REQUIREMENTS

for the degree

DOCTOR OF PHILOSOPHY

Field of Physics

By

James Phearl Jenkins Jr.

EVANSTON, ILLINOIS

June 2008

ABSTRACT

Model Independent Explorations of Majorana Neutrino Mass Origins

James Phearl Jenkins Jr.

The recent observation of nonzero neutrino mass is the first concrete indication of physics beyond the Standard Model. Their properties, unique among the other fermions, leads naturally to the idea of a Majorana neutrino mass term. Despite the strong theoretical prejudice toward this concept, it must be tested experimentally. This is indeed possible in the context of next generation experiments. Unfortunately, the scale of neutrino mass generation may be too large to explore directly, but useful information may still be extracted from independent experimental channels. Here I survey various model independent probes of Majorana neutrino mass origins. A brief introduction to the concepts relevant to the analysis is followed by a discussion of the physical ranges of neutrino mass and mixing parameters within the context of standard and non-standard interactions. Armed with this, I move on to systematically analyze the properties of radiatively generated neutrino masses induced by nonrenormalizable lepton number violating effective operators of mass dimensions five through eleven. By fitting these to the observed light mass scale, I extract predictions for neutrino mixing as well as neutrinoless double

beta decay, rare meson/tau decays and collider phenomenology. I find that many such models are already constrained by current data and many more will be probed in the near future. I then move on demonstrate the utility of a low scale see saw mechanism via a viable $3 + 2 + 1$ sterile neutrino model that satisfies all oscillation data as well as solves problems associated with supernova kicks and heavy element nucleosynthesis. From this I extract predictions for tritium and neutrinoless double beta decay searches. This is supplemented throughout by descriptions of practical limitations in addition to suggestions for future work.

Acknowledgements

I would like to acknowledge the help of many friends and colleges, without whom this work could never have begun. First, I thank my advisor Andre de Gouvea for his advice, support and patience. On the same note, I thank the remainder of my thesis committee, Heidi Schellman and Robert Oakes for their kind remarks and encouragement throughout my years of graduate study. Finally, I would like to thank Tina Jakubosky for editing services.

The success of my graduate career also depended heavily on my vast exposure to scholarly dialog/instruction. For this reason I also take this opportunity to acknowledge the faculty of Northwestern University's high energy physics group as well as the Fermilab and Argonne theory groups. Additionally, I thank the organizers, participants, and lecturers of the TASI 2006 and PITP 2007 summer schools for many useful discussions and insights into this thesis topic.

Dedication

This thesis is dedicated to my best friend and companion Tina Jakubosky for her unending love and support.

Preface

While there exists many astrophysical hints of physics beyond the Standard Model, the observation of nonzero neutrino mass is the only undisputed terrestrial evidence. It is set apart from the rest because it is not (directly) related to poorly understood gravitational interactions. If it were just the fact that neutrinos have mass, this observation would be important but not earth shattering... After all, the quarks and charged leptons have nonzero mass values that span nearly six orders of magnitude (this is puzzling by itself). The neutrinos' mystique is enhanced because they are so different from the charged fermions in both structure and magnitude. Specifically, we find that the neutrinos possess unprecedented tiny masses, nearly twelve orders of magnitude smaller than the largest quark mass, or equivalently the electroweak scale (another puzzle). Additionally, we observe large (perhaps maximal) mixing which is quite distinct from the observed quark mixings. It is likely not a coincidence that neutrinos are the only known electrically neutral fundamental fermion. They are not protected by this $U(1)_Q$ gauge symmetry and consequently may have new types of interactions of the Majorana type. On the grander scale, neutrino data unambiguously confirms that the pattern of fermion masses begs for an explanation. Fitting the known Yukawa couplings as well as neutrino masses (of either Dirac or Majorana type) into the Standard Model can be easily accomplished, but there is likely something more. Flavor constraints are some of the strongest in all of particle physics and, enhanced by information in the neutrino sector, are currently poised to select

the next set of fundamental laws that govern the universe. The next step on this journey is the exploration of neutrino mass origins.

It is possible that this goal is beyond the reach of next generation experiments due to the possibility of potentially ultra high energy scales involved in neutrino mass generation. Still, it is my biased hope that, by combining information from distinct terrestrial, astrophysical and cosmological probes, the physics community can at least narrow down the set of model possibilities, if not choose the correct one. Of course completeness dictates that such analysis should be as model independent as possible. This spirit is the inspiration for the majority of my research interests and, in particular, the present analysis. Here, I embark on a model independent survey of (potentially) testable models of Majorana neutrino mass.

This thesis is taken from three previously published papers done in collaboration with Andre de Gouvea and Nirmala Vasudevan [**1**, **2**, **3**]. They were selected and modified to reflect the unifying themes outlined above. While this work does not cover all possible models of neutrino mass, it is easily broad enough to aid in the analysis of current and future neutrino data. This analysis will help constrain large classes of new physics models as well as lead the way for other theoretical/phenomenological studies.

Table of Contents

ABSTRACT	2
Acknowledgements	4
Preface	6
List of Tables	10
List of Figures	11
Chapter 1. Introduction	13
Chapter 2. The Physical Range of Neutrino Parameters	17
2.1. Within the Minimally extended standard model	18
2.2. Nonstandard Interactions	38
2.3. Conclusions	43
Chapter 3. A Survey of Lepton Number Violation Via Effective Operators	44
3.1. The lepton number violating scale	48
3.2. General operator constraints and predictions	77
3.3. Neutrino mixing	107
3.4. Phenomenologically interesting operators: Sample Renormalizable Model	117
3.5. Conclusion	124

Chapter 4. Neutrino Phenomenology of Very Low-Energy Seesaws	128
4.1. The Seesaw Mechanism and electron volt neutrino masses: preliminaries	130
4.2. Oscillation Phenomenology and Current Evidence for Low-Energy Seesaw	135
4.3. Other Probes of the Seesaw Energy Scale	153
4.4. Conclusions	162
References	165
Appendix A. Standard Model of Particle Physics	174
Appendix B. Extended $SU(2)$ neutrino mixing matrix notation	178

List of Tables

2.1	Exhaustive summary of two neutrino mixing symmetries	21
2.2	Summary of selected three neutrino mixing symmetries	27
3.1	Summary of dimension 5-11 LNV operators surveyed here	66
4.1	Parameter values used in analysis extracted from global $3 + 2$ fit	138
A.1	Standard Model fermion content with quantum numbers	175

List of Figures

2.1	Mapping the inverted neutrino hierarchy between popular schemes	30
2.2	Neutrino electron quasi-elastic scattering diagrams via W' and Z'	41
3.1	Sample diagrams that radiatively generate Majorana neutrino masses	61
3.2	Summary histogram of the scale Λ extracted from 129 LNV operators	73
3.3	Feynman diagrams contributing to neutrinoless double-beta decay	82
3.4	m_{ee}^{eff} distribution derived for neutrinoless double-beta decay process	86
3.5	Parton level Feynman diagrams contributing to LNV meson decay	92
3.6	$m_{\alpha\beta}^{\text{eff}}$ distribution derived for several rare LNV meson and τ decays	94
3.7	Cross-section distribution for $e^-e^- \rightarrow q\bar{q}q\bar{q}$ at an e^-e^- collider	101
3.8	Parton level gluon–gluon and gluon–quark LNV interaction diagrams	106
3.9	Scatter plots of normalized Majorana neutrino mass matrix elements	115
3.10	Sample scalar interactions that lead to the effective operator \mathcal{O}_{56}	121
4.1	Viable $3 + 2 + 1$ neutrino mass spectrum with flavor composition	140
4.2	Cosmological and astrophysical constraints on the $ U_{\alpha 6} ^2 \times m_6$ -plane	143
4.3	$1 - S/S_0$ as a function of the tritium β -ray energy	156
4.4	Contour plot of constant R assuming an energy window $\Delta E = 25$ eV	158

4.5	Effective m_{ee} for neutrinoless double-beta decay as a function of m_6	161
-----	--	-----

CHAPTER 1

Introduction

The Standard Model (SM) of particle physics has enjoyed tremendous success in recent decades. Indeed, consistency between experiments and theoretical calculations has been demonstrated in a variety of terrestrial channels over a wide range of energy scales exceeding twelve orders of magnitude¹. Despite extensive searches, the majority of experiments have not yet uncovered a shred of (convincing) evidence of new physics Beyond the Standard Model (BSM). On the contrary, most results agree with SM predictions to an unprecedented and often puzzling degree. See appendix A for a brief review of the SM.

Despite its success, there is still strong reason to believe that there exists new physics BSM. These are of both an indirect and direct nature. Indirectly, one is naturally led to the idea of new physics above the electroweak scale to stabilize the scalar Higgs mass to radiative corrections [4]. Additionally, the running and approximate intersection of the SM gauge couplings at high energies hint at a possible grand unification of particle physics within a single (broken) gauge group [5]. The details of this unification requires the existence of supersymmetry for full consistency. Direct evidence for phenomenon BSM is also available from astrophysical/cosmological observations. Specifically, an analysis of the energy budget of the universe reveals that only a small fraction of the universe is composed of the SM particles with the majority residing in dark energy (70%) and dark

¹This conservative range is taken from the sub-eV scale associated with atomic fine structure to the ultra-GeV scale accessible to present day colliders.

matter (26%) [6]. Finally, as will become clear shortly, the discovery of neutrino mass via flavor oscillations is a clear sign of physics BSM and is the motivation of this thesis. Originally, the evidence of this phenomenon was also of astrophysical origin but has been convincingly confirmed by terrestrial experiments. All of these “problems” suggest the existence of new physics for full resolution.

The observation of nonzero neutrino mass is the first unambiguous evidence for physics BSM. In other words, neutrino mass can not be accommodated within the SM as currently formulated. This is easy to understand by considering the “types” of masses available to the neutrino. First, neutrinos may be Dirac particles and thus possess a mass term similar to that of the charged fermions, of the general form

$$\mathcal{L}_{Dirac} = M_D (\bar{\nu}N + \bar{N}\nu) \quad (1.1)$$

where N is a *new* right-handed SM singlet dubbed “right handed neutrino.” This mass term arises after electroweak symmetry breaking from the Yukawa coupling of the $\bar{\nu}N$ combination to the neutral component of the SM Higgs doublet. Notice that these terms involve two different fields, the familiar left-handed neutrino and the new right-handed state. The addition of N is already an indication of new physics, but as is often overlooked in such discussions, it is not the only BSM effects guaranteed to arise from Dirac neutrinos. Since the singlet N carries no unbroken charge, it should combine to form a mass term $\overline{N^c}N$, which ultimately spoils the Dirac nature of the physical neutrino state upon diagonalization. A new global symmetry must be imposed on the system by hand to forbid it whereas it is accidental within the SM. Indirectly, the Dirac nature of the neutrino suggests more substantial modifications to the SM in order to explain the tiny

Yukawa coupling constant needed to yield the observed sub-eV neutrino mass, roughly 10^{-12} .

The second type of neutrino mass term is allowed since the neutrino carries no unbroken gauge quantum numbers. This is of the Majorana form written as

$$\mathcal{L}_{Majorana} = M_M (\bar{\nu}^c \nu + \bar{\nu} \nu^c). \quad (1.2)$$

Notice that this mass is written entirely in terms of a single field ν and so no new field content is required for its construction. Physically, such an interaction states that left-handed neutrinos have a small but nonzero probability (proportional to M_M^2) of being observed as right-handed antineutrinos. In this case, neutrinos and antineutrinos are equivalent. The only reason the distinction between them is convenient is that the numerical coefficient M_M is so small. This mass term, however, is not invariant under the full unbroken electroweak symmetry of SM $SU(2)_L \times U(1)_Y$ where the neutrino is charged under both weak isospin and hypercharge. The only means of such a construction is via the Higgs boson, but unlike the Dirac case, the Higgs quantum numbers do not allow the required renormalizable interaction. This necessarily requires the addition of new physics of various types. One can form the required term by coupling to a pair of Higgs doublets as $(1/\Lambda)HH\bar{\nu}^c\nu$, but this is of dimension five and as such, nonrenormalizable. It requires an ultraviolet completion at or below the scale Λ to preserve unitarity. This is in fact the effective operator induced by the seesaw mechanisms [7] and yields a mass of order v^2/Λ after electroweak symmetry breaking. The seesaw neutrino mass mechanism will be discussed at length in chapter 4. The case of neutrino mass generation by more general high dimensional operators is discussed in chapter 3. Alternatively, to construct Eq. (1.2), one

could simply introduce a new scalar ϕ , in addition to the SM Higgs that transforms as a triplet under $SU(2)_L$ to form the SM singlet $\phi\bar{\nu}^c\nu$. It will yield a Majorana mass after the neutral component of ϕ acquires a vacuum expectation value either directly, or indirectly via a trilinear Higgs coupling ϕHH . In the first case the vacuum expectation of ϕ must be unnaturally small to accomodate the tiny observed neutrino masses. However, in the latter case, provided the mass of ϕ is large, the system reduces down to the previously mentioned dimension five seesaw operator after electroweak symmetry breaking with the scalar mass acting as the suppression scale Λ .

It is natural to wonder about the consequences of introducing both Dirac and Majorana masses. It is well known that any such combination will yield physical Majorana neutrinos after diagonalization to the mass basis. This is the principle behind the type-I seesaw mechanism. From this it seems that the Majorana nature of the neutrino is the most natural choice and indeed it is a majority prejudice within the theoretical neutrino physics community. I emphasize that the construction of Dirac-type neutrinos *requires* the existence of a new symmetry imposed to protect lepton number (L) or more precisely Baryon minus Lepton Number (B-L). While B-L is accidental within the SM there is no reason to believe that it will be so with the addition of new physics. Ultimately, the nature of the neutrino is one we must answer experimentally. The overall purpose of my thesis is to aid in this endeavor by exploiting the connection between Majorana neutrinos, Lepton Number Violation (LNV), and mixing phenomena and thereby extract predictions for a variety of physics experiments.

CHAPTER 2

The Physical Range of Neutrino Parameters

In order to properly study Majorana neutrino interactions, it is important to understand how to fully parameterize neutrino mixing both within the SM, minimally extended to include neutrino mass, and in the context of more general BSM interactions. This involves questions that arise regarding both the number of free parameters and their physical ranges. Parameter counting arguments are well known in both the Dirac and Majorana cases. In words, these go as follows for the general case of n Majorana neutrinos. The transformation from the flavor bases, where the gauge interactions are diagonal, to the mass basis is accomplished by an $n \times n$ complex matrix. These $2n^2$ degrees of freedom minus n^2 unitarity conditions and n field rephasings leaves room for $n(n-1)$ parameters. For Dirac neutrinos, one is allowed to rephase both the left-handed lepton doublet and right handed neutrino fields separately, thus reducing the parameter count by $n-1$ where the additional “1” arises from the universal ability to rephase the entire system. The freedom is shared between real mixing angles, Majorana phases, and Dirac phases.

While this much is known, the complex relationship between the physical ranges of these parameters has not been explored fully. It turns out that one may limit the range of a particular parameter set by simply extending the range of another in a non-trivial way. Furthermore, this relationship is modified in the presence of new physics. In what follows, I develop a framework in which to study these ranges via symmetries of the mass matrix. The reasoning behind this is simple: If a symmetry exists between the mixing values, it

implies the existence of two or more degenerate regions within the parameter space. One may choose to exclusively populate any one of them while at the same time taking heed of the consequences imposed by this choice on other parameters. This is accomplished using an extension of the $SU(2)$ algebra defined in Appendix B. Admittedly, the use of this system is not optimal for a specified neutrino system. It is natural to use the well known algebra of $SU(n)$ to study the symmetries of an n neutrino system. The drawback of this approach is that one must use a different algebra to analyze each different system. The utility of the approach adopted here is that it works for all cases, as will become apparent.

In this chapter, I explore the physical ranges of neutrino mixing parameters within the SM for the minimal case of two neutrinos, the realistic case of three neutrinos, and the general case of n neutrinos. Special emphasis is placed on the parameter implications of additional sterile neutrinos and their mixing. This is followed by a discussion of the modifications to these relationships under the influence of new physics.

2.1. Within the Minimally extended standard model

With the introduction offered in Appendix A, it is easy to see that the neutrino sector of the SM extended to accommodate Majorana neutrino mass may be expressed by the Lagrangian

$$\mathcal{L}_{\nu SM} \supset \frac{g}{\sqrt{2}} (\bar{\nu}_\alpha \gamma^\mu \ell_\alpha W_\mu^+ + \bar{\ell}_\alpha \gamma^\mu \nu_\alpha W_\mu^-) + \frac{g}{2 \cos \theta_W} \bar{\nu}_\alpha \gamma^\mu \nu_\alpha Z_\mu + \frac{1}{2} \bar{\nu}_\alpha^c M_{\alpha\beta} \nu_\beta. \quad (2.1)$$

Where $M_{\alpha\beta}$ is the Majorana neutrino mass matrix. This expression is written in the flavor bases where the charged lepton masses and neutrino interaction terms are diagonal. I now

determine the transformations of the neutrino mixing matrix that leaves this invariant. The reader should note for future use that an overall sign change of any neutrino field, either in the flavor or mass basis, is unphysical, in that it will not affect any observable process and is a common property of all quantum field theories. This follows directly from the rephasing freedom already discussed in the previous section. Using this I analyze the symmetries of the mass matrix.

2.1.1. The Two Neutrino Case

In the case of only two Majorana neutrinos, the mass eigenstates ν_1 and ν_2 are related to the flavor eigenstates ν_α and ν_β by the unitary transformation U^\dagger . This can be parameterized as

$$\begin{aligned} \begin{pmatrix} \nu_1 \\ \nu_2 \end{pmatrix} &= \mathbf{P}^2(\phi)\mathbf{R}^{12}(\theta) \begin{pmatrix} \nu_\alpha \\ \nu_\beta \end{pmatrix} \\ &= \begin{pmatrix} 1 & 0 \\ 0 & e^{i\phi} \end{pmatrix} \begin{pmatrix} \cos \theta & -\sin \theta \\ \sin \theta & \cos \theta \end{pmatrix} \begin{pmatrix} \nu_\alpha \\ \nu_\beta \end{pmatrix} \end{aligned} \quad (2.2)$$

where the phase matrix \mathbf{P}^2 and rotation matrix \mathbf{R}^{12} are defined in Appendix B Here, all physics is contained in four parameters expressible as two real and positive masses m_1, m_2 , one real mixing angle θ , and one CP violating Majorana phase ϕ . The symmetries of Eq. (2.3) may be used to limit the physical ranges of these quantities. To this end, I must find transformations up to an overall rephasing that renders

$$\mathbf{N}_m\mathbf{P}^2(\phi)\mathbf{R}^{12}(\theta)\mathbf{N}_f = \mathbf{S}^{12}\mathbf{P}^2(\phi')\mathbf{R}^{12}(\theta'), \quad (2.3)$$

where \mathbf{N}_m and \mathbf{N}_f are unphysical shifts of the mass and flavor eigenstates respectively, and \mathbf{S}^{12} is a discrete permutation matrix that flips 1-2 vector elements. Assuming the Standard Model Lagrangian augmented by Majorana neutrino masses, these are just simple field sign redefinitions. All possible physical transformations are contained in the continuous shifts of mixing parameters $\mathbf{P}^2(\phi + \delta\phi)\mathbf{R}^{12}(\theta + \delta\theta)$, as well as the discrete interchange of mass eigenstates. This is accomplished by the operation $\mathbf{S}^{12} = \mathbf{P}^2(\pi)\mathbf{R}^{12}(-\pi/2)$ which changes the sign of the mass squared difference $\Delta m^2 = m_2^2 - m_1^2$. To perform a systematic symmetry search, I put both sides of Eq. (2.3) into the same form for easy comparison. Beginning on the right hand side, I find that the case without the mass eigenstate flip is trivially $\mathbf{P}^2(\phi)\mathbf{P}^2(\delta\phi)\mathbf{R}^{12}(\delta\theta)\mathbf{R}^{12}(\theta)$. Adding the $\nu_1 \leftrightarrow \nu_2$ operation I commute to find

$$\begin{aligned}
\mathbf{S}\mathbf{P}^2(\phi + \delta\phi)\mathbf{R}^{12}(\theta + \delta\theta) &= \mathbf{P}^2(\pi)\mathbf{R}^{12}\left(-\frac{\pi}{2}\right)\mathbf{P}^2(\phi)\mathbf{P}^2(\delta\phi)\mathbf{R}^{12}(\delta\theta)\mathbf{R}^{12}(\theta) & (2.4) \\
&= \mathbf{P}^2(\pi)\mathbf{P}^1(\phi)\mathbf{P}^1(\delta\phi)\mathbf{R}^{12}\left(-\frac{\pi}{2}\right)\mathbf{R}^{12}(\delta\theta)\mathbf{R}^{12}(\theta) \\
&= \mathbf{P}^2(\phi)\mathbf{P}^2(\pi - \phi)\mathbf{P}^1(\phi + \delta\phi)\mathbf{R}^{12}\left(\delta\theta - \frac{\pi}{2}\right)\mathbf{R}^{12}(\theta) \\
&= \mathbf{P}^2(\phi)\mathbf{P}^2(\pi - 2\phi - \delta\phi)\mathbf{R}^{12}\left(\delta\theta - \frac{\pi}{2}\right)\mathbf{R}^{12}(\theta).
\end{aligned}$$

The last step utilizes a total rephasing by $e^{-i(\phi+\delta\phi)}$ to yield the requisite form. On the left of Eq. (2.3) I must consider eight cases defined by the matrix pairs

$$\begin{aligned}
(\mathbf{N}_m, \mathbf{N}_f) &= \{(\mathbf{I}, \mathbf{I}), (\mathbf{I}, -\mathbf{I}), (\mathbf{P}^2(\pi), \mathbf{I}), (\mathbf{P}^1(\pi), \mathbf{I}), (\mathbf{P}^2(\pi), \mathbf{P}^2(\pi)), (\mathbf{P}^2(\pi), \mathbf{P}^1(\pi)), \\
&\quad (\mathbf{I}, \mathbf{P}^2(\pi)), (\mathbf{I}, \mathbf{P}^1(\pi))\}. & (2.5)
\end{aligned}$$

Matrix		$\mathbf{P}^2(\delta\phi)\mathbf{R}^{12}(\delta\theta)$	$\mathbf{P}^2(\pi - 2\phi - \delta\phi)\mathbf{R}^{12}(\delta\theta - \pi/2)$
$\mathbf{P}^2(0)\mathbf{R}^{12}(0)$	None	$(\phi, \theta) \rightarrow (\phi, \theta)$	$(\phi, \theta) \rightarrow (-\phi + \pi, \theta + \pi/2)$
$\mathbf{P}^2(0)\mathbf{R}^{12}(\pi)$	$\nu_\alpha \rightarrow -\nu_\alpha, \nu_\beta \rightarrow -\nu_\beta$	$(\phi, \theta) \rightarrow (\phi, \theta + \pi)$	$(\phi, \theta) \rightarrow (-\phi + \pi, \theta - \pi/2)$
$\mathbf{P}^2(\pi)\mathbf{R}^{12}(0)$	$\nu_2 \rightarrow -\nu_2$	$(\phi, \theta) \rightarrow (\phi + \pi, \theta)$	$(\phi, \theta) \rightarrow (-\phi, \theta + \pi/2)$
$\mathbf{P}^2(\pi)\mathbf{R}^{12}(\pi)$	$\nu_1 \rightarrow -\nu_1$	$(\phi, \theta) \rightarrow (\phi + \pi, \theta + \pi)$	$(\phi, \theta) \rightarrow (-\phi, \theta - \pi/2)$
$\mathbf{P}^2(0)\mathbf{R}^{12}(-2\theta)$	$\nu_2 \rightarrow -\nu_2, \nu_\beta \rightarrow -\nu_\beta$	$(\phi, \theta) \rightarrow (\phi, -\theta)$	$(\phi, \theta) \rightarrow (-\phi + \pi, -\theta + \pi/2)$
$\mathbf{P}^2(0)\mathbf{R}^{12}(-2\theta + \pi)$	$\nu_2 \rightarrow -\nu_2, \nu_\alpha \rightarrow -\nu_\alpha$	$(\phi, \theta) \rightarrow (\phi, -\theta + \pi)$	$(\phi, \theta) \rightarrow (-\phi + \pi, -\theta - \pi/2)$
$\mathbf{P}^2(\pi)\mathbf{R}^{12}(-2\theta)$	$\nu_\beta \rightarrow -\nu_\beta$	$(\phi, \theta) \rightarrow (\phi + \pi, -\theta)$	$(\phi, \theta) \rightarrow (-\phi, -\theta + \pi/2)$
$\mathbf{P}^2(\pi)\mathbf{R}^{12}(-2\theta + \pi)$	$\nu_\alpha \rightarrow -\nu_\alpha$	$(\phi, \theta) \rightarrow (\phi + \pi, -\theta + \pi)$	$(\phi, \theta) \rightarrow (-\phi, -\theta - \pi/2)$

Table 2.1. Exhaustive summary of two neutrino mixing symmetries. See text for details.

The only difficulty arises from a nontrivial \mathbf{N}_f commuting with the rotation matrix. Since $\mathbf{P}^1(\pi) = -\mathbf{P}^2(\pi)$ in this two dimensional case, it is enough to consider only

$$\mathbf{N}_m \mathbf{P}^2(\phi) \mathbf{R}^{12}(\theta) \mathbf{P}^1(\pi) = \mathbf{P}^2(\phi) \mathbf{N}_m \mathbf{R}^{12}(\theta) \mathbf{P}^1(\pi) \mathbf{R}^{12}(-\theta) \mathbf{R}^{12}(\theta) \quad (2.6)$$

$$= \mathbf{P}^2(\phi) \mathbf{N}_m \mathbf{P}^1(\pi) \mathbf{R}^{12}(-2\theta) \mathbf{R}^{12}(\theta)$$

$$= \mathbf{P}^2(\phi) \mathbf{N}_m \mathbf{P}^2(\pi) \mathbf{R}^{12}(-2\theta + \pi) \mathbf{R}^{12}(\theta) \quad (2.7)$$

and change overall signs as needed, with the operation $\mathbf{R}^{12}(\pi)$, to match the intended structure. Once this is done to both sides of Eq. (2.3), the outer factors of $\mathbf{P}^2(\phi)$ and $\mathbf{R}^{12}(\theta)$ cancel, revealing simplified equations that may be easily solved for the physical parameter shifts $\delta\phi$ and $\delta\theta$.

Table 2.1.1 shows the solutions to these equations for every possible case. The first column and row displays the simplified matrix equations obtained from manipulations of the left and right side of Eq. (2.3), respectively. For convenience, the second column displays the unphysical field redefinitions associated with each corresponding row. The remaining columns contain an exhaustive list of physical transformations that leave the two neutrino Majorana mixing matrix invariant. All of these take the general form

$(\phi, \theta) \rightarrow (\pm\phi + \delta\phi, \pm\theta + \delta\theta)$. Notice that many of the listed transformations yield equivalent information. In particular, I find that the phase $\phi \rightarrow -\phi$ for all cases where the mass eigenstates are exchanged since $\nu_1 \leftrightarrow \nu_2 \Rightarrow \mathbf{P}^2(\phi) \rightarrow \mathbf{P}^1(\phi)$, which must be countered by a total rephasing by $-\phi$. Additionally, I see that ϕ is invariant under translations by π in cases defined by the number of unphysical field redefinitions. In a similar way, it is clear that the mixing angle θ is only invariant under discrete sign changes as well as shifts by π and $\pi/2$. Each invariance listed in the table may be interpreted as a single constraint on the physical parameter ranges. I follow [8], choosing independent entries, and limit these as:

- (1) $\nu_2 \rightarrow -\nu_2$, and $\phi \rightarrow \phi + \pi$.

Here I find that the phase ϕ is invariant under shifts by π , given a nonphysical mass eigenstate redefinition. This suggests degeneracies between the ϕ parameter regions of size π . I choose $\phi \in [-\pi/2, \pi/2]$ without loss of generality. This result conforms via direct symmetry arguments to the common conception of Majorana phase ranges.

- (2) $\theta \rightarrow \theta + \pi$, $\nu_1 \rightarrow -\nu_1$, and $\nu_2 \rightarrow -\nu_2$.

The mixing angle shift suggests parameter space degeneracies of size π . Hence, θ is limited to span π radians, half its original range, to the interval $\theta \in [-\pi/2, \pi/2]$, chosen for convenience.

- (3) $\theta \rightarrow -\theta$, $\nu_\beta \rightarrow -\nu_\beta$, and $\nu_2 \rightarrow -\nu_2$.

Thus, neutrino mixing is invariant under reflections about $\theta = 0$, implying a degeneracy between positive and negative values. This suggests a halving of the mixing angle physical range to $\theta \in [0, \pi/2]$.

(4) $\theta \rightarrow \theta + \pi/2$, $\nu_2 \rightarrow -\nu_2$, $\nu_1 \leftrightarrow \nu_2$ and $\phi \rightarrow -\phi$.

This symmetry relates three distinct physical transformations, and it is clear from Table 2.1.1 that no smaller set will yield the same results. Hence, this relation may be interpreted in one of three ways. First, if θ and ϕ are allowed to move within their full range as constrained above, one may choose a particular ordering of mass eigenstates, or equivalently, the sign of the neutrino mass squared difference. This is typically done in full, two neutrino oscillation analysis where Δm^2 is taken positive. If both positive and negative Δm^2 are allowed, one has the freedom to limit *either* $\theta \in [0, \pi/4]$ or $\phi \in [0, \pi/2]$. In the case of standard vacuum oscillations, the sign of Δm^2 is unphysical, leading to the notion that the mixing parameter ranges are automatically limited as described here. While true for pure neutrino mixing, the SM charged current interactions shown in Eq. (2.1), relevant for matter effects, break this degeneracy and one must explicitly choose how to limit and interpret the resulting parameter space.

I point out that the Majorana neutrino mass matrix, which governs such lepton number violating processes as neutrinoless double beta decay, is invariant under these transformations by construction. It is also easy to check that other processes such as neutrino flavor oscillations and neutrino-antineutrino oscillations share this property since their amplitudes are strongly related to the mass matrix. I illustrate some of the above observations by example in this simple two neutrino context. Most conclusions are apparent by inspection here, but carry over to the more general case of n neutrino flavors in a much less obvious way.

First, consider the two flavor neutrino oscillation probability of a ν_α being measured as a ν_β after traversing a baseline L with energy E . In vacuum, this is given by

$$P_{\nu_\alpha \rightarrow \nu_\beta}^{\text{vacuum}}(L, E) = \sin^2 2\theta \sin^2 \left(\frac{\Delta m^2 L}{4E} \right). \quad (2.8)$$

Here, the Majorana phase, as well as the sign of Δm^2 , is unphysical. It is clear that the physical range of θ is only in the $[0, \pi/4]$ interval from the factor $\sin^2 2\theta$. To introduce the Δm^2 sign as a physical degree of freedom, I must introduce matter effects. For neutrinos propagating in a constant electron density background, the mixing parameters of Eq. (2.8) must be replaced by effective matter quantities. In terms of the dimensionless parameter $A = 2\sqrt{2}EG_F N_e / \Delta m^2$, where N_e is the local electron number density, the modified oscillation probability is

$$P_{\nu_\alpha \rightarrow \nu_\beta}^{\text{matter}}(L, E) = \frac{\sin^2 2\theta}{1 + A^2 - 2A \cos 2\theta} \sin^2 \left(\frac{\Delta m^2 L}{4E} \sqrt{1 + A^2 - 2A \cos 2\theta} \right). \quad (2.9)$$

Since $\cos 2\theta$ now appears independently, I have lost the freedom to constrain θ beyond $[0, \pi/2]$. However, if I allow for a mass eigenstate flip, which induces an $A \rightarrow -A$ transformation, the angular degeneracy is restored. I see that one may choose to confine either Δm^2 positive *or* $\theta \in [0, \pi/4]$.

To see how the Majorana phases enter into this discussion, I must move to lepton number violating processes where they contribute to important physical effects. These are much harder to observe/constrain since all rates must be proportional to neutrino mass values, as opposed to the interferometric dependence in standard neutrino oscillations.

Consider the rate for neutrino-antineutrino oscillation which goes like [9, 10]

$$\Gamma_{\nu \rightarrow \bar{\nu}} \propto \frac{\sin^2 2\theta}{4E^2} \left\{ m_1^2 + m_2^2 - 2m_1 m_2 \cos \left(\frac{\Delta m^2 L}{2E} - 2\phi \right) \right\}. \quad (2.10)$$

This is similar to the neutrino vacuum flavor oscillation formulae, except that this rate is directly proportional to the neutrino mass scale and shows a Majorana phase dependence. Here the physical range of θ is still of size $\pi/4$, but now the sign of Δm^2 and ϕ are physical. I may limit the range for one of these by noting that a negative ϕ value can be compensated by mass eigenstate flip. This is the physical manifestation of the ambiguity noted in the final entry of the above symmetry list. The next logical step is to consider neutrino-antineutrino oscillations in matter, where, as in the flavor cases, the mass matrix diagonalization is modified by an effective matter potential. The process carries through as before, yielding no new information except for an illustration of the interplay between θ , Δm^2 and ϕ at the same time. I leave this to the reader and move on to the more realistic three neutrino case.

2.1.2. The Three Neutrino Case

The case of three Majorana neutrinos is more complicated than the two neutrino analysis performed in Subsection 2.1.1. Nevertheless, the methodology and many features of the previous example carry over directly. Here, neutrino mixing is defined in terms of nine parameters, conventionally chosen as three mass eigenvalues $\{m_1, m_2, m_3\}$ taken real and positive, three real mixing angles $\{\theta_{12}, \theta_{13}, \theta_{23}\}$, and three CP violating phases $\{\delta, \phi_2, \phi_3\}$. The Majorana phases ϕ_2 and ϕ_3 are not physical, meaning that they may be phased away, when neutrinos are Dirac particles. The mixing between the mass eigenstates ν_1 , ν_2 and

ν_3 and the flavor eigenstates ν_e , ν_μ , and ν_τ may be parameterized by

$$\begin{aligned}
\begin{pmatrix} \nu_1 \\ \nu_2 \\ \nu_3 \end{pmatrix} &= [\mathbf{P}^2(\phi_2)\mathbf{P}^3(\phi_3)] [\mathbf{R}^{12}(\theta_{12})] [\mathbf{P}^1(-\delta)\mathbf{P}^3(\delta)\mathbf{R}^{13}(\theta_{13})\mathbf{P}^1(\delta)\mathbf{P}^3(-\delta)] \\
&\quad \times [\mathbf{R}^{23}(\theta_{23})] \begin{pmatrix} \nu_e \\ \nu_\mu \\ \nu_\tau \end{pmatrix} \\
&= \begin{pmatrix} 1 & 0 & 0 \\ 0 & e^{i\phi_2} & 0 \\ 0 & 0 & e^{i\phi_3} \end{pmatrix} \begin{pmatrix} c_{12} & -s_{12} & 0 \\ s_{12} & c_{12} & 0 \\ 0 & 0 & 1 \end{pmatrix} \begin{pmatrix} c_{13} & 0 & -s_{13}e^{-i\delta} \\ 0 & 1 & 0 \\ s_{13}e^{i\delta} & 0 & c_{13} \end{pmatrix} \quad (2.11) \\
&\quad \times \begin{pmatrix} 1 & 0 & 0 \\ 0 & c_{23} & -s_{23} \\ 0 & s_{23} & c_{23} \end{pmatrix} \begin{pmatrix} \nu_e \\ \nu_\mu \\ \nu_\tau \end{pmatrix},
\end{aligned}$$

where, to conserve space, I employ the shorthand $c_{ij} \equiv \cos \theta_{ij}$ and $s_{ij} \equiv \sin \theta_{ij}$.

As in the previous case, I search for physical transformations of the mixing variables that leave Eq. (2.12) invariant and interpret these as degeneracies within their parameter spaces, which lead directly to range limitations. Here, it is not useful to list every possible symmetry due to the overwhelming number of possibilities, many of which yield equivalent physical information. Rather, I enumerate in Table 2.1.2 a subset of simple cases that best reveal the underlying physics. The first column labels the transformation number referred to in the text, followed by the unphysical field redefinitions and the physical shifts

#	Unphysical	Physical
1	$\nu_2 \rightarrow -\nu_2$	$\phi_2 \rightarrow \phi_2 + \pi$
2	$\nu_3 \rightarrow -\nu_3$	$\phi_3 \rightarrow \phi_3 + \pi$
3		$\theta_{13} \rightarrow -\theta_{13}, \delta \rightarrow \delta + \pi$
4	$\nu_\tau \rightarrow -\nu_\tau, \nu_3 \rightarrow -\nu_3$	$\theta_{23} \rightarrow -\theta_{23}, \theta_{13} \rightarrow -\theta_{13}$
5	$\nu_\mu \rightarrow -\nu_\mu, \nu_2 \rightarrow -\nu_2$	$\theta_{12} \rightarrow -\theta_{12}, \theta_{23} \rightarrow -\theta_{23}$
6	$\nu_1 \rightarrow -\nu_1, \nu_2 \rightarrow -\nu_2$	$\theta_{12} \rightarrow \theta_{12} + \pi$
7	$\nu_2 \rightarrow -\nu_2, \nu_3 \rightarrow -\nu_3$	$\theta_{23} \rightarrow \theta_{23} + \pi, \theta_{13} \rightarrow -\theta_{13}, \theta_{12} \rightarrow -\theta_{12}$
8		$\theta_{13} \rightarrow \theta_{13} + \pi, \theta_{12} \rightarrow \theta_{12} + \pi, \theta_{23} \rightarrow \theta_{23} + \pi, \delta \rightarrow \delta + \pi$

Table 2.2. Summary of selected three neutrino mixing symmetries. Although this list is not exhaustive it is a complete representation of the symmetry structure. See text for details.

in columns two and three, respectively. For convenience, the symmetry ordering is set such that the first physical transformation in each row may be used to limit a particular parameter provided the constraints listed above it are imposed. In this way, one may run down the list systematically to reveal the most constrained parameter spaces available to the system. One should note a few key features of this table. First, for simplicity, I only include those transformations that lead to parameter space degeneracies and skip nontrivial parameter redefinitions of the form $P_i \rightarrow P_i(P_1, P_2 \dots P_n)$ for arbitrary mixing variables P_i . Such cases that mix parameters are addressed separately. Furthermore, the entries listed here are in no way unique, but they do constitute a complete set, since combining them in various ways will produce all other elements. These variations, however, yield no new physical insight and are therefore neglected.

From this, the physical mixing parameters may be limited in the following way. The first two entries tell us that I may halve the ranges of the Majorana phases to π with impunity. The next entry constrains the θ_{13} mixing angle and its associated phase δ . Here, one may chose either variable to be limited to a range of π provided the other occupies

the full 2π region. This suggests that one may have either $\delta \in [0, \pi]$ and $\theta_{13} \in [-\pi, \pi]$ or $\delta \in [0, 2\pi]$ and $\theta_{13} \in [0, \pi]$, but not both. Typically, the latter option is chosen by experimental analyses to maintain consistency with the two neutrino case where the Dirac phase, and therefore this ambiguity, is not present. It will become clear that, since these two symmetries are independent of unphysical transformations they are thus robust to the effects on non-standard interactions. Entries 4 and 5 allow for the similar range limitation of the mixing angles θ_{12} and θ_{23} to $[0, \pi]$. Notice that while naively requiring both positive and negative θ_{13} values, this is independent of the previously described ambiguity. This is because $\theta_{13} \rightarrow -\theta_{13}$ and $\delta \rightarrow \delta + \pi$ are interchangeable transformations, such that the mixing angle sign change may be compensated by a phase shift. Entries 6, 7 and 8 permit one to further limit each mixing angle to a range of $\pi/2$, which I take to be $[-\pi/2, \pi/2]$ without loss of generality. I see here that these actions utilize the nonphysical sign change of the mass eigenstates. Finally, making these standard choices, I see that the physical ranges of each mixing angle is limited to $\theta_{ij} \in [0, \pi/2]$ and the Majorana phases are limited to $\phi_i \in [-\pi/2, \pi/2]$, while the Dirac phase is unconfined within its full $\delta \in [0, 2\pi]$ range.

Unfortunately, without an exhaustive search, it is impossible to know if and when I include all relevant transformations. To this end, I must submit to plausibility arguments supplemented by numerical examples. The invariance criterion is simple if I consider each of the six parameters of the mixing matrix Eq. (2.12) to transform as $P_i \rightarrow P_i + \delta P_i$ and formally commute the result into the form $\mathbf{N}_m U^\dagger(p_i, \delta P_i) = U^\dagger(P_i) M(P_i, \delta P_i)$. One must then find all possible $\delta P_i = \delta P_i(P_j)$ that renders the matrix M proportional to some product of $\mathbf{P}^k(\pi)$ s, which are just nonphysical field redefinitions. Working through this manipulation, I make the observation that only factors of $\mathbf{P}^k(\pi)$ commute through the

rotation matrices trivially, only inducing parameter sign changes. All other attempts do not commute and lead to additional terms directly proportional to some of the mixing parameters. It follows that M is a product of such factors, so it is natural to conclude that solutions $\delta P_i(P_j)$ can not exist in general for all parameter values. This statement holds true in the case of three parameter variations, which may be checked analytically, but is not obvious when all six parameters are allowed to shift. To establish confidence that no symmetries are missed in the general case, I perform a comprehensive numerical scan for solutions. Due to the large number of possible variations, this operation is coarse by necessity. That being said, our methodology did find the class of solutions already explored with no indication of other possibilities. I therefore conclude that the symmetries spanned by the transformations listed in Table 2.1.2 are complete.

In addition to the symmetries outlined in Table 2.1.2, physically distinct transformations also exist that do not limit parameter spaces, but should rather be interpreted as variable redefinitions. These are cases where parameters mix with each other in a nontrivial way. The simplest example that still supplies physical insight is the three neutrino analog of symmetry four in the two neutrino case involving the exchange of mass eigenstates. Here I see that the Lagrangian is invariant under $\theta_{12} \rightarrow \theta_{12} - \pi/2$, $\phi_2 \rightarrow -\phi_2$, $\phi_3 \rightarrow \phi_3 - \phi_2$, $\nu_1 \leftrightarrow \nu_2$ provided the unphysical sign redefinition $\nu_2 \rightarrow -\nu_2$. No phase space limitations may be extracted from this due to the mixing of the Majorana phases ϕ_2 and ϕ_3 . It requires a nontrivial relabeling of the ϕ_3 parameter. The utility of this transformation is clear when the Majorana phases are unphysical, as is the case for Dirac neutrinos, where the troublesome shifts may be phased away, or in all lepton number conserving processes where ϕ_2 and ϕ_3 simply do not show up. Under these circumstances, one may use this

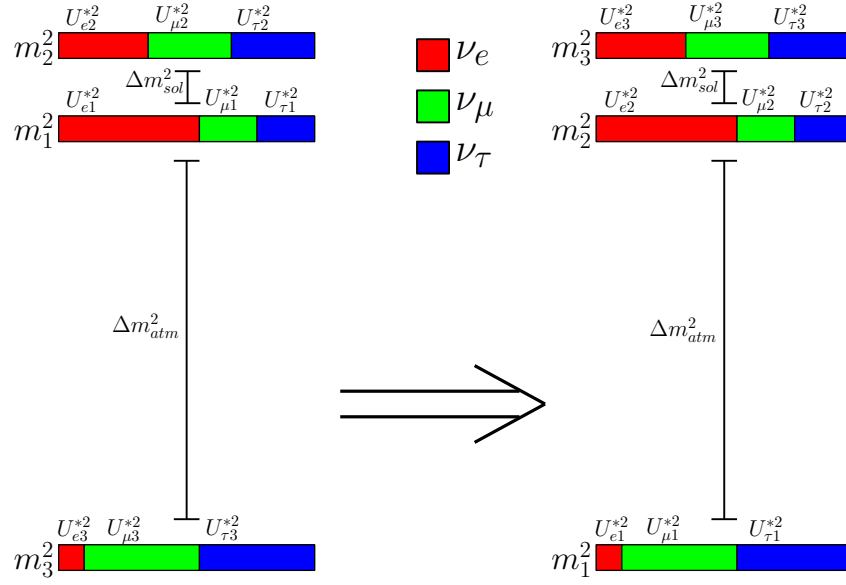


Figure 2.1. Mapping of the inverted neutrino mass hierarchy between the popular (312) and (123)schemes. The relationship between mixing elements is clear from this plot, but the mapping between the specific mixing parameters is highly nontrivial as given in the text.

symmetry to limit parameters in much the same way as in the two neutrino scenario. Namely, one may choose either positive Δm_{12}^2 , or $\theta_{12} \in [0, \pi/4]$. The central position of the 1 – 2 parameters in this discussion is unambiguously chosen by our standard mixing matrix parameterizations. The general conclusion is that the $i - j$ plane may enjoy this constraint if it contains the *first* Euler rotation of the mass eigenstates in the transformation to the flavor basis. The noncommutative nature of orthogonal rotations renders the effects of any other $\nu_{i'} \leftrightarrow \nu_{j'}$ much more complex. In particular, all other mass eigenstate exchange symmetries require mixing/relabeling of the mixing angles and Dirac phase that cannot be phased away in any reasonable situation. Therefore, most such transformations are of little practical importance and are not considered further.

The only exception to this involves the permutations of two eigenstate pairs $\nu_1 \leftrightarrow \nu_2$ followed by $\nu_3 \leftrightarrow \nu_2$. This transformation is of interest because it defines the mapping between two popular parameterizations of three neutrino mixing within the context of the inverted mass hierarchy displayed in Figure 2.1. On one hand, as shown in the leftmost spectrum, one may assume the mass states ordered, from smallest to largest, as m_3, m_1, m_2 (henceforth the 312-case), so as to maintain the mixing angle definitions obtained for the normal hierarchy. On the other hand, one may wish to maintain the mass ordering scheme m_1, m_2, m_3 (the 123-case) as shown in the rightmost spectrum [11]. It is natural to explore the mapping between the mixing parameters in these two cases. Figure 2.1, which indicates the flavor composition of each state by color coding, represents this transformation between the mixing matrix elements $U_{\alpha i}^*$ via explicit labeling. From this alone I see, for example, that $U_{e3}^{(312)*} = U_{e1}^{(123)*}$ which implies that $s_{12}^{(312)} s_{23}^{(312)} + c_{12}^{(312)} c_{23}^{(312)} s_{13}^{(312)} e^{-i\delta^{(312)}} = c_{12}^{(123)} c_{13}^{(123)}$, where the parameter superscripts indicate the mass ordering. This is one of the simplest cases taken from the figure, but it still provides a very nontrivial relation between the variables. I proceed formally, using the language of Appendix B, to complete the mapping. Specifically, I study the effect of the following operation

$$\mathbf{H} \begin{pmatrix} \nu_3 \\ \nu_1 \\ \nu_2 \end{pmatrix} = \mathbf{R}^{23}\left(\frac{\pi}{2}\right) \mathbf{P}^3(\pi) \mathbf{R}^{13}\left(\frac{\pi}{2}\right) \mathbf{P}^3(\pi) \begin{pmatrix} \nu_3 \\ \nu_1 \\ \nu_2 \end{pmatrix} = \begin{pmatrix} \nu_1 \\ \nu_2 \\ \nu_3 \end{pmatrix} \quad (2.12)$$

on the mixing matrix. Here, one of the phase rotations $\mathbf{P}^3(\pi)$ may commute through the real rotations to cancel out, leaving only a simple sign change. Acting on the mixing

matrix, this has the following effect:

$$\begin{aligned}
\mathbf{H}^{-1}\mathbf{U}^\dagger &= \mathbf{R}^{13}\left(\frac{\pi}{2}\right)\mathbf{R}^{23}\left(-\frac{\pi}{2}\right)\mathbf{P}^2(\phi_2)\mathbf{P}^3(\phi_3)\mathbf{R}^{12}(\theta_{12})\mathbf{P}^1(-\delta)\mathbf{P}^3(\delta)\mathbf{R}^{13}(\theta_{13}) \quad (2.13) \\
&\quad \times \mathbf{P}^1(\delta)\mathbf{P}^3(-\delta)\mathbf{R}^{23}(\theta_{23}) \\
&= \mathbf{R}^{13}\left(\frac{\pi}{2}\right)\mathbf{P}^3(\phi_2)\mathbf{P}^2(\phi_3)\mathbf{R}^{13}(\theta_{12})\mathbf{P}^1(-\delta)\mathbf{P}^2(\delta)\mathbf{R}^{12}(\theta_{13})\mathbf{P}^1(\delta) \\
&\quad \times \mathbf{P}^2(-\delta)\mathbf{R}^{23}\left(\theta_{23} - \frac{\pi}{2}\right) \\
&= \mathbf{P}^1(\phi_2)\mathbf{P}^2(\phi_3)\mathbf{R}^{13}\left(\theta_{12} + \frac{\pi}{2}\right)\mathbf{P}^1(-\delta)\mathbf{P}^2(\delta)\mathbf{R}^{12}(\theta_{13})\mathbf{P}^1(\delta) \times \mathbf{P}^2(-\delta) \\
&\quad \mathbf{R}^{23}\left(\theta_{23} - \frac{\pi}{2}\right).
\end{aligned}$$

Notice that the entire transformation may be absorbed into shifts of the physical mixing parameters leaving no nonphysical sign change requirements. Formally, the transformations shown in Eq. (2.14) are very simple. The largest change arises from the relabeling of the mixing planes which leads to a situation where the complex rotation governed by θ_{13} and δ now acts in the 1 – 2 plane, while θ_{12} governs the 1 – 3 rotation. As intuitively expected, it exchanges the roles of θ_{12} and θ_{13} . The main difficulty arises operationally while massaging the Euler rotations into the conventional order, since they do not commute. To put the result of Eq. (2.14) into the form of Eq. (2.12) one must commute the 1 – 2 and 1 – 3 rotations. A little thought reveals that this alone is not enough, as no consistent parameter mapping may exist for all relevant angles in this case. Thus, to proceed, one must also search for highly nontrivial transformations of θ_{23} . Commuting the matrices formally for the full transformation, I find the following mapping of mixing

parameters from the 312 to the 123 spectral cases.

$$\Delta m_{13}^2 \rightarrow -\Delta m_{12}^2$$

$$\Delta m_{23}^2 \rightarrow -\Delta m_{31}^2 \Rightarrow$$

$$\Delta m_{12}^2 \rightarrow \Delta m_{23}^2$$

$$\left\{ \begin{array}{l} c_{12}^2 \rightarrow \frac{s_{13}^2}{1-c_{13}^2 s_{12}^2} \\ s_{13}^2 \rightarrow c_{13}^2 s_{12}^2 \\ c_{23}^2 \rightarrow \frac{c_{23}^2 s_{12}^2 s_{13}^2 + c_{12}^2 s_{23}^2 + 2 \cos \delta c_{12} c_{23} s_{12} s_{23} s_{13}}{1-c_{13}^2 s_{12}^2} \\ \delta \rightarrow \cos^{-1} \left(\frac{c_{12} s_{23} + \cos \delta c_{12} s_{23} s_{13}}{\sqrt{c_{23}^2 s_{12}^2 s_{13}^2 + c_{12}^2 s_{23}^2 + 2 \cos \delta c_{12} c_{23} s_{12} s_{23} s_{13}}} \right) \\ \phi_3 \rightarrow \phi_2 - \phi_3 - \delta - \cos^{-1} \left(\frac{c_{12} s_{23} + \cos \delta c_{12} s_{23} s_{13}}{\sqrt{c_{23}^2 s_{12}^2 s_{13}^2 + c_{12}^2 s_{23}^2 + 2 \cos \delta c_{12} c_{23} s_{12} s_{23} s_{13}}} \right) \\ \phi_2 \rightarrow -\phi_3 - \delta \end{array} \right. \quad (2.14)$$

These are unique up to trivial sign changes, provided the overall nonphysical rephasing by $e^{i(\delta+\phi_3)}$. The transformations are relatively simple for the θ_{12} and θ_{13} parameters, but the redefinition is less attractive for θ_{23} due to its induced dependence on δ . In the case of Dirac CP conservation, the properties $\delta = 0$ and $\delta = \pi$ are maintained in the mapping (as they should) and the troublesome transformations are simplified to $\phi_2 \rightarrow -\phi_3 + (-\pi)$, $\phi_3 \rightarrow \phi_2 - \phi_3 + (-\pi)$ and $c_{23}^2 \rightarrow (c_{23} s_{12} s_{13} + c_{12} s_{23})^2 / (c_{13}^2 s_{12}^2 - 1)$.

2.1.3. Comments on the n Neutrino case

The results of the previous subsections may be directly generalized to the case of n neutrinos. Here, all physics may be parameterized by n real and positive masses m_i and $n(n-1)$ mixing angles/phases. This arises from the $2n^2$ degrees of freedom in an arbitrary complex $n \times n$ matrix minus n^2 unitarity conditions and n field rephasing. Choosing the standard parameterizations, the remaining freedom may be categorized into $n(n-1)/2$ real mixing angles θ_{ij} , $(n-1)(n-2)/2$ Dirac phases δ_{ij} and $n-1$ Majorana phases ϕ_i . Due to the limited rephasing freedom, I may define select elements of the mixing matrix real.

Following [12] I choose to remove all Dirac phases from the three row main diagonal band so that rotations between the neighboring $(a-1) - a$ planes are taken to be real, while the rest are not, and thus, include a CP violating Dirac phase. Taking these complex rotations in the $i-j$ plane to be $\tilde{\mathbf{R}}^{ij}(\theta_{ij}, \delta_{ij}) \equiv \mathbf{P}^i(-\delta_{ij}/2)\mathbf{P}^j(\delta_{ij}/2)\mathbf{R}^{ij}(\theta_{ij})\mathbf{P}^i(\delta_{ij}/2)\mathbf{P}^j(-\delta_{ij}/2)$, I find that an arbitrary $n \times n$ Majorana mixing matrix may be written as:

$$\begin{aligned} U_n^\dagger &= \prod_{i=2}^n \left[\mathbf{P}^i(\phi_i) \prod_{j=1}^{i-2} \left[\tilde{\mathbf{R}}^{ji}(\theta_{ji}, \delta_{ji}) \right] \mathbf{R}^{i-1,i}(\theta_{i-1,i}) \right] \\ &= \mathbf{P}^n(\phi_n) U_{n-1}^\dagger \prod_{j=1}^{n-2} \left[\tilde{\mathbf{R}}^{jn}(\theta_{jn}, \delta_{jn}) \right] \mathbf{R}^{n-1,n}(\theta_{n-1,n}), \end{aligned} \quad (2.15)$$

where the products are taken on the right such that $\prod_{i=1}^n A_i = A_1 A_2 A_3 \dots A_n$. The U_{n-1}^2 in the second line is actually of dimension $n \times n$, but is suggestively written to indicate that the upper $n-1 \times n-1$ diagonal block is the reduced $n-1$ neutrino mixing matrix. This reproduces the standard mixing matrices for the previous $n=2$ and $n=3$ cases and one may, in principle, compute this structure for an arbitrary number of states. For example, assuming $n=4$ Eq. (2.16) takes the form

$$U_4^\dagger = \mathbf{P}^2(\phi_2) \mathbf{R}^{12}(\theta_{12}) \mathbf{P}^3(\phi_3) \tilde{\mathbf{R}}^{13}(\theta_{13}, \delta_{13}) \mathbf{R}^{23}(\theta_{23}) \mathbf{P}^4(\phi_4) \tilde{\mathbf{R}}^{14}(\theta_{14}, \delta_{14}) \tilde{\mathbf{R}}^{24}(\theta_{24}, \delta_{24}) \mathbf{R}^{34}(\theta_{34}). \quad (2.16)$$

In order for this analysis to make contact with observed reality, I now describe the parameterization of the $3+n$ sterile neutrino scenario. Assuming the standard three light neutrinos that mix among themselves via the 3×3 matrix U_ℓ and n sterile states that

mix via the approximately unitary $n \times n$ matrix U_H . The total mixing matrix $[U_{tot}]_{n+3}$ to first order in the light-heavy mixing is

$$[U_{tot}]_{n+3} = \begin{pmatrix} [U_\ell]_3 & [\Theta^\dagger]_{3 \times n} \\ -[U_H]_n [\Theta]_{n \times 3} [U_\ell]_3 & [U_H]_3 \end{pmatrix}, \quad (2.17)$$

where

$$[\Theta]_{n \times 3} = \sum_{j=1}^n [U_{H,j-1}]_n [\Theta_j]_{n \times 3}. \quad (2.18)$$

Here, $[U_{H,0}]_n = [U_{H,1}]_n = 1$ and Θ_j is zero for all elements a, b except the row $a = i$ where it is

$$\theta_{b,a+3} e^{i\delta_{b,a+3}}. \quad (2.19)$$

Note that all Dirac phases are present, per my outlined convention, except $\delta_{34} = 0$ (since I hold rotations between adjacent planes real).

In the special 3 + 1 sterile neutrino case I can work out the mixing matrix to second order.

$$\begin{pmatrix} U_\ell^\dagger & \mathbf{0}_{3 \times 1} \\ \mathbf{0}_{1 \times 3} & 1 \end{pmatrix} \begin{pmatrix} 1 - \frac{1}{2}\theta_{14}^2 & -\theta_{14}\theta_{24}e^{-i(\delta_{14}-\delta_{24})} & -\theta_{14}\theta_{34}e^{-i\delta_{14}} & -\theta_{14}e^{-i\delta_{14}} \\ 0 & 1 - \frac{1}{2}\theta_{24}^2 & -\theta_{24}\theta_{34}e^{-i\delta_{24}} & -\theta_{24}e^{-i\delta_{24}} \\ 0 & 0 & 1 - \frac{1}{2}\theta_{34}^2 & -\theta_{34} \\ \theta_{14}e^{i\delta_{14}} & \theta_{24}e^{i\delta_{24}} & \theta_{34} & 1 - \frac{1}{2}(\theta_{14}^2 + \theta_{24}^2 + \theta_{34}^2) \end{pmatrix} \quad (2.20)$$

The schematic form of the sterile-active mixing

$$\begin{pmatrix} C \approx 1 - \frac{1}{2}\theta^2 & S^\dagger \approx \theta^\dagger \\ S \approx \theta & C \approx 1 - \frac{1}{2}\theta^2 \end{pmatrix} \quad (2.21)$$

is clear in all cases and will be very useful in Chapter 4.

I may now search for symmetries of U_n^\dagger . To limit the parameter space in a systematic fashion, I present the symmetries in the same order as in the three neutrino case. The transformations outlined here are equally complete. First, notice that all Majorana phases may be trivially commuted to the left of the expression. As such, for all integers $i \in (2, n)$, a phase shift $\phi_i \rightarrow \phi_i + \pi$ may be absorbed by a sign redefinition of the mass eigenstate $\nu_i \rightarrow -\nu_i$. Hence, as was recently shown in [13] using different methods, each Majorana phase may be limited to a range of π . Next, I find that $\theta_{ij} \rightarrow -\theta_{ij}$, followed by $\delta_{ij} \rightarrow \delta_{ij} + \pi$ is also an invariance for integers $i + 1 \neq j$. Thus, for the complex rotations one may compensate for negative angle values, provided a corresponding shift π of the Dirac phase. In a similar way, the angles governing real rotations participate in this invariance via the symmetries $\theta_{a-1,a} \rightarrow -\theta_{a-1,a}, \theta_{ia} \rightarrow -\theta_{ia}, \theta_{aj} \rightarrow -\theta_{aj}$ for all integers $i \in (1, a - 2)$ and $j \in (a + 1, n)$ provided the unphysical redefinitions $\nu_a \rightarrow -\nu_a$ and $\nu_{\alpha_a} \rightarrow -\nu_{\alpha_a}$ of the mass and flavor states, respectively. Here, one may systematically limit the angles $\theta_{a-1,a}$ since all other angles are either constrained by the previous transformations, or show up to the right of the real rotation in question. In this latter case one may proceed inductively from the rightmost rotation $\mathbf{R}^{n-1,n}(\theta_{n-1,n})$. Finally, I see that our system obeys the symmetry $\theta_{ab} \rightarrow \theta_{ab} + \pi, \theta_{ib} \rightarrow -\theta_{ib}, \theta_{aj} \rightarrow -\theta_{aj}$ for all integers $i < a$ and $a < j < b$, provided the unphysical redefinitions $\nu_a \rightarrow -\nu_a$ and $\nu_b \rightarrow -\nu_b$ of the mass and

flavor states, respectively. Hence, I obtain the expected result that the physical range of *all* mixing angles, Majorana phases, and Dirac phases are $\theta_{ij} \in [0, \pi/2]$, $\phi \in [-\pi/2, \pi/2]$, and $\delta_{ij} \in [0, 2\pi]$, respectively. As in the three neutrino case, no simple invariance may be formed with mass eigenstate permutations.

That being said, some relations still hold among the mixing angles and phases in these most general cases. Such instances are highly nontrivial and a full exploration is beyond the scope of this analysis and not very enlightening. In any case, all of the examples outlined in subsections 2.1.1 and 2.1.2 are still valid in the full n neutrino case. To see this, I show that if U_{n-1}^\dagger is invariant under some symmetry up to allowed state sign changes, then U_n^\dagger is also invariant. In this context, invariant is taken to mean $U_{n-1}^{\dagger'} = \mathbf{N}_m U_{n-1}^\dagger \mathbf{N}_f$ where, as in subsection 2.1.1, \mathbf{N}_m and \mathbf{N}_f are simply sign change matrices acting on the mass and flavor eigenstates, respectively. Both of these may be written as products of $\mathbf{P}^i(\pi)$ and handled with the algebra outlined in Appendix B. To begin, I note that \mathbf{N}_m can always be absorbed by mass eigenstate sign changes, as can a π phase shift of $\mathbf{P}^n(\phi_n)$. Thus, it is enough to show that an arbitrary $\mathbf{P}^a(\pi)$ from \mathbf{N}_f commutes through the remaining rotations to the flavor state vector. Since $a \leq n-1$, only the commutation with \mathbf{R}^{an} is nontrivial. For $a < n-1$ I have $\mathbf{P}^a(\pi) \tilde{\mathbf{R}}^{\text{an}}(\theta_{an}, \delta_{an}) = \tilde{\mathbf{R}}^{\text{an}}(-\theta_{an}, \delta_{an}) \mathbf{P}^a(\pi) = \tilde{\mathbf{R}}^{\text{an}}(\theta_{an}, \delta_{an} + \pi) \mathbf{P}^a(\pi)$, which yields only a δ_{an} shift by π . For the case $a = n-1$ I am left with $\mathbf{P}^{n-1}(\pi) \mathbf{R}^{n-1, \text{n}}(\theta_{n-1, n}) = \mathbf{P}^{n-1}(\pi) \mathbf{P}^{n-1}(\pi) \mathbf{P}^n(\pi) \mathbf{R}^{n-1, \text{n}}(\theta_{n-1, n} + \pi) = \mathbf{P}^n(\pi) \mathbf{R}^{n-1, \text{n}}(\theta_{n-1, n} + \pi)$, where the remaining phase shift is absorbed by a ν_n sign change after commuting through each $\tilde{\mathbf{R}}^{\text{in}}$, which induces a $\delta_{in} \rightarrow \delta_{in} + \pi$ for all $i < n$. The $\theta_{n-1, n} \rightarrow \theta_{n-1, n} + \pi$ is absorbed by a separate

$\nu_{\alpha_{n-1}} \rightarrow -\nu_{\alpha_{n-1}}, \nu_{\alpha_n} \rightarrow -\nu_{\alpha_n}$ transformation. Hence, I see that the invariance of U_{n-1}^\dagger is preserved, provided each δ_{in} occupy its full physical range of 2π .

2.2. Nonstandard Interactions

Many conclusions derived in the previous sections will be modified when nonstandard neutrino interactions are introduced into the SM Lagrangian of Eq. (2.1). These can take the form of lepton number conserving interactions given by

$$\mathcal{L}_{NS}^{LNC} = \xi_{\alpha\beta}^n \bar{\nu}_\alpha \gamma_\mu \nu_\beta Z'^\mu + \xi_{\alpha\beta}^c \bar{\nu}_\alpha \gamma_\mu \ell_\beta W'^\mu + \text{h.c.} \quad (2.22)$$

and lepton number violating interactions such as

$$\mathcal{L}_{NS}^{LNV} = \eta_{\alpha\beta}^n \bar{\nu}_\alpha^c \nu_\beta S_n + \eta_{\alpha\beta}^c \bar{\nu}_\alpha^c \ell_\beta S_c + \text{h.c.} \quad (2.23)$$

Here, each line contains a neutral current type and charged current type interaction denoted by the superscripts on the coupling constants ξ and η . To be concrete, these are written in terms of renormalizable expressions where neutrinos couple to vectors Z' and W' , as well as charged and neutral scalars denoted by S_c and S_n , respectively. All that is needed for my purpose is the neutrino structure, so one may substitute a general fermion current in place of the bosons to yield effective operators if desired. All four of the couplings listed are general complex matrices in flavor space defined by the flavor subscripts α and β . These are not diagonal in either the flavor or mass basis. I point out that terms in Eq. (2.23) violate lepton number by two units and as such, will themselves lead to radiatively generated Majorana neutrino masses at some order in perturbation

theory [1]. If this is the dominant source of neutrino masses generation, $\eta^{n(c)}$ would then be approximately aligned with the mass basis.

Upon transforming to the mass basis with the unitary matrix U , I find that the coupling constants shift to

$$\begin{aligned}
 \xi^n &\rightarrow U^\dagger \xi^n U & (2.24) \\
 \xi^c &\rightarrow U^\dagger \xi^n \\
 \eta^n &\rightarrow U^T \eta^n U \\
 \eta^c &\rightarrow U^T \eta^n.
 \end{aligned}$$

Using the invariance condition $U^\dagger \rightarrow \mathbf{N}_m U^\dagger \mathbf{N}_f$ as before, I search for the symmetries of these interactions. First, by recalling that both \mathbf{N} matrices are Hermitian, it is clear that both the lepton number violating and conserving interactions yield the same conditions, so it is enough to discuss the transformation of ξ . For the neutral current term I want $\mathbf{N}_m U^\dagger \mathbf{N}_f \xi^n \mathbf{N}_f U \mathbf{N}_m = U^\dagger \xi^n U$ up to field sign redefinitions which can clearly absorb the \mathbf{N}_m factors. Thus, a given symmetry of the mixing matrix is also a symmetry of neutral current nonstandard interactions if the resulting \mathbf{N}_f commutes with ξ^n . Since \mathbf{N}_f is some product of $\mathbf{P}^{a_i}(\pi)$, for some set of integers a_i , this translates to the condition that $\xi_{a_i j}^n = \xi_{j a_i}^n = 0$ for all $j \neq a_i$. The charged current case is even less restrictive in that all that is required is $\mathbf{N}_m U^\dagger \mathbf{N}_f \xi^c = U^\dagger \xi^n$ up to field sign redefinitions. Here, this reduces to $\mathbf{N}_f \xi^c = \xi^c \mathbf{N}_f'$, where \mathbf{N}_f' is some other product of $\mathbf{P}^{b_i}(\pi)$. In component form, this translates to the condition that for each b_i there exists a c_i such that $\xi_{b_i, j}^c = 0$ for all $j \neq c_i$ and $\xi_{k, c_i}^c = 0$ for all $k \neq b_i$. This is a much looser set of conditions than for the

neutral current case. I point out that any symmetries of the mixing matrix broken by the nonstandard interactions may be restored by allowing for coupling constant sign changes of the form $\xi^n \rightarrow \mathbf{N}_f \xi^n \mathbf{N}_f$ or $\xi^c \rightarrow \mathbf{N}_f \xi^c$.

In terms of the specific symmetries found in Section 2.1, I see that most parameter limitations still hold in the face of general new physics. These are transformations whose \mathbf{N}_f may be commuted and absorbed entirely into a redefinition of the mass eigenstates. In particular, within the n neutrino scenario, the invariance involving $\theta_{a-1,a} \rightarrow -\theta_{a-1,a}$ is broken while the following symmetries still hold:

- (1) $\phi_i \rightarrow \phi_i + \pi, \nu_i \rightarrow -\nu_i$ for all integers $1 \leq i$.
- (2) $\theta_{ij} \rightarrow -\theta_{ij}, \delta_{ij} \rightarrow \delta_{ij} + \pi$ for all integers $i \neq j - 1$.
- (3) $\theta_{ij} \rightarrow \theta_{ij} + \pi, \theta_{i,i+1} \rightarrow -\theta_{i,i+1}, \theta_{ia} \rightarrow -\theta_{ia}, \theta_{bj} \rightarrow -\theta_{bj}, \nu_i \rightarrow -\nu_i, \nu_j \rightarrow -\nu_j$ for all integers $b < i$ and $i + 1 < a < j$.

In the last entry the $\theta_{i,i+1} \rightarrow -\theta_{i,i+1}$ transformation is factored out of the other operations, as it may not be independently addressed by another unbroken symmetry. Therefore, in the case where the $\theta_{i,i+1}$ positive-negative symmetry is broken, one must choose which degeneracy to exploit when limiting the parameter space. In either case, this leads to an expanded mixing angle range $\theta_{ij} \in [-\pi/2, \pi/2]$. This occurs when the nonstandard interactions, written in the flavor basis, have a structure where there exists at least one nondiagonal ξ^n entry in each of the i^{th} and $(i + 1)^{\text{th}}$ row or column for the neutral current case. The situation is similar for charged current new terms, except that here one must have a nondiagonal ξ^n entry in both the i^{th} and $(i + 1)^{\text{th}}$ rows, or at least one in each column.

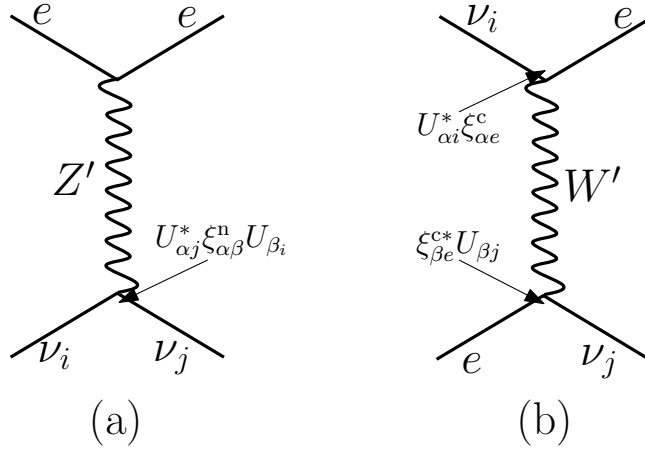


Figure 2.2. Neutrino electron quasi-elastic scattering diagrams via the exchange of massive W' and Z' vector bosons.

It is useful to explore this result with examples taken from the two neutrino scenario. Of course many processes may be used to illustrate these points, but for simplicity, I focus on neutrino electron scattering $\nu_i e \rightarrow \nu_j e$. The Standard Model contribution to this via t-channel Z and W exchange is easy to understand and is responsible for coherent forward neutrino scattering in dense media that leads to matter effects in neutrino oscillations. For this, one may subtract the diagonal Z couplings from the effective matter potential as a common factor and consider only the charged current interactions. In a similar way, nonstandard neutrino couplings will modify matter affected neutrino oscillations. One may calculate the modified probabilities, but for my purpose it is enough to simply consider the relative amplitudes. I consider the SM contributions as well as new neutral and charged current interactions mediated by Z' and W' , respectively. The relevant diagrams are shown in Figure 2.2 along with explicitly labeled vertex couplings. In this example, I assume that new physics has nonzero coupling to first generation charged

leptons, but this is not a general requirement. The amplitude for this process is

$$\mathcal{A}_{ij} = F_Z \delta_{ij} + F_W U_{ie}^* U_{ej} + F_{Z'} U_{\alpha j}^* \xi_{\alpha\beta}^n U_{\beta i} + F_{W'} U_{\alpha i}^* \xi_{\alpha e}^c \xi_{\beta e}^{c*} U_{\beta j}, \quad (2.25)$$

where F_i is some function containing process-dependent kinematical factors and irrelevant coupling constants. For my purpose, it is enough to know that these functions are independent of neutrino mixing parameters and couplings. The full expression may be calculated within the context of a specific model if needed. I point out that all Majorana phase dependency washes out of this expression since it conserves lepton number. For illustrative purposes, I evaluate the $i = j = 1$ elastic scattering case since it has contributions from all four interaction types identifiable by their F_i factors. In component form, the amplitude is

$$\begin{aligned} \mathcal{A}_{11} = & F_Z + F_W \cos^2 \theta + \frac{1}{2} F_{Z'} (\xi_{ee}^n + \xi_{\mu\mu}^n + (\xi_{ee}^n - \xi_{\mu\mu}^n) \cos 2\theta - (\xi_{e\mu}^n + \xi_{\mu e}^n) \sin 2\theta) \\ & + F_{W'} (\xi_{ee}^c \cos \theta - \xi_{\mu e}^c \sin \theta)^2. \end{aligned} \quad (2.26)$$

I explore this term by term, beginning with the SM contributions. Clearly, the Z exchange terms do not effect the symmetry structure of neutrino mixing, but W mediation breaks the θ degeneracy between $[0, \pi/4]$ and $[\pi/2, \pi/2]$ due to the $\cos^2 \theta$ factor. This is the reason behind the physical interpretation of the Δm^2 sign discussed by example in Subsection 2.1.1. Moving to the new physics contrabutions I see that W' mediation maintains $\theta \rightarrow \theta + \pi$ while breaking the $\theta \rightarrow -\theta$ symmetry, unless compensated by a corresponding sign flip of the off diagonal coupling constant $\xi_{\mu e}^c$. The same is true for the Z' interaction which breaks $\theta \rightarrow -\theta$ unless $\xi_{e\mu}^n + \xi_{\mu e}^n \rightarrow -(\xi_{e\mu}^n + \xi_{\mu e}^n)$. Therefore, I see explicitly that

flavor off diagonal nonstandard interactions expand the physical mixing angle range to $\theta \in [-\pi/2, \pi/2]$, as expected.

2.3. Conclusions

I conclude with a brief summary of the key issues explored in this chapter. From exploiting the symmetries of the neutrino mixing matrix, I explore degeneracies within the neutrino parameter space. There is a significant amount of freedom in choosing the physical ranges of these quantities and care must be taken to ensure consistent analysis of neutrino data. This is particularly true when comparing the results of experiments that rely on different “physical” parameter combinations as in, for example, lepton number violating and lepton number conserving phenomena where Majorana neutrino phases are physical and non-physical, respectively. With this in mind, it is best to choose a parameter scheme and stick with it. Following the majority of the literature, I chose to restrict all Majorana phases $\phi_i \in [-\pi/2, \pi/2]$, Dirac phases $\delta_{ij} \in [0, 2\pi]$, and mixing angles $\theta_{ij} \in [0, \pi/2]$ for the remainder of this thesis. Such a convention can accommodate all of the physics of neutrino mixing, assuming SM interactions. Interestingly, this also holds in the case of arbitrary BSM effects, provided that some select new physics coupling constants are allowed to take on both positive and negative values.

CHAPTER 3

A Survey of Lepton Number Violation Via Effective Operators

As previously emphasized, the discovery of neutrino masses via their flavor oscillations over long baselines constitutes the first solid evidence of physics beyond the standard model (SM) of particle physics [14]. While this is an important first step toward a deeper understanding of nature, it poses many more questions than it answers. A number of theoretically well-motivated models have been proposed and explored to address the origin of the neutrino mass but, strictly speaking, these represent only a handful out of an infinite set of possibilities. The question of how well future experiments can probe and distinguish different scenarios arises naturally and is quite relevant given the current state of high energy physics. The coming years promise detailed explorations of the terascale with the Large Hadron Collider (LHC) and the more distant International Linear Collider (ILC) or variants thereof. Expectations are that combined information from these two facilities, coupled with high precision, low energy results and cosmological observations will shed light on some of the current mysteries of physics, including that of the neutrino mass.

Here, I concentrate on the possibility that the neutrino masses are generated at some high energy scale Λ where $U(1)_{B-L}$, the only non-anomalous global symmetry of the standard model, is broken. Such a scenario is well-motivated by the observed properties of the light neutrinos including tiny masses, large mixings and the fact that neutrinos are the only electrically neutral fundamental fermions. More specifically, once $U(1)_{B-L}$ is broken,

neutrinos are not protected from getting non-zero Majorana masses after electroweak symmetry breaking. On the other hand, since the renormalizable minimal standard model¹ preserves $U(1)_{B-L}$, $B - L$ breaking effects will only manifest themselves at low energies through higher dimensional operators. This being the case, one generically expects neutrino masses to be suppressed with respect to charged fermion masses by $(v/\Lambda)^n$, $n \geq 1$, where v is the Higgs boson vacuum expectation value.

By further assuming that all new degrees of freedom are much heavier than the weak scale, I am guaranteed that, regardless of the details of the new physics sector, all phenomena below the weak scale are described by irrelevant, higher dimensional operators. In this spirit, the observable consequences of all high energy models that lead to small Majorana neutrino masses can be catalogued by understanding the consequences of irrelevant operators that break $B - L$ by two units. With this in mind, I will survey all such non-renormalizable effective operators for phenomenological signatures at future and current experiments. I restrict myself to operators that will lead to lepton number violation (LNV), as these will be directly connected to the existence of small Majorana neutrino masses. This means that I do not consider operators that conserve L but violate B , and hence also $B - L$, by two units (such operators lead to, for example, neutron–antineutron oscillations), nor do I include operators that respect $B - L$. Most of the time, the latter will not mediate any observable consequences for large enough Λ , except for operators of dimension-six and above that can mediate proton decay.

¹Throughout, I will assume that the weak scale degrees of freedoms are the known standard model fields, plus a minimal Higgs sector. Hence, I assume that there are no gauge singlet “right-handed neutrino” fermions or higher $SU(2)_L$ Higgs boson representations, such as Higgs boson triplets.

To begin, I systematically name and classify all relevant LNV operators. Fortunately, this has already been done² in [15] up to and including operators of mass dimension eleven.³ For each operator I then calculate/estimate the analytic form of the radiatively generated neutrino mass matrix. Upon setting this expression equal to the experimentally measured neutrino masses, I extract the energy scale Λ associated to the new LNV physics. Armed with these scales, I proceed to calculate each operator’s phenomenological signatures at a variety of experimental settings. Additionally, having explicitly calculated the operator-induced neutrino mass *matrices*, I may also verify, under some generic assumptions, whether one can account for the observable lepton mixing pattern. After such a general survey, one is adequately equipped to take a step back and select phenomenologically/theoretically interesting operators for further detailed study by “expanding” effective vertices to reveal particular ultraviolet completions. In this way, one can use the results presented here as a means of systematically generating renormalizable models with well-defined experimental predictions.

This chapter is organized as follows. Sec. 3.1 is devoted to an introduction to the effective operators and methods. In Sec. 3.1.1, I derive and comment on the scales Λ of new physics that are used throughout the remainder of the text. In Sec. 3.2, I survey various experimental probes of LNV for each operator, and address if and when our analysis breaks

²The authors of [15] discuss all possible effective operators of dimensions up to and including eleven, but only explicitly list those deemed unique in the sense that they cannot be written as the product of any previous operator with a Standard Model interaction. I append their list and naming scheme to include these into our analysis.

³I will argue later that irrelevant operators with mass dimension thirteen and higher, if related to neutrino masses, will require new physics below the electroweak scale so that I would have already observed new physics if neutrino masses were generated in this way. Furthermore, from a model building perspective, it is difficult to develop models that predominantly yield effective operators of very high mass dimension. The probability that such scenarios are both theoretically well-motivated and evade all observations appears to be slim.

down due to added model structure or additional assumptions. Specifically, I study both current constraints and future prospects for neutrinoless double-beta decay experiments in Sec. 3.2.1, followed, in Sec. 3.2.2, by a similar analysis of other rare decay modes, including those of various mesons and W/Z gauge bosons. In Sec. 3.2.3, I present collider signatures of LNV as they apply to future linear collider facilities running in the e^-e^- collision mode, and describe extensions of our analysis to include associated $\gamma\gamma$ collisions. I also comment on searches for LNV in future hadron machines. Sec. 3.3 describes current constraints from neutrino oscillation phenomenology due to the general structure of the derived neutrino mass matrices. In Sec. 3.4, I highlight a number of “interesting” operators, defined by low cutoff scales and prominence of experimental signatures, which are still allowed by current constraints on LNV. I undertake a slightly more detailed discussion of their characteristics and signatures and present some sample ultraviolet completions. I conclude in Sec. 3.5 with a summary of our assumptions and results, augmented by commentary on future prospects for LNV searches. Our results are tabulated by operator name in Table 3.1 for easy reference.

I hope that this analysis will prove useful to various audiences on a number of distinct levels. In the most superficial sense, the casual reader should note the general features of LNV as well as the diversity of model variations. Such information is best expressed in terms of the operator distribution histograms scattered throughout the text. These are color-coded by operator dimension or cutoff scale, and typically contain additional information, including current experimental prospects. On the more technical side, those interested in specific neutrino mass generating models will find detailed, operator specific, information that may be utilized as crude model predictions. Additionally, as already

alluded to, one may even “hand-pick” operators for model development based on specific phenomenological criteria. Finally, I urge experimentalists to search for new physics in all accessible channels. It is our ultimate goal to provide motivation for experimental considerations of non-standard LNV effects, beyond neutrinoless double-beta decay.

3.1. The lepton number violating scale

Here I analyze $SU(3)_c \times SU(2)_L \times U(1)_Y$ invariant $\Delta L = 2$ non-renormalizable effective operators of mass dimension up to and including eleven. They are composed of only the SM field content as all other, presumably heavy, degrees of freedom are integrated out. As already emphasized, I do not allow for the existence of SM singlet states (right-handed neutrinos) or any other “enablers” of renormalizable neutrino masses, such as Higgs $SU(2)_L$ triplet states. I therefore assume that all lepton number violation originates from new ultraviolet physics and that neutrino masses are generated at some order in perturbation theory.

A d -dimensional operator \mathcal{O}^d is suppressed by $d - 4$ powers of a mass scale Λ that characterizes the new physics, in addition to a dimensionless coupling constant λ :

$$\mathcal{L} \in \sum_i \frac{\lambda_i \mathcal{O}_i^d}{\Lambda^{d-4}}, \quad (3.1)$$

where I sum over all possible flavor combinations that make up the same “operator-type,” as defined below. For each operator, Λ/λ is approximately the maximum energy scale below which the new perturbative ultraviolet physics is guaranteed to reside, and Λ is used as a hard momentum cutoff in the effective field theory. Among all d -dimensional

operators, I define Λ so that the largest dimensionless coupling λ is equal to unity. Unless otherwise noted, I will assume that all other λ are of order one.

In the first two columns of Table 3.1, I exhaustively enumerate all possible lepton number violating operators of mass dimension less than or equal to eleven. All together, this amounts to 129 different types of operators, most of which, 101 to be exact, are of dimension eleven and consist of six fermion and two Higgs fields. Remaining are 21, 6 and 1 operator of dimension nine, seven, and five, respectively. The dimension-nine operators can be of two different kinds, as defined by their respective field content. They either contain four fermion and three Higgs fields or simply six fermion fields with no Higgs field content. For consistency, I use the notation of reference [15], where such a listing was first introduced. Our operator naming scheme is also derived from the same list, which I trivially extend to include 21 elements only mentioned in that analysis. These are the dimension-nine and dimension-eleven LNV operators that can be constructed from the “product” of the previously listed dimension-five and dimension-seven operators with the SM Yukawa interactions. I individually identify those operators with the same field content but different $SU(2)_L$ gauge structure with an additional roman character subscript added onto the original designation from [15]. This is done in order to render our discussion of the various operators clearer, since specific gauge structures can play an important role in the derived energy scale and predictions of a given operator. Note that I neglect effective operators that contain SM gauge fields, since, as argued in [15], these are not typically generated by renormalizable models of new physics.

Our notation is as follows.

$$L = \begin{pmatrix} \nu_L \\ e_L \end{pmatrix} \text{ and } Q = \begin{pmatrix} u_L \\ d_L \end{pmatrix} \quad (3.2)$$

are the left-handed lepton and quark $SU(2)_L$ doublets, respectively. e^c , u^c and d^c are the charge-conjugate of the $SU(2)_L$ singlet right-handed charged lepton and quark fermion operators, respectively. Conjugate fields are denoted with the usual “bar” notation (\bar{L} , \bar{Q} , \bar{e}^c). For simplicity, I am omitting flavor indices, but it is understood that each matter fermion field comes in three flavors. All matter fields defined above are to be understood as flavor eigenstates: all SM gauge interactions, including those of the W -boson, are diagonal. Without loss of generality, I will also define the L and e^c fields so that the charged-lepton Yukawa interactions are flavor-diagonal.

I take the $SU(2)_L$ doublet Higgs scalar to be

$$H = \begin{pmatrix} H^+ \\ H^0 \end{pmatrix}, \quad (3.3)$$

and assume that, after electroweak symmetry breaking, its neutral component acquires a vacuum expectation value (vev) of magnitude $v \approx 0.174$ TeV,¹ thus spontaneously breaking the electroweak gauge symmetry $SU(2)_L \times U(1)_Y \rightarrow U(1)_{\text{em}}$. In Table 3.1, the components of the $SU(2)_L$ doublets are explicitly listed and labeled with $i, j, k, \dots = 1, 2$. In order to form gauge singlets, operators are contracted either by the antisymmetric tensor ϵ_{ij} , defined such that $\epsilon_{12} = 1$, or by trivial contractions with a conjugate doublet

¹Our numerical value for v is distinct from many treatments of the SM where v is taken to be 0.246 TeV. These are equivalent up to a factor of $\sqrt{2}$ and are both valid provided a consistent treatment of the interaction Lagrangian.

field. Different gauge contractions are partially responsible for the wide variety of operator structures encountered in this study.

In order to avoid unnecessarily messy expressions, several features are missing from the operators as listed in Table 3.1. To begin, $SU(3)_c$ color indices are suppressed in these expressions. Color contractions are only implied here because $SU(3)_c$ is an unbroken symmetry of the SM and hence there is no sense in distinguishing the various quark field components. I assume that the parent ultraviolet completion to each operator treats the color gauge symmetry properly by introducing appropriately chosen heavy colored particles to render the theory gauge invariant. Slightly more serious is the omission of flavor indices to label the fermion generations. For most of this analysis, I assume that all new physics effects are generation universal and thus, flavor independent. This is not guaranteed to be the case, as is painfully obvious within the SM. One will also note that, depending on the $SU(2)$ structure of the effective operator, different flavor-dependent coefficients will be strictly related. For example, including flavor dependent couplings $\lambda_{\alpha\beta}^1$, \mathcal{O}_1 should read $\lambda_{\alpha\beta}^1 L_\alpha^i L_\beta^j H^k H^l \epsilon_{ik} \epsilon_{jl}$, where $\lambda_{\alpha\beta}^1 = \lambda_{\beta\alpha}^1$ (symmetric) for all $\alpha, \beta = e, \mu, \tau$. On the other hand, \mathcal{O}_{3a} should read (for fixed Q and d^c flavors) $\lambda_{\alpha\beta}^{3a} L_\alpha^i L_\beta^j Q^k d^c H^l \epsilon_{ij} \epsilon_{kl}$, where $\lambda_{\alpha\beta}^{3a} = -\lambda_{\beta\alpha}^{3a}$ (antisymmetric) for all $\alpha, \beta = e, \mu, \tau$. Large differences among the various flavor structures of each operator may very well exist. Flavor is an important facet of LNV phenomenology, and is addressed where relevant within the text.

The final feature missing from our notation is explicit Lorentz structure. Each operator must, of course, form a Lorentz scalar, but there are numerous field configurations that can bring this about. The Higgs field is a scalar, and as such, transforms trivially under the Lorentz group and is thus of no relevance to this discussion. The fermions, however,

transform non-trivially and their contractions must be accounted for in each operator. Simple combinatorics dictate that there are at most 45 such possibilities for the six-fermion operators that comprise the bulk of our sample, 3 in the four-fermion case and only 1 for the lone dimension five operator. Additionally, each contraction can be made in a variety of ways, corresponding to the bilinear Dirac operators $\mathbf{1}$, γ^μ and $\sigma^{\mu\nu} = \frac{i}{2}[\gamma^\mu, \gamma^\nu]$ of the scalar, vector and tensor types, respectively. Since I am dealing with chiral fields, the addition of the γ_5 matrix to form the pseudoscalar and axial-vector bilinears is redundant. While this helps reduce the number of possibilities, the task of listing, categorizing, and analyzing all possible Lorentz structures for each operator is still quite overwhelming and is not undertaken in this general survey. Fortunately, different Lorentz structures for the same operator-type lead to the same predictions up to order one effects. This is especially true for the “interesting” operators characterized by TeV Λ scales. I shall quantify this statement and mention specific structures when relevant. That being said, the Lorentz structure of an effective operator can suggest a lot of information about its parent renormalizable model. For example, it can suggest the spin of the heavy intermediate states and the forms of various vertices.

Armed with these operators, I can calculate the amplitude of any $\Delta L = 2$ LNV process. It is important to emphasize that when addressing the phenomenological consequences of any particular operator \mathcal{O} , I assume that it characterizes the dominant tree-level effect of the new heavy physics, and that all other effects – also characterized by other LNV effective operators of lower mass dimension – occur at higher orders in perturbation theory. Our approach is purely diagrammatic, in that I begin with an operator-defined vertex and then proceed to close loops and add SM interactions as needed to yield the correct external

state particles. In this sense, special care must be taken to respect the chiral structure as defined by each operator. In order to reach the intended external states, to couple to particular gauge bosons, or to close fermion loops, one must often induce a helicity flip with a SM mass insertion. I express these inserted fermion masses in terms of the respective Yukawa couplings, y_f ($f = \ell, u, d$) and the Higgs vev, v . The Higgs field can be incorporated into this procedure in a number of ways. I treat the two charged and single neutral Nambu-Goldstone Higgs bosons, H^\pm and H^0 , respectively, within the Feynman-'t Hooft gauge as propagating degrees of freedom with electroweak scale masses. The physical neutral Higgs, h_0 , can be either chosen to propagate as a virtual intermediate state, or couple to the vacuum with amplitude v .

In order to avoid the task of explicitly evaluating a huge number of multiloop Feynman diagrams, I succumb to approximate LNV amplitudes based on reasonable assumptions and well-motivated rules. Our methodology is motivated by exact computations with one-loop, dimension 7 operators where the work is analytically tractable, as well as on general theoretical grounds. For select operators, I have also checked our assumptions against predictions from ultraviolet complete models with success. In order to perform a particular calculation, I draw the appropriate diagram(s), taking care that no momentum loop integral vanishes by symmetry reasons. This step is potentially quite involved, as multiple diagrams can give sizable amplitude contributions depending on the characteristic energy transfer in the system, not to mention the cumbersome Dirac algebra within the respective loops. Given the high, often super-TeV, mass scale associated with our calculations, it is often convenient to work in the gauge field basis where each boson state

is associated with a single SM group generator, as is natural before electroweak symmetry breaking. In a similar sense, all fermions, including those of the third generation, are taken to be massless to zeroth order. All masses are included perturbatively where needed via mass insertions. At first guess, it would seem that our results are only valid in the rather subjective limit $\Lambda \gg v$. By direct comparison with other more complete approximations, however, I find that our predictions are very reasonable at all scales above 0.5 TeV. Keeping all of this in mind, I apply the following “rules” to obtain approximate amplitude expressions.

- (1) *Trivial numerical factors*: A number of numerical factors can be read off trivially from the Feynman diagrams. Specifically, one can extract the presence of the suppression scale $\Lambda^{-(d-4)}$ directly from the dimension d operator, as well as the dimensionless coupling constants λ . Generally, λ is a generation dependent quantity, but for lack of any experimental evidence to the contrary, I take $\lambda = 1$ universally unless stated otherwise. In the case of scenarios already constrained by current data, I will relax this assumption to “save” the operator and comment on the phenomenological consequences of the change.

Furthermore, various factors of the electroweak scale v may be extracted from the operator’s Higgs field content, in addition to fermion/gauge boson mass terms. In this way, I may also include the various Yukawa and gauge coupling factors y_f ($f = \ell, u, d$) and g_i , respectively, where i runs over the three SM gauge groups. For simplicity, I neglect the gauge subscript i in further analytic expressions. Finally, a color factor of 3 associated with each quark loop should also be included in our computations, but can (and will) be neglected for simplicity

from algebraic expressions where order one factors are irrelevant and only serve to render expressions more cumbersome. I note that all coupling constants are subject to renormalization group running. In particular, those occurring within a loop should be evaluated at the scale Λ . I neglect this order one effect since it is most important at large Λ scales where operators tend to have less of a phenomenological impact due to the $(1/\Lambda)^n$ suppression.

- (2) *Loop factors:* In all of our calculations, I assume that each operator defines an effective field theory, characterized by the scale Λ . This implies that all momentum integrals are effectively cut off at Λ , above which new states will emerge to regularize the theory. Divergences in such loops tend to cancel the large scale suppressions inherent to the bare operators, and thus enhance predicted LNV rates. Specific divergences can be determined by simple power counting of momentum factors. Of course, multiple loop integrals are often convoluted to the point where substantial simplification is needed to determine the dominant divergent term. Such a complication is in part due to the numerator of the Dirac propagators, which include single momentum factors and must therefore be present in pairs to contribute effectively to an ultraviolet divergence. The process of adding loops to induce Λ power law divergences should only be pursued to the point where the suppression of the induced effective term is no less than Λ^{-1} . Any further divergent contribution must be treated as a renormalization to lower order terms, and hence, can only add small finite corrections to the total amplitude. In any case, those diagrams with the smallest scale suppressions are

not always the most dominant, as will become clear later when I discuss specific results.

In addition to power-law divergences, each loop is also associated with a numerical suppression factor. This arises from the proper normalization of the loop four-momentum integral as a factor of $(2\pi)^{-4}$, the characteristic phase space “volume” of a quantum state. It allows one to view the integral as a coherent sum over all possible intermediate configurations in a consistent way. Partially evaluating these integrals for a number of examples, one quickly finds that two powers of π cancel with the four dimensional Euclidian space solid angle $\int d\Omega_4$. I introduce a suppression factor of $(16\pi^2)^{-1} \sim 0.0063$ for each diagram loop, which tends to offset enhancements from associated divergent factors. A quadratically divergent loop diagram is often proportional to the lowest order contribution times $(1/16\pi^2)(\Lambda/v)^2$ to the power n (number of loops in the diagram). This contribution is larger than the leading order one if $\Lambda > 4\pi v \sim 2$ TeV for any number of loops. The situation is often more involved, as many loops turn out to be logarithmically divergent or even convergent. The important conclusion is that adding loops is not an efficient way to enhance LNV rates at the low scales accessible to future experiments. This fact is demonstrated by example in Sec. 3.2.

Finally, as already alluded to, many diagram loops will exhibit logarithmic divergences, as is the standard case in renormalizable theories involving fermion and vector fields. This occurrence typically reflects the differences between the two characteristic scales inherent to the system, namely Λ and v , and are of

the general form $\xi \log^n(\Lambda/v)$ for some power n . ξ is a small, loop suppressed, dimensionless coupling coefficient. Numerically, these logarithms are much softer than their quadratically divergent counterparts seen elsewhere in the diagrams and can safely be neglected.

- (3) *Intermediate states*: I treat all virtual intermediate states, outside of loops, as if they carry the characteristic momentum of the interaction Q and neglect Dirac structure, unless stated otherwise. In particular, goldstone bosons are assigned the propagator $(Q^2 - M_g^2)^{-1}$ and fermions are assigned $(Q - M_f)^{-1}$. In the case of an intermediate neutrino, this reduces to a simple factor of Q^{-1} for all realistic Q values. Hence, for very low energy processes ($Q \ll 100$ MeV), neutrino exchange diagrams tend to dominate LNV rates.
- (4) *Lorentz structure*: For the purposes of our analysis, I assume that all Lorentz contractions between fermions are scalar-like. As previously mentioned, the absolute magnitude of most LNV amplitudes is robust under this assumption up to order one factors. The only qualitative exception to this occurs in some cases involving fermion bilinear terms with a tensor Lorentz structure $(\bar{\psi}' \sigma_{\mu\nu} \psi)$. This factor, when coupled between two fermions contracted in a loop, will yield a vanishing rate due to its antisymmetry inside of a trace, since $Tr(\sigma_{\mu\nu}) = 0$. This can be bypassed by introducing a new momentum vector into the trace, implying the addition of another loop. In most cases, this is most efficiently accomplished with a new gauge boson line, which is accompanied by a logarithmic divergence. The combination of both factors leads to a marginal amplitude suppression (with

respect to the same operator where all fermion bilinears are Lorentz scalars) for all energies of interest.

With these approximations in hand, it is a simple matter to estimate the amplitude associated to any given diagram. Still, one must wonder about the uncertainty induced onto the calculations by such varied assumptions. Can results obtained by such methods supply valid physical predictions? The answer, of course, depends on the question that is being asked. Here, I will only be interested in estimating order of magnitude effects, including what value of Λ is required in order to explain the observed neutrino masses and, once Λ is so constrained, what is the order of magnitude of other related observable effects.

One may wonder whether a more detailed estimate of the effects of each individual operator would lead to more reliable results. The answer is negative. It is easy to show that different renormalizable theories that lead to the same effective operator at tree-level will mediate different processes at the loop-level with order one different relative strengths. Furthermore, the derived cutoff scales inherit the uncertainty from the absolute value of the heaviest neutrino mass, which is only loosely bounded between 0.05 eV and 1 eV by the extracted atmospheric mass squared difference [16] and tritium beta decay kinematic measurements [17, 18]. This is an order of magnitude uncertainty that cannot be avoided even if one were to perform a detailed computation within a well-defined ultraviolet complete theory.

In summary, given all approximations and uncertainties, our results are only valid up to \pm an order of magnitude. In this spirit, one need not explicitly consider order one factors that will necessarily yield negligible corrections by these standards. Such a large

error tolerance supplies the need for care when interpreting results. In particular, one should not place too much emphasis on any one bound or prediction, unless it is very robust, *i.e.*, able to withstand variations of at least a factor of ten. Of course, for those operators constrained by several different independent sources one can, and should, take more marginal results seriously.

3.1.1. Neutrino Masses and the Scale of New Physics

Having defined the set of LNV operators, I now extract the scale of new physics from the direct comparison of radiatively generated neutrino mass expressions to their observed values. Since there are three light neutrino masses, I will use the heaviest of these to set the overall mass scale. Neutrino oscillation data, currently providing the only evidence for neutrino masses, constrain the relative magnitudes of the mass eigenstates but not the overall scale [14]. Such data only supply a lower bound on the heaviest neutrino mass, derived from the largest observed mass squared difference $\Delta m_{13}^2 = |m_3^2 - m_1^2| \approx 0.0025 \text{ eV}^2$, the atmospheric mass squared difference [16]. At least one neutrino mass must be greater than $\sqrt{\Delta m_{13}^2} \approx 0.05 \text{ eV}$. Neutrino oscillations also teach us that the next-to-heaviest neutrino weighs at least $\sqrt{\Delta m_{12}^2} \approx 0.009 \text{ eV}$ (the solar mass-squared difference), in such a way that the ratio of the heaviest to the next-to-heaviest neutrino masses is guaranteed to be larger than, approximately, 0.2. No lower bounds can be placed on the lightest neutrino mass. An upper bound on the heaviest neutrino mass is provided by several non-oscillation neutrino probes. Cosmology provides interesting constraints on the sum of light neutrino masses, but these are quite dependent on unconfirmed details of the thermal history of the universe and its composition [19, 20, 21, 22]. Most direct are

kinematic measurements of the tritium beta decay electron endpoint spectrum [23]. Both types of probes provide upper bounds near 1 eV, likely to improve in coming years. I choose to perform our calculations assuming the mass scale $m_\nu \approx 0.05$ eV, corresponding to the experimental lower bound. In this way, each extracted operator scale Λ , inversely related to the neutrino mass, represents a loose upper bound. Since most rates for LNV observables are proportional to some inverse power of Λ , this choice implies the added interpretation that, all else remaining equal, our results for such rates should conservatively reflect lower limit predictions.

LNV neutrino masses are nothing more than self-energy diagrams evaluated at vanishing momentum transfer. These must couple together the left-handed neutrino state ν_α with the right-handed anti-neutrino state ν_β , as shown schematically in diagram (a) of Fig. 3.1. Here the flavor indices α and β can accommodate any of the three lepton flavors ($\alpha, \beta = e, \mu, \tau$). The derived Majorana masses $m_{\alpha\beta} = m_{\beta\alpha}$ are generally complex. The large grey circle in this diagram represents all possible contributions to the neutrino mass. Specifically, it contains the underlying $\Delta L = 2$ operator along with all modifications needed to yield the correct external state structure. This includes such objects as loops, additional gauge boson propagators and SM coupling constants. Generally, several diagrams can contribute to this mass generation, but special care must be taken that these are not proportional to any positive power of Q , the momentum carried by the neutrino legs, as this would not lead to a nonzero rest mass correction.

Diagrams (b)–(e) of Fig. 3.1 are examples that serve to illustrate some typical features encountered in our effective operator induced self-energy calculations. The underlying LNV operators shown in each diagram contain six fermion fields and are therefore of

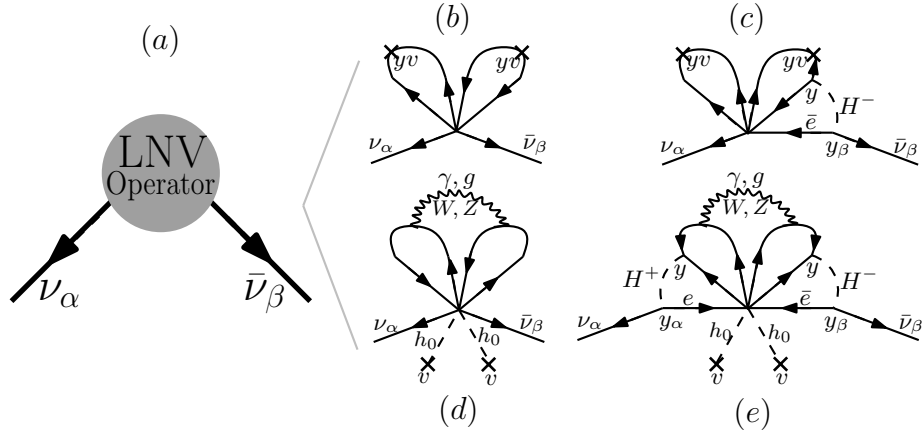


Figure 3.1. Sample diagrams that radiatively generate Majorana neutrino masses. Diagram (a) is representative of all operators that can generate the needed external state neutrinos. This usually proceeds via loop contractions and other couplings, hidden within the light gray region. Diagrams (b) – (e) help illustrate the methodology of this analysis. Despite obvious differences, all of these generate effective dimension-five interactions of calculable strength. See the text for more details.

dimension nine or eleven, as are the majority of the analyzed operators. Each of these diagrams generates an effective dimension-five interaction

$$\mathcal{L}_5 = \xi_{\alpha\beta}^{(5)} \frac{(L^\alpha H)(L^\beta H)}{\Lambda}, \quad (3.4)$$

where $\xi_{\alpha\beta}^{(5)} = \xi_{\beta\alpha}^{(5)}$ is a generation dependent coupling constant that is calculable, given the structure of the original operator. This is easily verifiable via direct power counting, despite differences in dimension, loop number, field content, and helicity structure. It turns out that most operators, especially those characterized by super-TeV scales, possess this property.

I describe each sample diagram in turn to point out important features. A subset of the subtleties described below is encountered when estimating the neutrino masses $m_{\alpha\beta}$

for the entire effective operator set. Diagram (b) is a simple two-loop radiatively generated mass term proceeding from dimension-nine operators, such as $\mathcal{O}_{11b} = L^i L^j Q^k d^c Q^l d^c \epsilon_{ik} \epsilon_{jl}$, containing the fermion structure $f_L f_R^c f_L' f_R'^c$, where the fields f and f' are contracted into loops with mass insertions that supply the needed field chirality flip. Masses arising from such operators are proportional to two powers of fermion Yukawa couplings. Strictly speaking, allowed fermions from all three generations traverse the closed loops and contribute to the mass. However, assuming universal new physics coupling constants, third generation fermions will strongly dominate the induced neutrino mass. In cases such as these, one can freely suppress couplings to the lighter two generations without modifying the expected value of Λ . Since diagrams arising from the majority of our operator set contain at least one loop of this kind, this property proves quite useful when attempting to avoid low energy nuclear physics constraints, as will be discussed in more detail later.

Diagram (d) involves an operator of dimension eleven, such as $\mathcal{O}_{22} = L^i L^j L^k e^c \bar{L}_k \bar{e}^c H^l H^m \epsilon_{il} \epsilon_{jm}$, but has a similar structure to Diagram (b) since both neutral Higgs fields h_0 couple to the vacuum, yielding a v^2 factor. In this case, the parent underlying operators contain the fermion structure $f_{L(R)} f_{L(R)}^c f_{L(R)}' f_{L(R)}'^c$, or simple variants thereof. From this, it is clear that such operators will create and annihilate the *same* field and one can close the fermion loops without mass insertions. A little thought reveals that such loops, if left on their own, will vanish by symmetry, since $\int d^4k [k^\mu / g(k^2)] = 0$ for all functions $g(k^2)$. Hence, non-zero neutrino masses only appear at a higher order in perturbation theory (*i.e.*, I need to add another loop). To maintain the chiral structure of the diagram a gauge boson line insertion is always the most effective. The specific gauge field required in this step depends critically on the quantum numbers of the fermions f

and f' contained in the operator itself and must be determined on a case-by-case basis. The absence of Yukawa dependence renders the estimated value of the cutoff scale Λ insensitive to the values of the dimensionless operator couplings (λ), given the way Λ is defined. Notice that this three-loop diagram, like Diagram (b), predicts an anarchic neutrino Majorana mass matrix, currently allowed by the neutrino oscillation data [24]. That is, up to order one corrections, all entries are of the same magnitude, $m_\nu \approx 0.05$ eV. This is in contrast to the remaining sample diagrams ((c) and (e)), which both suggest flavor-structured mass matrices.

Dimension-nine operators, such as $\mathcal{O}_{19} = L^i Q^j d^c d^c \bar{e}^c \bar{u}^c \epsilon_{ij}$, yielding diagram (c) have the peculiar property that, upon expanding out the various $SU(2)_L$ contractions in terms of component fields, no $\nu_\alpha \nu_\beta$ content is present to form the external legs of a mass diagram. Here the LNV is introduced via the fermion structure $\nu_\alpha e_{R\beta}$, which annihilates a left-handed neutrino and creates a left-handed positron. Hence, to tie in the needed antineutrino line, one must both flip the charge lepton helicity and carry away the excess charge with some bosonic state. Of course, such a charged boson is guaranteed by charge conservation to be needed elsewhere in the system to close some f/f' loop. In this particular example, the process is illustrated by the exchange of a charged Higgs goldstone boson H^- to clearly visualize the chiral structure, but of course, one may equivalently think in terms of a transverse W^- boson. The crucial point is that this mass is necessarily proportional to a charged lepton Yukawa coupling y_{ℓ_β} , of the *same* flavor as the external neutrino, since I am working in the weak eigenbasis where the gauge couplings and the charged-lepton Yukawa couplings are flavor diagonal. By symmetry, the contribution to

the $m_{\alpha\beta}$ entry of the neutrino mass matrix is proportional to $y_{\ell_\alpha} + y_{\ell_\beta}$, which reduces to the largest coupling y_{ℓ_β} in the realistic case of hierarchial charged lepton Yukawa couplings.

Finally, Diagram (e) yields a five-loop suppressed neutrino self-energy originating from a dimension-eleven LNV operator such as $\mathcal{O}_{36} = \bar{e}^c \bar{e}^c Q^i d^c Q^j d^c H^k H^l \epsilon_{ik} \epsilon_{jl}$. This represents the most complicated structure considered in this analysis. As in Diagram (c), no explicit $\nu_\alpha \nu_\beta$ structure is available in the underlying operator, but in this case all of the LNV arises from $e_{R\alpha}^c e_{R\beta}^c$ -type interactions. Curiously, this interaction already flips helicity as it annihilates a left-handed positron and creates a right-handed electron. Unfortunately, being an $SU(2)_L$ singlet, e_R only couples to the neutrino via a charged Higgs induced Yukawa interaction; therefore, this amplitude must be proportional to the product $y_{\ell_\alpha} y_{\ell_\beta}$ to yield a legitimate neutrino mass contribution. One might imagine that the Higgs fields contained in the LNV operator could be used to produce the needed neutrino legs, but this is not possible since the resulting loop would have a structure of the form $\int d^4 k \frac{k^\mu + Q^\mu}{g(k^2)} \propto Q^\mu$ which vanishes in the “rest mass” limit. It is clear that both Higgs fields must again couple to the vacuum and the needed flip must come from the other fermion loops. The resulting loop integrals can be separated into two convoluted pieces corresponding to both loop/leg pairs. A little thought reveals that each loop set contains three fermion lines whose associated integral is again proportional to the momentum of the external neutrino, and thus is not a valid mass correction. To fix this last problem without further complicating the chiral structure, one can add a gauge boson exchange between the fermion loops, as was also done in Diagram (d).

Despite the dominance of the generated dimension-five interactions described by Eq. (3.4) for the majority of the studied LNV operators, I find that this need not be the case for all of

them. For some operators, the dimension-five neutrino-mass effective operator Eq. (3.4) occurs at higher order in perturbation theory than the dimension-seven neutrino-mass effective operator (schematically, $(LH)^2H^2$). For these, the neutrino mass matrix is generated after electroweak symmetry breaking from

$$\mathcal{L}_{57} = \frac{\xi_{\alpha\beta}^{(5)}}{16\pi^2} \frac{(LH)(LH)}{\Lambda} + \xi_{\alpha\beta}^{(7)} \frac{(LH)(LH)H\bar{H}}{\Lambda^3}, \quad (3.5)$$

where $\xi_{\alpha\beta}^{(7)}$ are new calculable coefficients. This type of structure is present in the following operators

$$\mathcal{O}_7, \mathcal{O}_{21_{a,b}}, \mathcal{O}_{22}, \mathcal{O}_{23}, \mathcal{O}_{25}, \mathcal{O}_{26_b}, \mathcal{O}_{27_b}, \mathcal{O}_{29_a}, \mathcal{O}_{30_b}, \mathcal{O}_{31}, \mathcal{O}_{44_c}, \mathcal{O}_{57}. \quad (3.6)$$

In general, they are associated with dimension-eleven operators² whose mass diagrams are found trivially by connecting the external fermion loops and coupling the neutral Higgs fields to the vacuum. This adds two factors of the electroweak scale to the mass expressions. Dimensional analysis dictates that the fermion loops must conspire to yield an addition factor of v^2 , usually from mass insertions utilized to flip helicities. For the dimension-seven operators in Eq. (3.5), the resulting neutrino mass expression is proportional to v^4/Λ^3 . If I assume, as is usually the case, that most of the dimensionless factors of Eq. (3.5) are common to both $\xi_{\alpha\beta}^{(5)}$ and $\xi_{\alpha\beta}^{(7)}$, I find $m_{\alpha\beta} \propto 1/16\pi^2 + v^2/\Lambda^2$. In such cases, the dimension-seven contribution is only relevant for operator cutoff scales $\Lambda \lesssim 4\pi v \approx 2$ TeV. Such low scales are seldom reached considering that these operators are efficient at mass generation at low orders and consequently do not possess the necessary suppression factors. Still, for completeness, I include these terms when relevant.

²This also occurs with operator \mathcal{O}_7 , which is of dimension nine. This operator is the exception, in that it explicitly contains three Higgs bosons which naturally aids in building the needed v^4 factors in a way similar to that discussed in the text.

Table 3.1: Dimension-five through dimension-eleven LNV operators analyzed in this survey. The first two columns display the operator name and field structure, respectively. Column three presents the induced neutrino mass expressions, followed by the inferred scale of new physics, Λ_ν . Column five lists favorable modes of experimental exploration. Column six describes an operator's current status according to the key U (Unconstrained), C (Constrained) and D (Disfavored). See text for details.

1	$L^i L^j H^k H^l \epsilon_{ik} \epsilon_{jl}$	$\frac{v^2}{\Lambda}$	6×10^{11}	$\beta\beta 0\nu$	U
2	$L^i L^j L^k e^c H^l \epsilon_{ij} \epsilon_{kl}$	$\frac{y_\ell}{16\pi^2} \frac{v^2}{\Lambda}$	4×10^7	$\beta\beta 0\nu$	U
3 _a	$L^i L^j Q^k d^c H^l \epsilon_{ij} \epsilon_{kl}$	$\frac{y_d g^2}{(16\pi^2)^2} \frac{v^2}{\Lambda}$	2×10^5	$\beta\beta 0\nu$	U
3 _b	$L^i L^j Q^k d^c H^l \epsilon_{ik} \epsilon_{jl}$	$\frac{y_d}{16\pi^2} \frac{v^2}{\Lambda}$	1×10^8	$\beta\beta 0\nu$	U
4 _a	$L^i L^j \bar{Q}_i \bar{u}^c H^k \epsilon_{jk}$	$\frac{y_u}{16\pi^2} \frac{v^2}{\Lambda}$	4×10^9	$\beta\beta 0\nu$	U
4 _b	$L^i L^j \bar{Q}_k \bar{u}^c H^k \epsilon_{ij}$	$\frac{y_u g^2}{(16\pi^2)^2} \frac{v^2}{\Lambda}$	6×10^6	$\beta\beta 0\nu$	U
5	$L^i L^j Q^k d^c H^l H^m \bar{H}_i \epsilon_{jl} \epsilon_{km}$	$\frac{y_d}{(16\pi^2)^2} \frac{v^2}{\Lambda}$	6×10^5	$\beta\beta 0\nu$	U
6	$L^i L^j \bar{Q}_k \bar{u}^c H^l H^k \bar{H}_i \epsilon_{jl}$	$\frac{y_u}{(16\pi^2)^2} \frac{v^2}{\Lambda}$	2×10^7	$\beta\beta 0\nu$	U
7	$L^i Q^j \bar{e}^c \bar{Q}_k H^k H^l H^m \epsilon_{il} \epsilon_{jm}$	$y_\ell y_\beta \frac{g^2}{(16\pi^2)^2} \frac{v^2}{\Lambda} \left(\frac{1}{16\pi^2} + \frac{v^2}{\Lambda^2} \right)$	4×10^2	mix	C
8	$L^i \bar{e}^c \bar{u}^c d^c H^j \epsilon_{ij}$	$y_\ell y_\beta \frac{y_d y_u}{(16\pi^2)^2} \frac{v^2}{\Lambda}$	6×10^3	mix	C
9	$L^i L^j L^k e^c L^l e^c \epsilon_{ij} \epsilon_{kl}$	$\frac{y_\ell^2}{(16\pi^2)^2} \frac{v^2}{\Lambda}$	3×10^3	$\beta\beta 0\nu$	U
10	$L^i L^j L^k e^c Q^l d^c \epsilon_{ij} \epsilon_{kl}$	$\frac{y_\ell y_d}{(16\pi^2)^2} \frac{v^2}{\Lambda}$	6×10^3	$\beta\beta 0\nu$	U
11 _a	$L^i L^j Q^k d^c Q^l d^c \epsilon_{ij} \epsilon_{kl}$	$\frac{y_d^2 g^2}{(16\pi^2)^3} \frac{v^2}{\Lambda}$	30	$\beta\beta 0\nu$	U
11 _b	$L^i L^j Q^k d^c Q^l d^c \epsilon_{ik} \epsilon_{jl}$	$\frac{y_d^2}{(16\pi^2)^2} \frac{v^2}{\Lambda}$	2×10^4	$\beta\beta 0\nu$	U
12 _a	$L^i L^j \bar{Q}_i \bar{u}^c \bar{Q}_j \bar{u}^c$	$\frac{y_u^2}{(16\pi^2)^2} \frac{v^2}{\Lambda}$	2×10^7	$\beta\beta 0\nu$	U
12 _b	$L^i L^j \bar{Q}_k \bar{u}^c \bar{Q}_l \bar{u}^c \epsilon_{ij} \epsilon^{kl}$	$\frac{y_u^2 g^2}{(16\pi^2)^3} \frac{v^2}{\Lambda}$	4×10^4	$\beta\beta 0\nu$	U
13	$L^i L^j \bar{Q}_i \bar{u}^c L^l e^c \epsilon_{jl}$	$\frac{y_\ell y_u}{(16\pi^2)^2} \frac{v^2}{\Lambda}$	2×10^5	$\beta\beta 0\nu$	U
14 _a	$L^i L^j \bar{Q}_k \bar{u}^c Q^k d^c \epsilon_{ij}$	$\frac{y_d y_u g^2}{(16\pi^2)^3} \frac{v^2}{\Lambda}$	1×10^3	$\beta\beta 0\nu$	U
14 _b	$L^i L^j \bar{Q}_i \bar{u}^c Q^l d^c \epsilon_{jl}$	$\frac{y_d y_u}{(16\pi^2)^2} \frac{v^2}{\Lambda}$	6×10^5	$\beta\beta 0\nu$	U
15	$L^i L^j L^k d^c \bar{L}_i \bar{u}^c \epsilon_{jk}$	$\frac{y_d y_u g^2}{(16\pi^2)^3} \frac{v^2}{\Lambda}$	1×10^3	$\beta\beta 0\nu$	U
16	$L^i L^j e^c d^c \bar{e}^c \bar{u}^c \epsilon_{ij}$	$\frac{y_d y_u g^4}{(16\pi^2)^4} \frac{v^2}{\Lambda}$	2	$\beta\beta 0\nu$, LHC	U
17	$L^i L^j d^c d^c \bar{d}^c \bar{u}^c \epsilon_{ij}$	$\frac{y_d y_u g^4}{(16\pi^2)^4} \frac{v^2}{\Lambda}$	2	$\beta\beta 0\nu$, LHC	U

\mathcal{O}	Operator	$m_{\alpha\beta}$	Λ_ν (TeV)	Best Probed	Disfavored
18	$L^i L^j d^c u^c \bar{u}^c \bar{u}^c \epsilon_{ij}$	$\frac{y_d y_u g^4}{(16\pi^2)^4} \frac{v^2}{\Lambda}$	2	$\beta\beta 0\nu$, LHC	U
19	$L^i Q^j d^c d^c \bar{e}^c \bar{u}^c \epsilon_{ij}$	$y_\ell y_\beta \frac{y_d^2 y_u}{(16\pi^2)^3} \frac{v^2}{\Lambda}$	1	$\beta\beta 0\nu$, HEInv, LHC, mix	C
20	$L^i d^c \bar{Q}_i \bar{u}^c \bar{e}^c \bar{u}^c$	$y_\ell y_\beta \frac{y_d y_u^2}{(16\pi^2)^3} \frac{v^2}{\Lambda}$	40	$\beta\beta 0\nu$, mix	C
21 _a	$L^i L^j L^k e^c Q^l u^c H^m H^n \epsilon_{ij} \epsilon_{km} \epsilon_{ln}$	$\frac{y_\ell y_u}{(16\pi^2)^2} \frac{v^2}{\Lambda} \left(\frac{1}{16\pi^2} + \frac{v^2}{\Lambda^2} \right)$	2×10^3	$\beta\beta 0\nu$	U
21 _b	$L^i L^j L^k e^c Q^l u^c H^m H^n \epsilon_{il} \epsilon_{jm} \epsilon_{kn}$	$\frac{y_\ell y_u}{(16\pi^2)^2} \frac{v^2}{\Lambda} \left(\frac{1}{16\pi^2} + \frac{v^2}{\Lambda^2} \right)$	2×10^3	$\beta\beta 0\nu$	U
22	$L^i L^j L^k e^c \bar{L}_k \bar{e}^c H^l H^m \epsilon_{il} \epsilon_{jm}$	$\frac{g^2}{(16\pi^2)^3} \frac{v^2}{\Lambda}$	4×10^4	$\beta\beta 0\nu$	U
23	$L^i L^j L^k e^c \bar{Q}_k \bar{d}^c H^l H^m \epsilon_{il} \epsilon_{jm}$	$\frac{y_\ell y_d}{(16\pi^2)^2} \frac{v^2}{\Lambda} \left(\frac{1}{16\pi^2} + \frac{v^2}{\Lambda^2} \right)$	40	$\beta\beta 0\nu$	U
24 _a	$L^i L^j Q^k d^c Q^l d^c H^m \bar{H}_i \epsilon_{jk} \epsilon_{lm}$	$\frac{y_d^2}{(16\pi^2)^3} \frac{v^2}{\Lambda}$	1×10^2	$\beta\beta 0\nu$	U
24 _b	$L^i L^j Q^k d^c Q^l d^c H^m \bar{H}_i \epsilon_{jm} \epsilon_{kl}$	$\frac{y_d^2}{(16\pi^2)^3} \frac{v^2}{\Lambda}$	1×10^2	$\beta\beta 0\nu$	U
25	$L^i L^j Q^k d^c Q^l u^c H^m H^n \epsilon_{im} \epsilon_{jn} \epsilon_{kl}$	$\frac{y_d y_u}{(16\pi^2)^2} \frac{v^2}{\Lambda} \left(\frac{1}{16\pi^2} + \frac{v^2}{\Lambda^2} \right)$	4×10^3	$\beta\beta 0\nu$	U
26 _a	$L^i L^j Q^k d^c \bar{L}_i \bar{e}^c H^l H^m \epsilon_{jl} \epsilon_{km}$	$\frac{y_\ell y_d}{(16\pi^2)^3} \frac{v^2}{\Lambda}$	40	$\beta\beta 0\nu$	U
26 _b	$L^i L^j Q^k d^c \bar{L}_k \bar{e}^c H^l H^m \epsilon_{il} \epsilon_{jm}$	$\frac{y_\ell y_d}{(16\pi^2)^2} \frac{v^2}{\Lambda} \left(\frac{1}{16\pi^2} + \frac{v^2}{\Lambda^2} \right)$	40	$\beta\beta 0\nu$	U
27 _a	$L^i L^j Q^k d^c \bar{Q}_i \bar{d}^c H^l H^m \epsilon_{jl} \epsilon_{km}$	$\frac{g^2}{(16\pi^2)^3} \frac{v^2}{\Lambda}$	4×10^4	$\beta\beta 0\nu$	U
27 _b	$L^i L^j Q^k d^c \bar{Q}_k \bar{d}^c H^l H^m \epsilon_{il} \epsilon_{jm}$	$\frac{g^2}{(16\pi^2)^3} \frac{v^2}{\Lambda}$	4×10^4	$\beta\beta 0\nu$	U
28 _a	$L^i L^j Q^k d^c \bar{Q}_j \bar{u}^c H^l \bar{H}_i \epsilon_{kl}$	$\frac{y_d y_u}{(16\pi^2)^3} \frac{v^2}{\Lambda}$	4×10^3	$\beta\beta 0\nu$	U
28 _b	$L^i L^j Q^k d^c \bar{Q}_k \bar{u}^c H^l \bar{H}_i \epsilon_{jl}$	$\frac{y_d y_u}{(16\pi^2)^3} \frac{v^2}{\Lambda}$	4×10^3	$\beta\beta 0\nu$	U
28 _c	$L^i L^j Q^k d^c \bar{Q}_l \bar{u}^c H^l \bar{H}_i \epsilon_{jk}$	$\frac{y_d y_u}{(16\pi^2)^3} \frac{v^2}{\Lambda}$	4×10^3	$\beta\beta 0\nu$	U
29 _a	$L^i L^j Q^k u^c \bar{Q}_k \bar{u}^c H^l H^m \epsilon_{il} \epsilon_{jm}$	$\frac{y_u^2}{(16\pi^2)^2} \frac{v^2}{\Lambda} \left(\frac{1}{16\pi^2} + \frac{v^2}{\Lambda^2} \right)$	2×10^5	$\beta\beta 0\nu$	U
29 _b	$L^i L^j Q^k u^c \bar{Q}_l \bar{u}^c H^l H^m \epsilon_{ik} \epsilon_{jm}$	$\frac{g^2}{(16\pi^2)^3} \frac{v^2}{\Lambda}$	4×10^4	$\beta\beta 0\nu$	U
30 _a	$L^i L^j \bar{L}_i \bar{e}^c \bar{Q}_k \bar{u}^c H^k H^l \epsilon_{jl}$	$\frac{y_\ell y_u}{(16\pi^2)^3} \frac{v^2}{\Lambda}$	2×10^3	$\beta\beta 0\nu$	U
30 _b	$L^i L^j \bar{L}_m \bar{e}^c \bar{Q}_n \bar{u}^c H^k H^l \epsilon_{ik} \epsilon_{jl} \epsilon^{mn}$	$\frac{y_\ell y_u}{(16\pi^2)^2} \frac{v^2}{\Lambda} \left(\frac{1}{16\pi^2} + \frac{v^2}{\Lambda^2} \right)$	2×10^3	$\beta\beta 0\nu$	U
31 _a	$L^i L^j \bar{Q}_i \bar{d}^c \bar{Q}_k \bar{u}^c H^k H^l \epsilon_{jl}$	$\frac{y_d y_u}{(16\pi^2)^2} \frac{v^2}{\Lambda} \left(\frac{1}{16\pi^2} + \frac{v^2}{\Lambda^2} \right)$	4×10^3	$\beta\beta 0\nu$	U
31 _b	$L^i L^j \bar{Q}_m \bar{d}^c \bar{Q}_n \bar{u}^c H^k H^l \epsilon_{ik} \epsilon_{jl} \epsilon^{mn}$	$\frac{y_d y_u}{(16\pi^2)^2} \frac{v^2}{\Lambda} \left(\frac{1}{16\pi^2} + \frac{v^2}{\Lambda^2} \right)$	4×10^3	$\beta\beta 0\nu$	U

\mathcal{O}	Operator	$m_{\alpha\beta}$	Λ_ν (TeV)	Best Probed	Disfavored
32 _a	$L^i L^j \bar{Q}_j \bar{u}^c \bar{Q}_k \bar{u}^c H^k \bar{H}_i$	$\frac{y_u^2}{(16\pi^2)^3} \frac{v^2}{\Lambda}$	2×10^5	$\beta\beta 0\nu$	U
32 _b	$L^i L^j \bar{Q}_m \bar{u}^c \bar{Q}_n \bar{u}^c H^k \bar{H}_i \epsilon_{jk} \epsilon^{mn}$	$\frac{y_u^2}{(16\pi^2)^3} \frac{v^2}{\Lambda}$	2×10^5	$\beta\beta 0\nu$	U
33	$\bar{e}^c \bar{e}^c L^i L^j e^c e^c H^k H^l \epsilon_{ik} \epsilon_{jl}$	$\frac{g^2}{(16\pi^2)^3} \frac{v^2}{\Lambda}$	4×10^4	$\beta\beta 0\nu$	U
34	$\bar{e}^c \bar{e}^c L^i Q^j e^c d^c H^k H^l \epsilon_{ik} \epsilon_{jl}$	$y_{\ell\beta} \frac{y_d g^2}{(16\pi^2)^4} \frac{v^2}{\Lambda}$	< 0.5	$\beta\beta 0\nu$, mix, ILC, LHC	C
35	$\bar{e}^c \bar{e}^c L^i e^c \bar{Q}_j \bar{u}^c H^j H^k \epsilon_{ik}$	$y_{\ell\beta} \frac{y_u g^2}{(16\pi^2)^4} \frac{v^2}{\Lambda}$	2	mix, LHC	C
36	$\bar{e}^c \bar{e}^c Q^i d^c Q^j d^c H^k H^l \epsilon_{ik} \epsilon_{jl}$	$y_{\ell\alpha} y_{\ell\beta} \frac{y_d^2 g^2}{(16\pi^2)^5} \frac{v^2}{\Lambda}$	< 0.5	$\beta\beta 0\nu$, mix, HEInu, ILC, LHC	D
37	$\bar{e}^c \bar{e}^c Q^i d^c \bar{Q}_j \bar{u}^c H^j H^k \epsilon_{ik}$	$y_{\ell\alpha} y_{\ell\beta} \frac{y_d y_u g^2}{(16\pi^2)^5} \frac{v^2}{\Lambda}$	< 0.5	$\beta\beta 0\nu$, mix, HEInu, ILC, LHC	D
38	$\bar{e}^c \bar{e}^c \bar{Q}_i \bar{u}^c \bar{Q}_j \bar{u}^c H^i H^j$	$y_{\ell\alpha} y_{\ell\beta} \frac{y_u^2 g^2}{(16\pi^2)^5} \frac{v^2}{\Lambda}$	< 0.5	$\beta\beta 0\nu$, mix, HEInu, ILC, LHC	D
39 _a	$L^i L^j L^k L^l \bar{L}_i \bar{L}_j H^m H^n \epsilon_{km} \epsilon_{ln}^3$	$\frac{g^2}{(16\pi^2)^3} \frac{v^2}{\Lambda}$	8×10^4	$\beta\beta 0\nu$	U
39 _b	$L^i L^j L^k L^l \bar{L}_m \bar{L}_n H^m H^n \epsilon_{ij} \epsilon_{kl}$	$\frac{g^2}{(16\pi^2)^3} \frac{v^2}{\Lambda}$	4×10^4	$\beta\beta 0\nu$	U
39 _c	$L^i L^j L^k L^l \bar{L}_i \bar{L}_m H^m H^n \epsilon_{jk} \epsilon_{ln}$	$\frac{g^2}{(16\pi^2)^3} \frac{v^2}{\Lambda}$	4×10^4	$\beta\beta 0\nu$	U
39 _d	$L^i L^j L^k L^l \bar{L}_p \bar{L}_q H^m H^n \epsilon_{ij} \epsilon_{km} \epsilon_{ln} \epsilon^{pq}$	$\frac{g^2}{(16\pi^2)^3} \frac{v^2}{\Lambda}$	4×10^4	$\beta\beta 0\nu$	U
40 _a	$L^i L^j L^k Q^l \bar{L}_i \bar{Q}_j H^m H^n \epsilon_{km} \epsilon_{ln}$	$\frac{g^2}{(16\pi^2)^3} \frac{v^2}{\Lambda}$	4×10^4	$\beta\beta 0\nu$	U
40 _b	$L^i L^j L^k Q^l \bar{L}_i \bar{Q}_l H^m H^n \epsilon_{jm} \epsilon_{kn}$	$\frac{g^2}{(16\pi^2)^3} \frac{v^2}{\Lambda}$	4×10^4	$\beta\beta 0\nu$	U
40 _c	$L^i L^j L^k Q^l \bar{L}_i \bar{Q}_i H^m H^n \epsilon_{jm} \epsilon_{kn}$	$\frac{g^2}{(16\pi^2)^3} \frac{v^2}{\Lambda}$	4×10^4	$\beta\beta 0\nu$	U
40 _d	$L^i L^j L^k Q^l \bar{L}_i \bar{Q}_m H^m H^n \epsilon_{jk} \epsilon_{ln}$	$\frac{g^2}{(16\pi^2)^3} \frac{v^2}{\Lambda}$	4×10^4	$\beta\beta 0\nu$	U
40 _e	$L^i L^j L^k Q^l \bar{L}_i \bar{Q}_m H^m H^n \epsilon_{jl} \epsilon_{kn}$	$\frac{g^2}{(16\pi^2)^3} \frac{v^2}{\Lambda}$	4×10^4	$\beta\beta 0\nu$	U
40 _f	$L^i L^j L^k Q^l \bar{L}_m \bar{Q}_i H^m H^n \epsilon_{jk} \epsilon_{ln}$	$\frac{g^2}{(16\pi^2)^3} \frac{v^2}{\Lambda}$	4×10^4	$\beta\beta 0\nu$	U
40 _g	$L^i L^j L^k Q^l \bar{L}_m \bar{Q}_i H^m H^n \epsilon_{jl} \epsilon_{kn}$	$\frac{g^2}{(16\pi^2)^3} \frac{v^2}{\Lambda}$	4×10^4	$\beta\beta 0\nu$	U
40 _h	$L^i L^j L^k Q^l \bar{L}_m \bar{Q}_n H^m H^n \epsilon_{ij} \epsilon_{kl}$	$\frac{g^2}{(16\pi^2)^3} \frac{v^2}{\Lambda}$	4×10^4	$\beta\beta 0\nu$	U
40 _i	$L^i L^j L^k Q^l \bar{L}_m \bar{Q}_n H^p H^q \epsilon_{ip} \epsilon_{jq} \epsilon_{kl} \epsilon^{mn}$	$\frac{g^2}{(16\pi^2)^3} \frac{v^2}{\Lambda}$	4×10^4	$\beta\beta 0\nu$	U
40 _j	$L^i L^j L^k Q^l \bar{L}_m \bar{Q}_n H^p H^q \epsilon_{ip} \epsilon_{lq} \epsilon_{jk} \epsilon^{mn}$	$\frac{g^2}{(16\pi^2)^3} \frac{v^2}{\Lambda}$	4×10^4	$\beta\beta 0\nu$	U

³This operator is modified slightly from its original form as given in reference [15] where it appeared as $\mathcal{O}_{39}(a) = L^i L^j L^k L^l \bar{L}_i \bar{L}_j H^m H^n \epsilon_{jm} \epsilon_{kl}$. I corrected this error.

\mathcal{O}	Operator	$m_{\alpha\beta}$	Λ_ν (TeV)	Best Probed	Disfavored
41 _a	$L^i L^j L^k d^c \bar{L}_i \bar{d}^c H^l H^m \epsilon_{jl} \epsilon_{km}$	$\frac{g^2}{(16\pi^2)^3} \frac{v^2}{\Lambda}$	4×10^4	$\beta\beta 0\nu$	U
41 _b	$L^i L^j L^k d^c \bar{L}_l \bar{d}^c H^l H^m \epsilon_{ij} \epsilon_{km}$	$\frac{g^2}{(16\pi^2)^3} \frac{v^2}{\Lambda}$	4×10^4	$\beta\beta 0\nu$	U
42 _a	$L^i L^j L^k u^c \bar{L}_i \bar{u}^c H^l H^m \epsilon_{jl} \epsilon_{km}$	$\frac{g^2}{(16\pi^2)^3} \frac{v^2}{\Lambda}$	4×10^4	$\beta\beta 0\nu$	U
42 _b	$L^i L^j L^k u^c \bar{L}_l \bar{u}^c H^l H^m \epsilon_{ij} \epsilon_{km}$	$\frac{g^2}{(16\pi^2)^3} \frac{v^2}{\Lambda}$	4×10^4	$\beta\beta 0\nu$	U
43 _a	$L^i L^j L^k d^c \bar{L}_l \bar{u}^c H^l \bar{H}_i \epsilon_{jk}$	$\frac{y_d y_u g^2}{(16\pi^2)^4} \frac{v^2}{\Lambda}$	6	$\beta\beta 0\nu$, LHC	U
43 _b	$L^i L^j L^k d^c \bar{L}_j \bar{u}^c H^l \bar{H}_i \epsilon_{kl}$	$\frac{y_d y_u g^2}{(16\pi^2)^4} \frac{v^2}{\Lambda}$	6	$\beta\beta 0\nu$, LHC	U
43 _c	$L^i L^j L^k d^c \bar{L}_l \bar{u}^c H^m \bar{H}_n \epsilon_{ij} \epsilon_{km} \epsilon^{ln}$	$\frac{y_d y_u g^2}{(16\pi^2)^4} \frac{v^2}{\Lambda}$	6	$\beta\beta 0\nu$, LHC	U
44 _a	$L^i L^j Q^k e^c \bar{Q}_i \bar{e}^c H^l H^m \epsilon_{jl} \epsilon_{km}$	$\frac{g^2}{(16\pi^2)^3} \frac{v^2}{\Lambda}$	4×10^4	$\beta\beta 0\nu$	U
44 _b	$L^i L^j Q^k e^c \bar{Q}_k \bar{e}^c H^l H^m \epsilon_{il} \epsilon_{jm}$	$\frac{g^2}{(16\pi^2)^3} \frac{v^2}{\Lambda}$	4×10^4	$\beta\beta 0\nu$	U
44 _c	$L^i L^j Q^k e^c \bar{Q}_l \bar{e}^c H^l H^m \epsilon_{ij} \epsilon_{km}$	$\frac{g^4}{(16\pi^2)^4} \frac{v^2}{\Lambda}$	60	$\beta\beta 0\nu$	U
44 _d	$L^i L^j Q^k e^c \bar{Q}_l \bar{e}^c H^l H^m \epsilon_{ik} \epsilon_{jm}$	$\frac{g^2}{(16\pi^2)^3} \frac{v^2}{\Lambda}$	4×10^4	$\beta\beta 0\nu$	U
45	$L^i L^j e^c d^c \bar{e}^c \bar{d}^c H^k H^l \epsilon_{ik} \epsilon_{jl}$	$\frac{g^2}{(16\pi^2)^3} \frac{v^2}{\Lambda}$	4×10^4	$\beta\beta 0\nu$	U
46	$L^i L^j e^c u^c \bar{e}^c \bar{u}^c H^k H^l \epsilon_{ik} \epsilon_{jl}$	$\frac{g^2}{(16\pi^2)^3} \frac{v^2}{\Lambda}$	4×10^4	$\beta\beta 0\nu$	U
47 _a	$L^i L^j Q^k Q^l \bar{Q}_i \bar{Q}_j H^m H^n \epsilon_{km} \epsilon_{ln}$	$\frac{g^2}{(16\pi^2)^3} \frac{v^2}{\Lambda}$	4×10^4	$\beta\beta 0\nu$	U
47 _b	$L^i L^j Q^k Q^l \bar{Q}_i \bar{Q}_k H^m H^n \epsilon_{jm} \epsilon_{ln}$	$\frac{g^2}{(16\pi^2)^3} \frac{v^2}{\Lambda}$	4×10^4	$\beta\beta 0\nu$	U
47 _c	$L^i L^j Q^k Q^l \bar{Q}_k \bar{Q}_l H^m H^n \epsilon_{im} \epsilon_{jn}$	$\frac{g^2}{(16\pi^2)^3} \frac{v^2}{\Lambda}$	4×10^4	$\beta\beta 0\nu$	U
47 _d	$L^i L^j Q^k Q^l \bar{Q}_i \bar{Q}_m H^m H^n \epsilon_{jk} \epsilon_{ln}$	$\frac{g^2}{(16\pi^2)^3} \frac{v^2}{\Lambda}$	4×10^4	$\beta\beta 0\nu$	U
47 _e	$L^i L^j Q^k Q^l \bar{Q}_i \bar{Q}_m H^m H^n \epsilon_{jn} \epsilon_{kl}$	$\frac{g^2}{(16\pi^2)^3} \frac{v^2}{\Lambda}$	4×10^4	$\beta\beta 0\nu$	U
47 _f	$L^i L^j Q^k Q^l \bar{Q}_k \bar{Q}_m H^m H^n \epsilon_{ij} \epsilon_{ln}$	$\frac{g^4}{(16\pi^2)^4} \frac{v^2}{\Lambda}$	60	$\beta\beta 0\nu$	U
47 _g	$L^i L^j Q^k Q^l \bar{Q}_k \bar{Q}_m H^m H^n \epsilon_{il} \epsilon_{jn}$	$\frac{g^2}{(16\pi^2)^3} \frac{v^2}{\Lambda}$	4×10^4	$\beta\beta 0\nu$	U
47 _h	$L^i L^j Q^k Q^l \bar{Q}_p \bar{Q}_q H^m H^n \epsilon_{ij} \epsilon_{km} \epsilon_{ln} \epsilon^{pq}$	$\frac{g^4}{(16\pi^2)^4} \frac{v^2}{\Lambda}$	60	$\beta\beta 0\nu$	U
47 _i	$L^i L^j Q^k Q^l \bar{Q}_p \bar{Q}_q H^m H^n \epsilon_{ik} \epsilon_{jm} \epsilon_{ln} \epsilon^{pq}$	$\frac{g^2}{(16\pi^2)^3} \frac{v^2}{\Lambda}$	4×10^4	$\beta\beta 0\nu$	U
47 _j	$L^i L^j Q^k Q^l \bar{Q}_p \bar{Q}_q H^m H^n \epsilon_{im} \epsilon_{jn} \epsilon_{kl} \epsilon^{pq}$	$\frac{g^2}{(16\pi^2)^3} \frac{v^2}{\Lambda}$	4×10^4	$\beta\beta 0\nu$	U
48	$L^i L^j d^c d^c \bar{d}^c \bar{d}^c H^k H^l \epsilon_{ik} \epsilon_{jl}$	$\frac{g^2}{(16\pi^2)^3} \frac{v^2}{\Lambda}$	4×10^4	$\beta\beta 0\nu$	U

\mathcal{O}	Operator	$m_{\alpha\beta}$	Λ_ν (TeV)	Best Probed	Disfavored
49	$L^i L^j d^c u^c \bar{d}^c \bar{u}^c H^k H^l \epsilon_{ik} \epsilon_{jl}$	$\frac{g^2}{(16\pi^2)^3} \frac{v^2}{\Lambda}$	4×10^4	$\beta\beta 0\nu$	U
50	$L^i L^j d^c d^c \bar{d}^c \bar{u}^c H^k \bar{H}_i \epsilon_{jk}$	$\frac{y_d y_u g^2}{(16\pi^2)^4} \frac{v^2}{\Lambda}$	6	$\beta\beta 0\nu$ LHC	U
51	$L^i L^j u^c u^c \bar{u}^c \bar{u}^c H^k H^l \epsilon_{ik} \epsilon_{jl}$	$\frac{g^2}{(16\pi^2)^3} \frac{v^2}{\Lambda}$	4×10^4	$\beta\beta 0\nu$	U
52	$L^i L^j d^c u^c \bar{u}^c \bar{u}^c H^k \bar{H}_i \epsilon_{jk}$	$\frac{y_d y_u g^2}{(16\pi^2)^4} \frac{v^2}{\Lambda}$	6	$\beta\beta 0\nu$, LHC	U
53	$L^i L^j d^c d^c \bar{u}^c \bar{u}^c \bar{H}_i \bar{H}_j$	$\frac{y_d^2 y_u^2 g^2}{(16\pi^2)^5} \frac{v^2}{\Lambda}$	< 0.5	$\beta\beta 0\nu$, HEInu, ILC, LHC	D
54 _a	$L^i Q^j Q^k d^c \bar{Q}_i \bar{e}^c H^l H^m \epsilon_{jl} \epsilon_{km}$	$y_{l\beta} \frac{y_d g^2}{(16\pi^2)^4} \frac{v^2}{\Lambda}$	< 0.5	$\beta\beta 0\nu$, mix, HEInu, ILC, LHC	D
54 _b	$L^i Q^j Q^k d^c \bar{Q}_j \bar{e}^c H^l H^m \epsilon_{il} \epsilon_{km}$	$y_{l\beta} \frac{y_d g^2}{(16\pi^2)^4} \frac{v^2}{\Lambda}$	< 0.5	$\beta\beta 0\nu$, mix, HEInu, ILC, LHC	D
54 _c	$L^i Q^j Q^k d^c \bar{Q}_l \bar{e}^c H^l H^m \epsilon_{im} \epsilon_{jk}$	$y_{l\beta} \frac{y_d g^2}{(16\pi^2)^4} \frac{v^2}{\Lambda}$	< 0.5	$\beta\beta 0\nu$, mix, ILC, LHC	D
54 _d	$L^i Q^j Q^k d^c \bar{Q}_l \bar{e}^c H^l H^m \epsilon_{ij} \epsilon_{km}$	$y_{l\beta} \frac{y_d g^2}{(16\pi^2)^4} \frac{v^2}{\Lambda}$	< 0.5	$\beta\beta 0\nu$, mix, HEInu, ILC, LHC	D
55 _a	$L^i Q^j \bar{Q}_i \bar{Q}_k \bar{e}^c \bar{u}^c H^k H^l \epsilon_{jl}$	$y_{l\beta} \frac{y_u g^2}{(16\pi^2)^4} \frac{v^2}{\Lambda}$	2	$\beta\beta 0\nu$, mix, LHC	C
55 _b	$L^i Q^j \bar{Q}_j \bar{Q}_k \bar{e}^c \bar{u}^c H^k H^l \epsilon_{il}$	$y_{l\beta} \frac{y_u g^2}{(16\pi^2)^4} \frac{v^2}{\Lambda}$	2	$\beta\beta 0\nu$, mix, LHC	C
55 _c	$L^i Q^j \bar{Q}_m \bar{Q}_n \bar{e}^c \bar{u}^c H^k H^l \epsilon_{ik} \epsilon_{jl} \epsilon^{mn}$	$y_{l\beta} \frac{y_u g^2}{(16\pi^2)^4} \frac{v^2}{\Lambda}$	2	$\beta\beta 0\nu$, mix, LHC	C
56	$L^i Q^j d^c d^c \bar{e}^c \bar{d}^c H^k H^l \epsilon_{ik} \epsilon_{jl}$	$y_{l\beta} \frac{y_d g^2}{(16\pi^2)^4} \frac{v^2}{\Lambda}$	< 0.5	$\beta\beta 0\nu$, mix, ILC, LHC	C
57	$L^i d^c \bar{Q}_j \bar{u}^c \bar{e}^c \bar{d}^c H^j H^k \epsilon_{ik}$	$y_{l\beta} \frac{y_u g^2}{(16\pi^2)^4} \frac{v^2}{\Lambda}$	2	$\beta\beta 0\nu$, mix, LHC	C
58	$L^i u^c \bar{Q}_j \bar{u}^c \bar{e}^c \bar{u}^c H^j H^k \epsilon_{ik}$	$y_{l\beta} \frac{y_u g^2}{(16\pi^2)^4} \frac{v^2}{\Lambda}$	2	mix, LHC	C
59	$L^i Q^j d^c d^c \bar{e}^c \bar{u}^c H^k \bar{H}_i \epsilon_{jk}$	$y_{l\beta} \frac{y_d^2 y_u}{(16\pi^2)^4} \frac{v^2}{\Lambda}$	< 0.5	$\beta\beta 0\nu$, mix, HEInu, ILC, LHC	D
60	$L^i d^c \bar{Q}_j \bar{u}^c \bar{e}^c \bar{u}^c H^j \bar{H}_i$	$y_{l\beta} \frac{y_d y_u^2}{(16\pi^2)^4} \frac{v^2}{\Lambda}$	< 0.5	$\beta\beta 0\nu$, mix, HEInu, ILC, LHC	D
61	$L^i L^j H^k H^l L^r e^c \bar{H}_r \epsilon_{ik} \epsilon_{jl}$	$\frac{y_\ell}{16\pi^2} \frac{v^2}{\Lambda} \left(\frac{1}{16\pi^2} + \frac{v^2}{\Lambda^2} \right)$	2×10^5	$\beta\beta 0\nu$	U
62	$L^i L^j L^k e^c H^l L^r e^c \bar{H}_r \epsilon_{ij} \epsilon_{kl}$	$\frac{y_\ell^2}{(16\pi^2)^2} \frac{v^2}{\Lambda} \left(\frac{1}{16\pi^2} + \frac{v^2}{\Lambda^2} \right)$	20	$\beta\beta 0\nu$	U
63 _a	$L^i L^j Q^k d^c H^l L^r e^c \bar{H}_r \epsilon_{ij} \epsilon_{kl}$	$\frac{y_\ell y_d}{(16\pi^2)^3} \frac{v^2}{\Lambda}$	40	$\beta\beta 0\nu$	U
63 _b	$L^i L^j Q^k d^c H^l L^r e^c \bar{H}_r \epsilon_{ik} \epsilon_{jl}$	$\frac{y_\ell y_d}{(16\pi^2)^2} \frac{v^2}{\Lambda} \left(\frac{1}{16\pi^2} + \frac{v^2}{\Lambda^2} \right)$	40	$\beta\beta 0\nu$	U
64 _a	$L^i L^j \bar{Q}_i \bar{u}^c H^k L^r e^c \bar{H}_r \epsilon_{jk}$	$\frac{y_\ell y_u}{(16\pi^2)^2} \frac{v^2}{\Lambda} \left(\frac{1}{16\pi^2} + \frac{v^2}{\Lambda^2} \right)$	2×10^3	$\beta\beta 0\nu$	U
64 _b	$L^i L^j \bar{Q}_k \bar{u}^c H^k L^r e^c \bar{H}_r \epsilon_{ij}$	$\frac{y_\ell y_u}{(16\pi^2)^3} \frac{v^2}{\Lambda}$	2×10^3	$\beta\beta 0\nu$	U
65	$L^i \bar{e}^c \bar{u}^c d^c H^j L^r e^c \bar{H}_r \epsilon_{ij}$	$\frac{y_d y_u g^2}{(16\pi^2)^4} \frac{v^2}{\Lambda}$	6	$\beta\beta 0\nu$, LHC	U

\mathcal{O}	Operator	$m_{\alpha\beta}$	Λ_ν (TeV)	Best Probed	Disfavored
66	$L^i L^j H^k H^l \epsilon_{ik} Q^r d^c \bar{H}_r \epsilon_{jl}$	$\frac{y_d}{16\pi^2} \frac{v^2}{\Lambda} \left(\frac{1}{16\pi^2} + \frac{v^2}{\Lambda^2} \right)$	6×10^5	$\beta\beta 0\nu$	U
67	$L^i L^j L^k e^c H^l Q^r d^c \bar{H}_r \epsilon_{ij} \epsilon_{kl}$	$\frac{y_\ell y_d}{(16\pi^2)^2} \frac{v^2}{\Lambda} \left(\frac{1}{16\pi^2} + \frac{v^2}{\Lambda^2} \right)$	40	$\beta\beta 0\nu$	U
68 _a	$L^i L^j Q^k d^c H^l Q^r d^c \bar{H}_r \epsilon_{ij} \epsilon_{kl}$	$\frac{y_d^2 g^2}{(16\pi^2)^3} \frac{v^2}{\Lambda} \left(\frac{1}{16\pi^2} + \frac{v^2}{\Lambda^2} \right)$	1	$\beta\beta 0\nu$, LHC	U
68 _b	$L^i L^j Q^k d^c H^l Q^r d^c \bar{H}_r \epsilon_{ik} \epsilon_{jl}$	$\frac{y_d^2}{(16\pi^2)^2} \frac{v^2}{\Lambda} \left(\frac{1}{16\pi^2} + \frac{v^2}{\Lambda^2} \right)$	1×10^2	$\beta\beta 0\nu$	U
69 _a	$L^i L^j \bar{Q}_i \bar{u}^c H^k Q^r d^c \bar{H}_r \epsilon_{jk}$	$\frac{y_d y_u}{(16\pi^2)^2} \frac{v^2}{\Lambda} \left(\frac{1}{16\pi^2} + \frac{v^2}{\Lambda^2} \right)$	4×10^3	$\beta\beta 0\nu$	U
69 _b	$L^i L^j \bar{Q}_k \bar{u}^c H^k Q^r d^c \bar{H}_r \epsilon_{ij}$	$\frac{y_d y_u g^2}{(16\pi^2)^3} \frac{v^2}{\Lambda} \left(\frac{1}{16\pi^2} + \frac{v^2}{\Lambda^2} \right)$	7	$\beta\beta 0\nu$, LHC	U
70	$L^i \bar{e}^c \bar{u}^c d^c H^j Q^r d^c \bar{H}_r \epsilon_{ij}$	$y_{\ell\beta} \frac{y_d^2 y_u}{(16\pi^2)^3} \frac{v^2}{\Lambda} \left(\frac{1}{16\pi^2} + \frac{v^2}{\Lambda^2} \right)$	< 0.5	$\beta\beta 0\nu$, mix, HEIn ν , ILC, LHC	D
71	$L^i L^j H^k H^l Q^r u^c H^s \epsilon_{rs} \epsilon_{ik} \epsilon_{jl}$	$\frac{y_u}{16\pi^2} \frac{v^2}{\Lambda} \left(\frac{1}{16\pi^2} + \frac{v^2}{\Lambda^2} \right)$	2×10^7	$\beta\beta 0\nu$	U
72	$L^i L^j L^k e^c H^l Q^r u^c H^s \epsilon_{rs} \epsilon_{ij} \epsilon_{kl}$	$\frac{y_\ell y_u}{(16\pi^2)^2} \frac{v^2}{\Lambda} \left(\frac{1}{16\pi^2} + \frac{v^2}{\Lambda^2} \right)$	2×10^3	$\beta\beta 0\nu$	U
73 _a	$L^i L^j Q^k d^c H^l Q^r u^c H^s \epsilon_{rs} \epsilon_{ij} \epsilon_{kl}$	$\frac{y_d y_u g^2}{(16\pi^2)^3} \frac{v^2}{\Lambda} \left(\frac{1}{16\pi^2} + \frac{v^2}{\Lambda^2} \right)$	7	$\beta\beta 0\nu$, LHC	U
73 _b	$L^i L^j Q^k d^c H^l Q^r u^c H^s \epsilon_{rs} \epsilon_{ik} \epsilon_{jl}$	$\frac{y_d y_u}{(16\pi^2)^2} \frac{v^2}{\Lambda} \left(\frac{1}{16\pi^2} + \frac{v^2}{\Lambda^2} \right)$	4×10^3	$\beta\beta 0\nu$	U
74 _a	$L^i L^j \bar{Q}_i \bar{u}^c H^k Q^r u^c H^s \epsilon_{rs} \epsilon_{jk}$	$\frac{y_u^2}{(16\pi^2)^2} \frac{v^2}{\Lambda} \left(\frac{1}{16\pi^2} + \frac{v^2}{\Lambda^2} \right)$	2×10^5	$\beta\beta 0\nu$	U
74 _b	$L^i L^j \bar{Q}_k \bar{u}^c H^k Q^r u^c H^s \epsilon_{rs} \epsilon_{ij}$	$\frac{y_u^2 g^2}{(16\pi^2)^3} \frac{v^2}{\Lambda} \left(\frac{1}{16\pi^2} + \frac{v^2}{\Lambda^2} \right)$	2×10^2	$\beta\beta 0\nu$	U
75	$L^i \bar{e}^c \bar{u}^c d^c H^j Q^r u^c H^s \epsilon_{rs} \epsilon_{ij}$	$y_{\ell\beta} \frac{y_d y_u^2}{(16\pi^2)^3} \frac{v^2}{\Lambda} \left(\frac{1}{16\pi^2} + \frac{v^2}{\Lambda^2} \right)$	1	$\beta\beta 0\nu$, mix	C

The third column of Table 3.1, labeled $m_{\alpha\beta}$, presents our estimate for the operator-induced Majorana neutrino mass expressions. These were derived based on the estimation procedure discussed earlier. Trivial order one factors, as well as the generation dependent coupling constants λ have been omitted, as already advertised. Flavor specific charged lepton Yukawa couplings are explicitly denoted y_{ℓ_α} and y_{ℓ_β} to distinguish them from y_ℓ , y_u and y_d , meant to represent α, β -independent Yukawa couplings. A summation over all “internal flavors” is assumed for each entry. For order one coupling constants, this sum is strongly dominated by third generation Yukawa couplings. Upon setting these mass expressions equal to the observed scale of light neutrino masses (0.05 eV), I extract the required cutoff scale Λ for each operator. This quantity, defined to be Λ_ν , is listed in column four in units of one TeV. Numerical results were obtained assuming the current best fit values for all SM parameters. Associated errors are negligibly small as far as our aspirations are concerned.

Fig. 3.2 displays the distribution of extracted cutoff scales, Λ_ν . The histogram bars are color coded to reflect the different operator mass dimensions. The distribution spans thirteen orders of magnitude, from the electroweak scale to 10^{12} TeV. It is interesting to note the general trend of operator dimension with scale: as expected, higher dimension operators are characterized by lower ultraviolet scales. For operators associated with the lowest ultraviolet cutoffs, the lepton number breaking physics occurs at the same energy scale as electroweak symmetry breaking. In this case, one needs to revisit some of the assumptions that go into obtaining the bounds and predictions discussed here. Regardless, it is fair to say that some of these effective operators should be severely constrained by other experimental probes, as will be discussed in the next section.

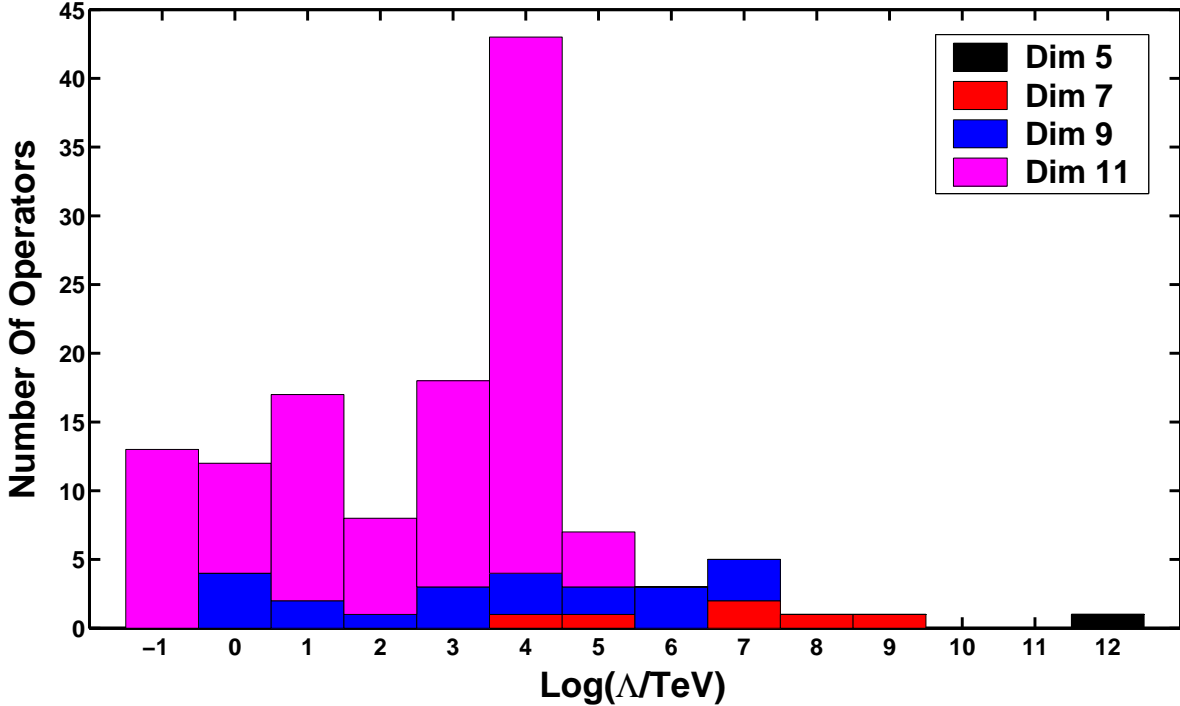


Figure 3.2. A summary histogram of the scale of new physics Λ_ν extracted from the 129 LNV operators introduced in Table 3.1. I assume a radiatively generated neutrino mass of 0.05 eV and universal order one coupling constants. The contributions of operators of different mass dimensions are associated to different colors (shades of gray), as indicated in the caption.

The natural scale for most of the explored operators is well above 10 TeV, and thus outside the reach of future experimental efforts except, perhaps, those looking for neutrinoless double-beta decay. The remainder, however, should yield observable consequences in next-generation experiments. This small subset arguably contains the most interesting cases on purely economic grounds, as they naturally predict tiny neutrino masses as well as TeV scale new physics, which is already thought to exist for independent reasons. It is aesthetically pleasing to imagine that all, or at least most, of nature's current puzzles

can arise from the same source, as opposed to postulating various solutions at different energy scales. It is important to note that one can “push” more of the operators into the observable TeV window by modifying the coupling of the new physics to different fermion generations. In particular, since many of the induced neutrino masses depend upon fermion Yukawa couplings, one can efficiently reduce scales by simply and uniformly decoupling the third generation. In most cases this can yield a Λ_ν reduction of several orders of magnitude; a factor that can be further enhanced by also decoupling the second generation. Under these conditions, the resulting distribution, analogous to Fig. 3.2, would show the majority of the operators piled up near and slightly above the electroweak scale. A detailed exploration of this possibility would be impractical and is not pursued further. I will, however, like to emphasize that this strategy of decoupling the new physics from the *heavy* fermions is very non-standard. In most cases, one is tempted to decouple *light* fermions from new physics both because these lead to the strongest constraints and because one tends to believe that the large Yukawa couplings of third generation fermions are entangled with the physics of electroweak symmetry breaking.

Not all extracted cutoff scales are subject to a strong dependency on SM Yukawa couplings. In particular, the Λ_ν values for the majority of dimension-eleven operators in the large histogram bar near 10^4 TeV would not shift down at all under this hypothetical decoupling of the third generation from the new physics. These are the operators, as shown in Diagram (d) of Fig. 3.1, whose induced neutrino mass matrix is independent of the Yukawa sector. In such cases, $m_{\alpha\beta}$ are only functions of the various gauge couplings. As such, these constitute the most robust results of our analysis. These operators all predict an anarchic Majorana neutrino mass matrix of overall scale given by

$m_\nu = g^2/(16\pi^2)^3 v^2/\Lambda$, implying an energy scale $\Lambda_\nu \sim 10^5$ TeV. The only other “Yukawa invariant” cutoff scale estimate arises for the dimension-five operator \mathcal{O}_1 . \mathcal{O}_1 captures the physics of all versions of the seesaw mechanism [7], and is at the heart of most of the model building currently done within the neutrino sector. Its ultraviolet completion can precede in only three distinct ways [25]. These possibilities are via the exchange of heavy gauge singlet fermions (type I seesaw), $SU(2)_L$ triplet scalars (type II seesaw) [26], $SU(2)_L$ triplet fermions (type III seesaw) [27], or some combination thereof. Its popularity is well-founded for a number of reasons, including its underlying simplicity in structure as well as the purely empirical fact that it is the “lowest order means” of neutrino mass, and as such is easily generated by a “generic” LNV model. Additionally, the high scale associated with the seesaw mechanism can be easily incorporated within existing theoretical models and serves to help explain the observed baryon antisymmetry of the universe via leptogenesis [28].

For the purposes of direct observation, \mathcal{O}_1 ’s high cutoff scale, nearly 10^{12} TeV, places it well outside of the “detectable region” ($\Lambda \lesssim 10$ TeV) and renders it uninteresting for the purposes of our analysis. Of course, there always remains the possibility that \mathcal{O}_1 is generated by very weakly coupled new physics (or very finely-tuned new physics [29]), in which case I expect to run into the new ultraviolet degrees of freedom at energies well below 10^{12} TeV. In the case of \mathcal{O}_1 , it has been argued that new physics at almost any energy scale (from well below the sub-eV realm to well above the weak scale) will lead to light neutrino masses [30, 31, 2, 32] without contradicting current experimental results. Such possibilities – related to the fact that the new physics is very weakly coupled – are

not being explored here, as I always assume that the new degrees of freedom are heavier than typical experimentally accessible energy scales.

Armed with our derived new physics scales Λ_ν , I proceed to plug them back into the different irrelevant LNV operators and search for possible means of future observation as well as already existing constraints. Generally, those operators that yield the largest experimental signals have the lowest cutoff scales. I conclude that, if associated to neutrino masses, the effective cutoff scale Λ_ν of the following effective operators is constrained to be less than 1 TeV:

$$\mathcal{O}_{34}, \mathcal{O}_{36}, \mathcal{O}_{37}, \mathcal{O}_{38}, \mathcal{O}_{53}, \mathcal{O}_{54_{a,b,c,d}}, \mathcal{O}_{56}, \mathcal{O}_{59}, \mathcal{O}_{60}, \mathcal{O}_{70}. \quad (3.7)$$

These may lead to observable effects at future high energy accelerator facilities. Additionally, such low scales may also indirectly lead to observable effects in “low energy” (but high sensitivity) experiments. There are more operators associated with slightly higher scales between (1 – 10) TeV that may manifest themselves experimentally via virtual effects. These are

$$\mathcal{O}_{16}, \mathcal{O}_{17}, \mathcal{O}_{18}, \mathcal{O}_{19}, \mathcal{O}_{35}, \mathcal{O}_{43_{a,b,c}}, \mathcal{O}_{50}, \mathcal{O}_{52}, \mathcal{O}_{55_{a,b,c}}, \mathcal{O}_{57}, \mathcal{O}_{58}, \mathcal{O}_{65}, \mathcal{O}_{68_{a,b}}, \mathcal{O}_{73_a}, \mathcal{O}_{75}. \quad (3.8)$$

These operators yield finite predictions for more than one observable, such that experimental efforts in seemingly unrelated fields can help constrain the class of possible LNV models or even help identify the true LNV model.

3.2. General operator constraints and predictions

There are, currently, bounds on LNV processes from a number of independent experimental sources [33, 34]. Many of these are presently too mild to constrain the operators listed in Table 3.1 once their ultraviolet cutoffs Λ are set to the required value indicated by the presence of non-zero neutrino masses, Λ_ν . The situation, however, is expected to improve in the next several years with increased rare decay sensitivities and higher collider energies. Here I survey the experimental signatures of these operators in terms of the minimal scenarios described above. Specifically, I address the potential of neutrinoless double-beta decay (Sec. 3.2.1), rare meson decays (Sec. 3.2.2), and collider experiments (Sec. 3.2.3) to constrain the effective operators in question, assuming that, indeed, they are responsible for the observed non-zero neutrino masses. As before, I will use the approximations discussed in Sec. 3.1, and warn readers that all the results presented are to be understood as order of magnitude estimates. The results, however, are useful as far as recognizing the most promising LNV probes and identifying different scenarios that may be probed by combinations of different LNV searches.

Most of this section will be devoted to probes of LNV via simple variants of the following process, which can be written schematically as

$$\ell_\alpha \ell_\beta \leftrightarrow d_\kappa d_\zeta \bar{u}_\rho \bar{u}_\omega. \quad (3.1)$$

Greek subscripts run over all different fermion flavors. Given the assumed democratic models, coupled with our present lack of experimental information, one would expect that all flavor combinations are equivalent to zeroth order. Any indication to the contrary would signify important deviations from simple expectations, and thus begin to reveal the

flavor structure of the new physics. The above selected “golden modes” often yield the largest LNV rates, but this is not always the case. For example, some operators do not allow tree-level charged dilepton events, but rather prefer to include neutrino initial or final states. LNV processes with initial and final state neutrinos are extremely difficult to identify. The only hope of such discovery channels is, perhaps, via neutrino scattering experiments on either electron or nucleon targets, using well understood neutrino beams. I point out that any neutrino/anti-neutrino cross contamination induces ambiguity onto the total lepton number of the incident beam and would serve as a crippling source of background for LNV searches. This reasoning rules out conventional superbeam [35] facilities as well as proposed neutrino factories [36], which contain both neutrino and anti-neutrino components, but does suggest modest possibilities for future beta-beams [37]. Given projected beta-beam luminosities and energies along with the derived cutoff scales Λ_ν , it seems unlikely that LNV can be observed in such experiments. Another possible discovery mode involves only two external state quarks and an associated gauge boson as in the sample process $\ell_\alpha \ell_\beta \rightarrow d\bar{u} + W^-$. It turns out that the rates for such processes are generally suppressed for the majority of operators involving six fermion fields, as I am trading a phase space suppression for a stronger loop suppression. For those operators with only four fermion fields, the situation is not as straightforward and, in some cases, the three particle final state is preferred. Typically, the neutrino mass induced cutoff scales of those operators are high ($\Lambda_\nu \gg 100$ TeV), so it would be quite difficult to observe such effects. Of course, any W -boson final state will either promptly decay leptonically, yielding missing energy and unknown total lepton number, or hadronically, reducing the reaction back to that of the golden mode.

Another possibility is to replace two or more of the external quark states in Eq. (3.1) with leptons in such a way as to preserve charge, baryon number, and $\Delta L = 2$ constraints. While many operators favor this structure, a little thought reveals that at least one external neutrino state is always present, which leaves only a missing energy signature, and little means of lepton number identification in a detector. Such events would not be clean, but of course, three final-state charged leptons and missing energy are enough to extract the existence of at least $\Delta L = 1$ LNV, provided that the number of invisible states is known to be no greater than one. This last requirement is difficult to achieve in the presence of the large backgrounds and the limited statistics expected at future collider facilities, but should still be possible given a concrete model probed near resonance (see for example [38]). Therefore, while important and potentially observable, this mode is not generally the best place to look for LNV and is neglected in the remainder of our analysis. From this perspective, the only other relevant channel of LNV discovery is related to W and Z rare decays into final states with non-zero total lepton number. This possibility is briefly addressed in Sec. 3.2.2.

3.2.1. Neutrinoless Double-Beta Decay

Here I probe the expectations for neutrinoless double-beta decay ($\beta\beta 0\nu$) for each operator listed in Table 3.1. $\beta\beta 0\nu$ is the LNV ($\Delta L = 2$) process where, within a nucleus, two down quarks convert into two up quarks with the emission of two electrons but no neutrinos, or in the language of nuclear physics $(A, Z) \rightarrow (A, Z + 2) + e^- e^-$. See [39, 40] and references therein for a comprehensive review. While precise computations of nuclear matrix elements are essential for making detailed predictions [41], the minimal parton-level

description given above is adequate for the purposes of this study. There is a continuing legacy of cutting edge experiments designed to search for $\beta\beta 0\nu$ with no success to date.¹ Currently the ^{76}Ge half-life for this process is bounded to be greater than 1.9×10^{25} yr and 1.57×10^{25} yr at 90% confidence by the Heidelberg-Moscow [43] and IGEX [44] experiments, respectively. Future experiments are poised to improve these limits (for several different nuclei) by a couple of orders of magnitude within the next five to ten years [45].

If one assumes that $\beta\beta 0\nu$ proceeds via the exchange of light Majorana neutrinos, its amplitude is proportional to the ee element of the Majorana neutrino mass matrix,

$$m_{ee} = \sum_{i=1}^3 m_i U_{ei}^2, \quad (3.2)$$

where m_i are the neutrino masses and U_{ei} are elements of the leptonic mixing matrix. With this, one can extract the upper bound $m_{ee} < 0.35$ eV (90% confidence level bound, [34]) from current experiments while next-generation experiments are aiming at $m_{ee} \gtrsim 0.05$ eV² [45]. In general, LNV new physics will lead to additional contributions to $\beta\beta 0\nu$, most of which are not proportional to m_{ee} . However, the amplitude for $\beta\beta 0\nu$ can still be expressed in terms of an effective m_{ee} , m_{ee}^{eff} , which is an operator-specific quantity that will be used to analyze new models of LNV.

Here, I define six different “classes” of diagrams one can construct out of LNV irrelevant operators that contribute to $\beta\beta 0\nu$ at the parton level. These are illustrated in Fig. 3.3, and classified by the dimension of the generated LNV interaction, depicted by

¹There is currently a positive report of $\beta\beta 0\nu$ at the 4.2σ level by a subset of the Heidelberg-Moscow collaboration [42]. They report a measured half-life of $1.74_{-0.16}^{+0.18} \times 10^{21}$ years which maps to $m_{ee}^{\text{eff}} \sim (0.2 - 0.6)$ eV. I choose to neglect this controversial result, which is still awaiting independent conformation.

²The parameter change from half-life to m_{ee} depends heavily on nuclear matrix element calculations. Current calculations induce an uncertainty of less than a factor of four on m_{ee} for most parent isotopes [41].

large gray dots. In order to unambiguously separate the different classes, note that the grey circles are defined in such a way that all fermion and Higgs legs that come out of it are part of the “parent” operator \mathcal{O} (and not attached on via reducible SM vertices), while all other interactions are SM vertices. The dots should be viewed as hiding the underlying LNV interactions. In general, they contain a mixture of coupling constants and loop factors that must be evaluated explicitly for each diagram. It is important to emphasize that the contribution of a generic operator \mathcal{O} to $\beta\beta 0\nu$ will consist of contributions from all different classes, while usually dominated by one of them. I show the lepton number conserving electroweak vertices (point-like) as effective four-fermion interactions, justified by the low energy scale of nuclear beta decays. The dotted lines indicate the exchange of W -bosons, labeled by W and H (charged Higgs goldstone boson). Helicity arrows are explicitly included where uniquely determined, implying that the arrowless legs can have any helicity.

D_ν describes the standard scenario of $\beta\beta 0\nu$ mediated by light Majorana neutrinos. It is simply two electroweak vertices held together by a Majorana mass term on which two neutrinos are annihilated. The amplitude for this diagram is proportional to m_{ee} , as defined in Eq. (3.2). The dependence on such a neutrino mass is intuitively clear considering the need for a helicity flip on the internal neutrino line. The remaining diagrams are qualitatively different from this standard case. Most importantly, none of them require “helicity flips” and are therefore not directly proportional to neutrino masses. They are, however, proportional to inverse powers of the new mass scale Λ_ν , and hence also suppressed. These effects are not entirely independent, since the value of Λ_ν was extracted from the requirement that neutrino masses are small, but correlations

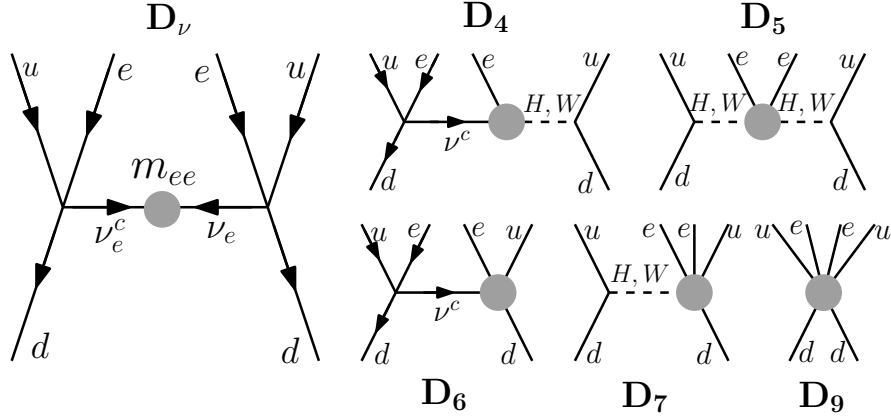


Figure 3.3. The parton level Feynman diagrams contributing to neutrinoless double-beta decay, labeled by the dimension of the underlying lepton number violating interaction, indicated by gray dots. Each diagram is generated, at some order in perturbation theory, by all analyzed interactions, but estimates of their magnitudes depend heavily on the details of the operators, including their associated scale Λ_ν , fermion content and helicity structure.

are relaxed enough to allow nontrivial consequences. It is this partial decoupling from neutrino masses that allows larger than naively expected contributions to $\beta\beta 0\nu$ from some of the LNV irrelevant operators. Before proceeding, I make the trivial observation that the amplitudes following from D_ν , D_4 and D_5 are additionally proportional to two powers of CKM matrix elements, namely $|V_{ud}|^2$, whereas D_6 and D_7 are only proportional to one power of V_{ud} .³ The tree-level diagram D_9 has no CKM “suppression.” While this is a purely academic fact in the case of $\beta\beta 0\nu$ ($|V_{ud}| \sim 1!$), it leads to important consequences for analogous rare decays that depend on the much smaller off-diagonal CKM matrix elements. I will return to these in the next subsection.

³This is true provided that I assume no flavor structure for the underlying operator, or, equivalently, that all dimensionless coupling constants are order one. If one is motivated by experiment to postulate a minimally flavor violating scenario, to perhaps ease constraints from flavor changing neutral currents, the statement must be modified accordingly.

For a given operator, the relative size of each diagram's contribution to the total decay rate depends on many factors including the operator's dimension, scale, fermion content and helicity structure. The dominant contributions must be calculated on a case by case basis. Generally, the high scale operators ($\Lambda_\nu \gtrsim 10$ TeV) are dominated by the two dimension-four diagrams D_ν and D_4 since many factors of Λ_ν will be canceled by divergent loops inside the gray dots thereby minimizing the $1/\Lambda_\nu$ suppression. All else being equal, D_ν is the strongest of the pair since it is enhanced by $\sim Q^{-2}$ from the two propagating neutrino lines as opposed to only $\sim Q^{-1}$ for the one neutrino case shown in diagram D_4 . For those operators with no tree-level $\nu\nu$ field content, D_4 can still be very important, but its dominance is nevertheless rare. As discussed in Sec. 3.1, these are precisely the operators that have the greatest loop suppressions and consequently lower energy scales suggesting the need for diagrams beyond D_4 . The effects of low cutoff scale operators ($\Lambda_\nu \lesssim 1$ TeV) are not severely suppressed by $1/\Lambda_\nu$ (by definition), so the dominant diagrams will typically be of the highest dimension allowed by the tree-level structure of the operator. For such low scales and for operators of the following schematic form $dd\bar{u}\bar{u}\bar{e}\bar{e}$ (dimension 9) or $dd\bar{u}\bar{u}\bar{e}\bar{e}H_0H_0$ (dimension 11), D_9 always dominates the $\beta\beta 0\nu$ rate yielding amplitudes proportional to $1/\Lambda_\nu^5$ and v^2/Λ_ν^7 , respectively. For intermediate scales, and when the operator's field content does not directly support $\beta\beta 0\nu$ due to lack of quark fields, the situation is not as straight forward and one must perform the relevant computations to determine the dominant diagrams. Still, it should be noted that diagrams containing internally propagating neutrinos are enhanced by inverse powers of Q and maintain a slight advantage over their neutrinoless counterparts. One can thus generally expect diagram D_6 to dominate the decay rates for low Λ_ν scale operators when

D_9 is suppressed. The opposite is true for interactions taking place at higher energies in, for example, next-generation colliders, as discussed in Sec. 3.2.3.

Since each diagram in Fig. 3.3 can have different external helicity structures, the different contributions to the total rate will be added incoherently, thus eliminating the effects of interference. There are some case specific coherent contributions that I neglected in our treatment since most rates are dominated by a single diagram. Another potential difference among the different contributions is related to nuclear matrix element calculations: can the calculations done assuming $\beta\beta 0\nu$ via the standard light Majorana neutrino exchange scenario of diagram D_ν be applied to the more general cases encountered here? I have nothing to add to this discussion except to naively note that there is no obvious reason why such rates should be severely suppressed or enhanced relative to the standard scenario. I therefore assume that all nuclear matrix elements are identical and can be factored out of the incoherent sum. I assume that this approximation is not more uncertain than the other sources of uncertainty inherent to our study (likely a very safe assumption).

As drawn, each diagram D_i contributes to the amplitude that characterizes $\beta\beta 0\nu$. For example, the amplitude associated with D_ν is proportional to

$$\mathcal{A}_{D_\nu} \equiv m_{ee} \frac{|V_{ud}|^2 G_F^2}{Q^2}, \quad (3.3)$$

where G_F is the Fermi constant. The remaining diagrams will contribute with $\mathcal{A}_{D_i} \propto \zeta(v, Q)\Lambda^{4-i}$, up to a dimensionless coefficient containing various numerical/loop factors, as well as general scale dependencies parameterized by some power of the ratio v/Λ . The function $\zeta(v, Q)$ has mass dimension $i - 9$ so that all \mathcal{A}_{D_i} have the same mass dimension.

Note that all aspects of \mathcal{A}_{D_i} are calculable given a LNV operator and diagram. I can analyze each operator in terms of an effective m_{ee}^{eff} , defined in terms of the underlying dimension nine amplitude \mathcal{A}_{D_i} by

$$m_{ee}^{\text{eff}} = \frac{Q^2}{G_F^2 |V_{ud}|^2} \sqrt{\sum_i \mathcal{A}_{D_i}^2}, \quad (3.4)$$

where i runs over the set $\{\nu, 4, 5, 6, 7, 9\}$ that labels the diagrams shown in Fig. 3.3, and $Q \sim 50$ MeV is the typical momentum transfer in $\beta\beta 0\nu$. m_{ee}^{eff} can be directly compared with experiment and used to make prediction for future observations. A few comments are in order regarding this quantity. First, it is a useful derived object that has no direct connection to a real neutrino mass and is valid to arbitrarily large values. Note that in the case of Majorana neutrino exchange, $m_{ee}^{\text{eff}} = m_{ee}$ only if $m_{ee} \ll Q$. When neutrino masses are greater than Q , $m_{ee}^{\text{eff}} \propto 1/m$. Our definition of m_{ee}^{eff} also conforms to the use of large effective masses in [33]. The second comment is that, unlike the case of m_{ee} , which is valid for any process involving the exchange of electron-like Majorana neutrinos, m_{ee}^{eff} is case specific. It must be calculated separately for each process, as each one, in general, is composed of different diagrams. In particular, the calculations of the effective mass for $\beta\beta 0\nu$ expressed here are not directly applicable to other LNV processes and should not be interpreted as such.

The m_{ee}^{eff} distribution extracted from all operators is shown in Fig. 3.4 assuming the scales Λ_ν derived in Sec. 3.1 and color-coded for convenience within the histogram. Specifically, I indicate in green the operators that are characterized by sub-TeV scales and thus accessible to next-generation experiments via direct production. The blue and red operators are characterized by scales between (1 – 5) TeV and (5 – 25) TeV respectively,

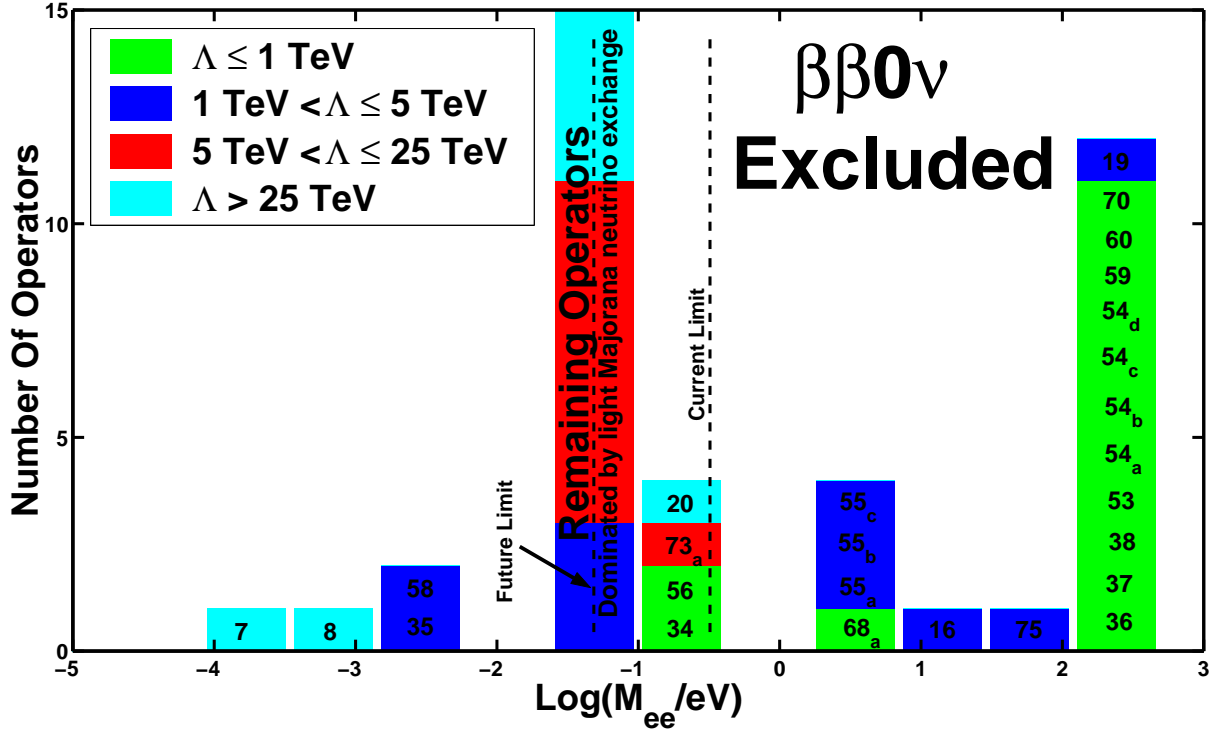


Figure 3.4. m_{ee}^{eff} distribution derived for the neutrinoless double-beta decay process as described in the text. The calculations were made assuming the scales Λ_ν derived in Sec. 3.1, as well as universally order one coupling constants. The histogram bars are labeled explicitly with operator names and color-coded by their cutoff scales. Also shown in light gray is the region probed by next-generation experiments. The vertical axis is truncated at 15 operators to best display the relevant features of the plot.

where virtual effects should be most important for collider searches. The majority of operators, shown in cyan, are suppressed by scales greater than 25 TeV and are hence quite difficult to observe in other search modes. I also explicitly label each operator within the histogram bars for easy identification and comparison. One should notice the expected general trend that increasing Λ_ν leads to a decrease in m_{ee}^{eff} and vice-versa. The vertical

axis is truncated at 15 operators, as the bar near 0.05 eV, dominated by the light Majorana neutrino exchange described above, would extend to nearly 100 operators. With broken vertical lines, I indicate the current 90% upper bound [34], $m_{ee}^{\text{eff}} = 0.35$ eV, and the potential reach of future experiments.

This distribution, which spans over six orders of magnitude (from 10^{-4} eV till 10^2 eV), reveals many important features of the effective operator set. Beginning at the largest m_{ee}^{eff} values, I find that the twelve operators appearing near 300 eV all have the expected common feature of low energy scales, including \mathcal{O}_{19} with Λ_ν only just above the 1 TeV mark. Additionally, the contribution of the majority of these operators to $\beta\beta 0\nu$ is dominated by the tree-level D_9 diagram. The exceptions are $\mathcal{O}_{54_{c,d}}$ and \mathcal{O}_{70} , all of which are characterized by sub 0.5 TeV scales and dominated by diagram D_6 . Consequently, these are subject to a loop and Yukawa/gauge⁴ suppression relative to their D_9 dominated cousins, but the difference is not visible given the resolution of the figure. It is interesting to note that these three operators have the correct quark and lepton content for large $\beta\beta 0\nu$, but their $SU(2)_L$ gauge structures forbid large tree-level contributions. Similarly, operators \mathcal{O}_{16} , $\mathcal{O}_{55_{a,b,c}}$, \mathcal{O}_{68_a} , and \mathcal{O}_{75} are also dominated by diagram D_6 accompanied by slightly higher cutoff scales. This drives down m_{ee}^{eff} significantly considering the leading one-loop scale suppressions of Λ^{-5} and Λ^{-3} for the dimension-eleven and dimension-nine operators respectively. I point out that operators $\mathcal{O}_{54_{a,b,c,d}}$ and $\mathcal{O}_{55_{a,b,c}}$ yield almost identical expressions for their respective $\beta\beta 0\nu$ amplitudes (as well as their radiatively generated neutrino mass expressions) with up and down quark Yukawa couplings exchanged. While this action enhances most of the \mathcal{O}_{55} $\beta\beta 0\nu$ couplings relative to those of \mathcal{O}_{54} , it also

⁴As it turns out these are all suppressed by a single bottom quark Yukawa coupling as well as two powers of the $SU(2)_L$ gauge coupling g , but this fact cannot be deduced from Fig. 3.4 alone.

raises the \mathcal{O}_{55} Λ_ν scale by nearly a factor of four and thus drives m_{ee}^{eff} down by orders of magnitude.

The remaining operators all predict $m_{ee}^{\text{eff}} < 1$ eV, close to current experimental bounds. The histogram bar near 0.1 eV is composed of operators of very different Λ_ν scales. \mathcal{O}_{34} and \mathcal{O}_{56} are both characterized by low cutoff energy scales around 0.5 TeV, but, due to their fermion and helicity structure, their contributions to $\beta\beta 0\nu$ are dominated by two-loop versions of diagram D_6 . The neutrino-mass-required cutoff for \mathcal{O}_{73_a} is around 7 TeV and its contribution to $\beta\beta 0\nu$ is also dominated by diagram D_6 . In this case, however, the two-loop version turns out to be larger than the allowed one-loop amplitude due to strong scale suppressions (the added loop reduces the cutoff dependency from Λ^{-5} to Λ^{-3}). This behavior is characteristic of operators with a larger value of Λ_ν . The $\Lambda_\nu = 40$ TeV operator \mathcal{O}_{20} , defines the lower edge of this histogram bar. It is dominated by the one-loop diagram D_6 enhanced by a top quark Yukawa coupling and, being a dimension nine operator, is only suppressed by Λ^{-3} from the start. The next bar down contains operators dominated by D_ν . Most of these are suppressed by a very high energy scale, but a small subset is characterized by scales $\Lambda_\nu < 25$ TeV. In particular operators \mathcal{O}_{17} , \mathcal{O}_{18} and \mathcal{O}_{57} are all cutoff at 2 TeV but, due to their fermion content they cannot participate in any of the non-standard interactions of Fig. 3.3 at a low enough order in perturbation theory. Similarly, the intermediately scaled operators $\mathcal{O}_{43_{a,b,c}}$, \mathcal{O}_{50} , \mathcal{O}_{52} , \mathcal{O}_{62} , \mathcal{O}_{65} , and \mathcal{O}_{69_b} have either the wrong fermion content or gauge structure to enhance any of the $\beta\beta 0\nu$ diagrams (other than D_ν) to an observable level. These operators are important because their minimal forms are experimentally unconstrained yet still potentially observable to both next-generation $\beta\beta 0\nu$ and collider experiments. The remaining histogram bars with

$m_{ee}^{\text{eff}} < 10^{-2}$ eV are not accessible to $\beta\beta 0\nu$ experiments in the foreseeable future. Each of these diagrams are dominated by D_ν , either due to high suppression scales as in the case of \mathcal{O}_7 and \mathcal{O}_8 , or, as in \mathcal{O}_{35} and \mathcal{O}_{58} , the operator’s fermion content simply disfavors other contributions to the $\beta\beta 0\nu$ amplitude. It is the general form of the neutrino mass matrix derived in Table 3.1, where I see that $m_{ee} \propto y_e$, that drives these operators away from their peers near $m_{ee}^{\text{eff}} = 0.05$ eV. It is unfortunate that the two “low” dimensionality operators \mathcal{O}_7 and \mathcal{O}_8 are cutoff by energy scales Λ_ν in excess of 100 TeV and are hence invisible to any direct probe. If either of these operators have anything to do with nature, it is unlikely that LNV will be observed in the foreseeable future in *any* experiment. On the other hand, any observation of LNV will rule out these types of scenarios. Additionally, as will become clear shortly in Sec. 3.3, current neutrino oscillation data already marginally disfavor such operators and have ample room to tighten constraints in the near future.

It is interesting to point out that the lower boundary of the currently excluded region falls within the m_{ee}^{eff} distribution, suggesting exciting prospects for the future. That being said, one should not read too much into current and future null results as, for most operators, relatively small cancelations and order one factors, not accounted for here, can push the relevant rates below the observable level depending on the underlying ultraviolet theory. On the other hand, one is allowed to interpret that operators that lead to $m_{ee}^{\text{eff}} \gtrsim 10$ eV are severely constrained (if not ruled out) as proper explanations for neutrino masses if one assumes the new physics to be flavor “indifferent” – order one factors cannot be evoked to save the scenario. Once this assumption is dropped, however, it is quite easy to “fix” these scenarios, since the large $\beta\beta 0\nu$ rate is a direct consequence of the universal order one couplings and the relatively low cutoff energy scale Λ_ν . For example, one can

suppress the coupling of new physics to first generation fermions (compared to second and third generation fermions), thereby suppressing the worrisome diagrams of Fig. 3.3. This will have little effect on the relation between Λ and the neutrino masses, discussed in Sec. 3.1, since these are either generation independent or highly reliant on third generation Yukawa couplings. Of course, by combining $\beta\beta 0\nu$ searches with other probes I can obtain a much better idea of the origins of LNV as well as the relevant model(s), if any, chosen by nature.

3.2.2. Other Rare LNV Decay Processes

Most of the qualitative discussions of Sec. 3.2.1, devoted to $\beta\beta 0\nu$, can be directly applied to other rare decay processes with the same underlying kernel interaction described by Eq. (3.1). For such processes one need only analyze simple variants of the diagrams listed in Fig. 3.3, using crossing amplitude symmetries to account for the needed initial and final state fermions. Other factors must be added to the various electroweak vertices to account for quark flavor mixing. The requisite CKM matrix elements can highly suppress many diagrams for processes involving cross-generational quark couplings. In fact, only tree-level D_9 diagrams are safe from such suppressions. Next, and most importantly, one must include the appropriate characteristic momentum transfer Q of the new system. Specific rates are highly dependent on this quantity as effective operator cross-sections typically grow with some power of Q . The particular exponent of the power law depends on the diagram, but naive dimensional analysis dictates that $\Gamma \propto Q^{12}$ for diagram D_9 , rendering it highly dependent on a reaction's energy transfer. The fact that each diagram varies with Q in a different way implies that predicting the dominant contributions to a

given process is non-trivial and must be addressed quantitatively. Finally, in the cases of hadronic decays, one must also account for initial/final state matrix elements. I assume that all factors can be simply estimated on dimensional grounds.

Unlike the $\beta\beta 0\nu$ case, some meson decay modes proceeding via new LNV tensor interactions are expected to be suppressed. Such processes are one instance in our analysis where an operator's Lorentz structure can qualitatively affect expected LNV decay rates. One can understand this by considering a meson decay mediated by a new tensor particle. The parton level interaction has the form $(\bar{u}\sigma_{\mu\nu}d)T^{\mu\nu}$ where the initial state quarks are explicitly shown and all other fields are contained in the tensor $T^{\mu\nu}$. Following the standard procedure I factor out the hadronic structure in the form of a free decay constant and write the amplitude as generally allowed by Lorentz invariance in terms of the external state's four-momentum. Due to the antisymmetry of $\sigma_{\mu\nu}$, this amplitude vanishes to first order. Non-zero contributions to this decay mode must necessarily involve individual parton momenta and are therefore suppressed relative to the usual vector-like decay calculations. From this, it is clear that models of LNV containing tensor couplings will often evade the predictions and bounds of this section. Tensor operators will mediate LNV meson decays into more complicated final states (one may include, say, initial/final state radiation). Associated rates are, however, subject to additional gauge coupling and phase space suppression that tend to further reduce the already tiny LNV rates beyond any hope of detection.

Rare LNV meson decays have been experimentally pursued for many years [34]. Here, I focus on the $\Delta L = 2$ processes $M' \rightarrow M + \ell_\alpha^\pm \ell_\beta^\pm$, where M' and M are the initial and final states mesons respectively and the ℓ s represent like-sign lepton pairs of arbitrary flavor.

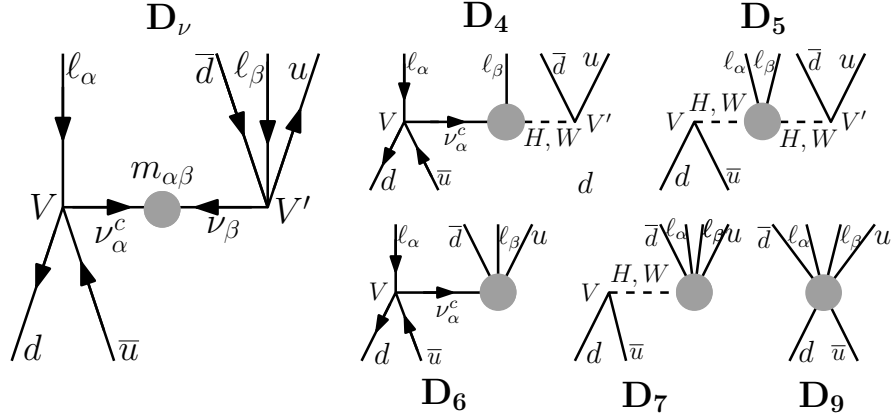


Figure 3.5. The parton level Feynman diagrams contributing to rare LNV meson decay labeled by the dimension of the underlying lepton number violating interaction, indicated by gray dots. Each diagram is generated, at some order in perturbation theory, by all analyzed interaction, but estimates of their magnitudes depend heavily on the details of the operators, including their associated scale Λ_ν , fermion content, and helicity structure.

Electric charge conservation dictates that M' and M have equal and opposite charge. Here I take each meson to consist of a color singlet up-type/antidown-type bound state¹ and factor out all long distance hadronic effects. In this way I can view the meson decay process as $d\bar{u} \rightarrow \ell_\alpha \ell_\beta + \bar{d}u$ for all up-type and down-type quark flavor combinations. The effective LNV diagrams contributing to this process are shown in Fig. 3.5 with the same naming scheme as their analogs in Fig. 3.3. Here, V and V' denote potentially distinct elements of the quark mixing matrix. I additionally point out the potential dependency on all entries of the Majorana neutrino mass matrix elements $m_{\alpha\beta}$ in diagram D_ν , as opposed to the $\beta\beta 0\nu$ case where D_ν depends only on m_{ee} . These processes probe combinations of the neutrino masses that are naively unconstrained by $\beta\beta 0\nu$ [46]. In general, the varied flavor structures encountered in meson decays allow for experimental probes into new

¹For simplicity I assume that both the process $M' \rightarrow M + \ell_\alpha \ell_\beta$ and its conjugate have similar amplitudes and therefore treat them symmetrically. Large CP-violating effects can invalidate this assumption.

physics couplings across the fermion generations. I pointed out earlier that some of the LNV operators lead to unacceptably large rates for $\beta\beta 0\nu$ unless first generation quarks participate in the new interactions with severely suppressed couplings (compared with second and third generation quarks). If such a scenario is realized in nature, rare D or B decays may be much more frequent than naive expectations. For this reason, improving rare decay sensitivities to all channels is essential to completely constrain models of new LNV physics beyond the minimal framework analyzed here.

Reference [33] summarizes LNV upper bounds on all of these processes in terms of the effective Majorana neutrino mass matrix element $m_{\alpha\beta}^{\text{eff}}$ that one would extract from observation assuming that all decay rates are dominated by the light neutrino exchange shown in D_ν . Hence, I can compare operator expectations with current experimental limits in exactly the same way as was done in Sec. 3.2.1. For a given LNV meson decay, $m_{\alpha\beta}^{\text{eff}}$ is defined from the contribution of the different classes of diagrams to the rare meson decay in question, exactly as m_{ee}^{eff} was defined in the previous subsection (see Eqs.(3.3,3.4)). Direct estimates for different process reveal m^{eff} distributions similar to that for m_{ee}^{eff} depicted Fig. 3.4, up to “rescalings” that reflect the different kinematics and the presence of small CKM mixing matrix elements. Results are summarized in Fig. 3.6 for a representative sample of charged meson decays. Each histogram is labeled by its associated decay mode and is color-coded to indicate the neutrino-mass constrained cutoff scale Λ_ν of the different LNV effective operators. For simplicity, I refrain from listing operator names on the individual histogram bars (as opposed to what was done in Fig. 3.4). The “operator ordering” is very similar to that of Fig. 3.4, especially in the low Λ_ν scale, high effective mass regime where decay rate predictions are particularly

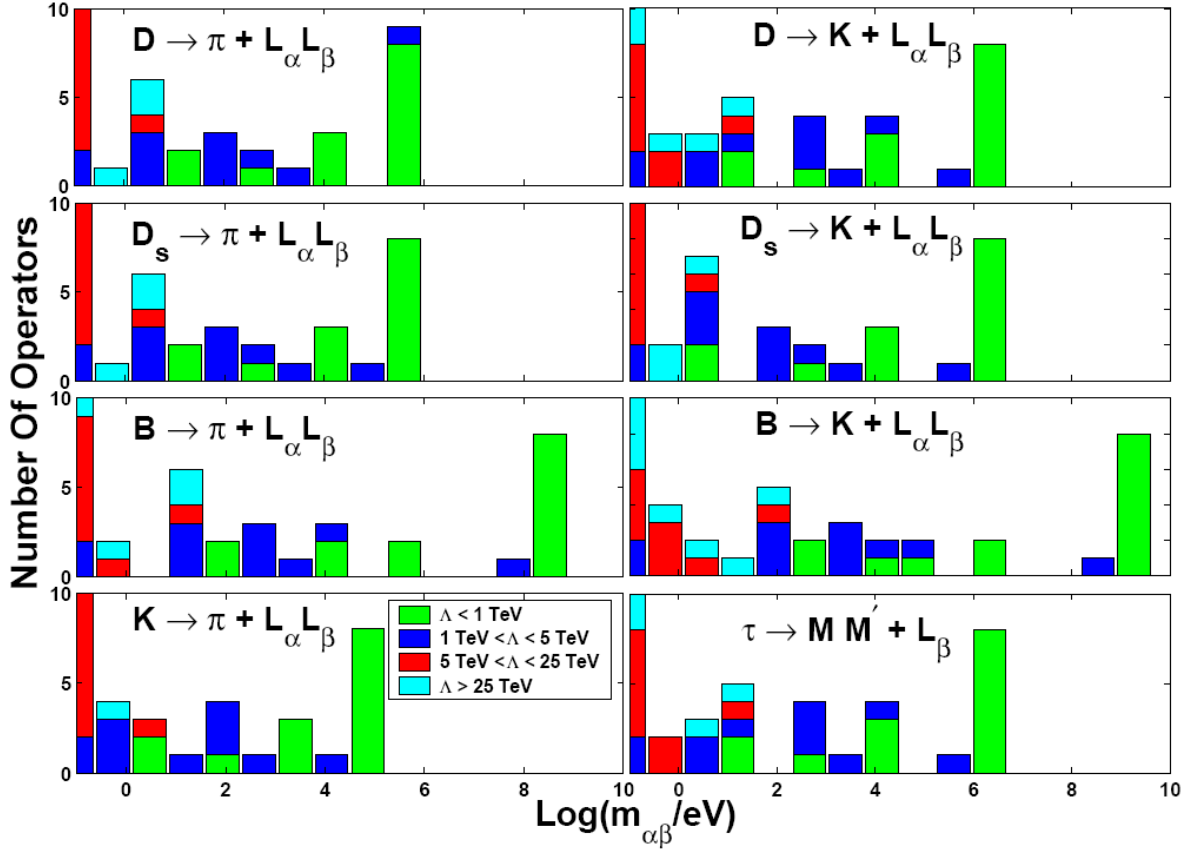


Figure 3.6. $m_{\alpha\beta}^{\text{eff}}$ distribution for several rare LNV meson and τ decays. Calculations assumed the charge lepton flavors $\ell_{\alpha\beta} = \mu e$, while the τ decay histogram (lower right-hand panel) was obtained assuming the final state mesons $MM' = KK$. The histogram bars are color-coded by suppression scale. Current bounds on these processes are typically above 1 TeV and are not visible at these small scales.

important. Note that the horizontal axes are relatively fixed for easy comparison and that the vertical direction is truncated and does not reflect the true “height” of the lowest mass bar (order one hundred operators).

Specifically, I present effective Majorana neutrino mass distributions for the processes, reading down the panels from left to right, $D \rightarrow \pi + \ell_{\alpha}^{\pm} \ell_{\beta}^{\pm}$, $D \rightarrow K + \ell_{\alpha}^{\pm} \ell_{\beta}^{\pm}$, $D_s \rightarrow \pi + \ell_{\alpha}^{\pm} \ell_{\beta}^{\pm}$, $D_s \rightarrow K + \ell_{\alpha}^{\pm} \ell_{\beta}^{\pm}$, $B \rightarrow \pi + \ell_{\alpha}^{\pm} \ell_{\beta}^{\pm}$, $B \rightarrow K + \ell_{\alpha}^{\pm} \ell_{\beta}^{\pm}$, $K \rightarrow \pi + \ell_{\alpha}^{\pm} \ell_{\beta}^{\pm}$, as well as the rare τ decay,

$\tau^\pm \rightarrow MM' + \ell_\beta^\mp$.² Here the final state leptons can be of any flavor allowed by energy conservation. Since, as previously discussed and explicitly verified numerically, the specific details of the distributions are mainly dictated by kinematics and CKM matrix elements, these results are robust under changes in the final state lepton flavors. The τ decay distribution shown in the lower right panel is representative of all possible decay products including first and second generation charged leptons and light meson states. One should notice the expected general operator trend within each histogram as the characteristic cutoff scale is decreased, as well as the expected peaks near 0.05 eV dominated by light Majorana neutrino exchange. Additionally, each distribution is much “broader” than the one in Fig. 3.4. This observation exemplifies the fact that effective mass calculations depend critically on the underlying process. Indeed, maximum m_{ee}^{eff} values can reach nearly 10^{10} eV for the $B^+ \rightarrow K^- + e^+e^+$ decay but only 10^3 eV for $\beta\beta 0\nu$. Current upper bounds for m^{eff} from these processes, mostly well above one TeV, are well beyond the largest operator predictions here, ranging from $m_{e\mu}^{\text{eff}} < 0.09$ TeV for the case of $K^+ \rightarrow \pi^- e^+ \mu^+$ to $m_{\mu\mu}^{\text{eff}} < 1800$ TeV for the case of $B^+ \rightarrow K^- \mu^+ \mu^+$ [33]. It is curious that the best meson decay bounds come from rare LNV kaon process but, as can be seen in the lower left panel of Fig. 3.6, these yield by far the lowest predictions. Future experiments have the potential for observing LNV for a select few operators only provided vast improvements in meson production luminosities. Current and upgraded B-factories [47] are expected to provide the most significant improvements, considering the large derived B -meson effective masses shown in Fig. 3.6. Still, the best cases from the figure yield only the tiny

²The actual calculations displayed in Fig. 3.6 assumed the charge lepton flavors $\ell_\alpha \ell_\beta = \mu e$, while the τ decay histogram (lower right-hand panel) was produced assuming the final state mesons $MM' = KK$.

branching fraction 1.8×10^{-17} for the case of the rare decay $B^+ \rightarrow \pi^- e^+ \mu^+$, nearly eleven orders of magnitude below the current experimental limit of 1.3×10^{-6} [34].

Another possible search mode involves the decay of the Z -boson into LNV final states. The dominant contributions to this process are generally unrelated to the reactions summarized in Eq. (3.1) and shown schematically in Figs. 3.3 and 3.5. While there is a slight connection between them as one can always attach a Z -boson to various fermion lines in each diagram, there are potentially large lower order contributions arising within the operators themselves. The latter, when present, can easily overtake the associated “golden mode” counterparts. In this context, such processes can be thought of as the decay of the longitudinally polarized Z -boson. Strict bounds exist on such decays from the LEP-I [48] and SLD [49] experiments. Each element of the operator set predicts decays into final state fermions with total lepton number $L = 2$. The dilepton pair can be of any flavor and is generally accompanied by two or four additional fermion states, depending on the dimension of the operator. I restrict our discussion to the dimension-eleven operators comprising the majority of the sample, as these are typically suppressed by lower cutoff Λ_ν scales and, equally important, explicitly contain Higgs doublets in their field content. In this case, tree-level decays result in a six-fermion final state which suffers from a large phase space suppression and cumbersome multiplicities that are likely to render even the most sophisticated search ineffective. The only possibility of this type that yields a charged dilepton signal is $Z \rightarrow \ell_\alpha^\pm \ell_\beta^\pm q\bar{q}q\bar{q}$ (quarks of all allowed flavors implied), but many other possibilities exist involving invisible final state neutrinos. A little thought also reveals that closing fermion loops in an attempt to obtain simpler final states and thus render the analysis more tractable will necessarily result in final state neutrinos.

Therefore, the majority of the Z -boson LNV decay channels involve invisible final states with practically undetermined total lepton number. The prospect of direct discovery by these means seems dismal, but indirect constraints on LNV are still possible from bounds on the Z -boson invisible decay width. There is currently a statistically insignificant, but nonetheless captivating, 2σ deviation between the observed invisible decay width and SM expectations assuming three light neutrino species [34]. The experimentally extracted branching ratio was found to be slightly *smaller* than its predicted value so that a new LNV contribution of the form $Z \rightarrow \nu_\alpha \nu_\beta$ would push the invisible branching ratio in the “wrong” direction. From these bounds the decay width of any new contribution to the Z -boson decay is constrained to be less than 2.0 MeV at the 95% confidence level [34, 50]. A quick estimate reveals that this constrains the dominant LNV amplitudes $A_Z < \sqrt{4\pi(2.0 \text{ MeV}/M_Z)} \sim 0.53$. For the dimension-eleven operators of interest, the largest possible amplitude is of order $y^2/(16\pi^2)^2(v/\Lambda)^3$ where y is an arbitrary fermion Yukawa coupling and four powers of the cutoff scale Λ are removed by divergences in the closed diagram loops. The constraint above translates into $y^2(v/\Lambda)^3 < 4.1 \times 10^2$, which is easily evaded by even the best case scenario of $y = y_t \approx 1$ and $\Lambda \approx v$. Experimental bounds on Γ_{inv} must be improved by a factor of a million before they start significantly constraining LNV (under the assumptions made here). This result holds for virtually all possible flavor structures. I conclude that rare Z -boson decays are not practical discovery modes for the LNV effects considered here, but look to future rare Z -boson decay studies for more information.

In a similar way, one can also dismiss the case of rare W -boson decays as promising probes of LNV. As in the Z -boson case, the W -boson can decay into a variety of $L = 2$

final states proceeding either through couplings to left-handed fermion lines or explicit operator content. Here, however, there is no six-fermion, same-sign dilepton final state with no neutrinos due to conservation of charge and weak isospin, so the lowest order observable mode is already loop suppressed to $W^- \rightarrow \ell_\alpha^- \ell_\beta^- + q\bar{q}$. Current W -boson decay bounds are far too weak to constrain such suppressed LNV [34] and are not likely to improve to the level implied by the operators under consideration, which predict the tiny decay rate $\Gamma_{LNV} \leq m_W(4\pi)/(16\pi^2)^5(v/\Lambda)^{10} \approx 10^{-5}$ MeV in the best case scenario of electroweak scale Λ_ν . I also point out that, contrary to the Z -boson decay limits, there are no robust, indirect bounds that can be used to constrain LNV in the case of the W -boson. Note that, despite dismal prospects for gauge boson decay driven LNV discovery within the minimal framework of “natural” effective operators, one can still construct theoretically well-motivated models that will yield observable signals. Particularly, in a weak-scale seesaw mechanism (\mathcal{O}_1), the new degrees of freedom, comprised mostly of Majorana gauge singlet fermions (right-handed neutrinos), can mediate visible, $\Delta L = 2$, W -boson mediated processes with little or no scale/loop suppression. This class of model is analyzed in [51] and is exempt from the discussion outlined here.

3.2.3. Collider LNV Signatures

If neutrino masses are a consequence of ultraviolet physics related to cutoff scales around the TeV scale, I expect future high energy collider searches to directly access the new LNV physics. For example, the direct, resonant, production of new states could lead to rather spectacular signals of these models. It would also indicate the breakdown of the effective field theory approach undertaken here. To pursue such possibilities, one must

assume a specific ultraviolet sector and study its signatures and implications on a case by case basis. In the looming shadow of the LHC, [52] and the more distant ILC [53], such an analysis is highly warranted but will not be pursued here. Instead, I assume that the masses of new ultraviolet degrees of freedom remain out of the reach of next-generation accelerator experiments. Such a situation can be easily accommodated within the context of the preceding results, considering the order of magnitude nature of the Λ_ν estimates.

I will concentrate on the process $e^-e^- \rightarrow q\bar{q}q\bar{q}$ (which will usually manifest themselves as jets) with no missing energy in an ILC-like environment [53] with a center-of-mass energy of 1 TeV and an integrated luminosity of 100 fb^{-1} . I also make the oversimplifying assumption that the detector system has equal acceptance to all quark flavors, and the ability to efficiently distinguish quarks, gluons and τ s. By summing over all possible quark final states it is simple to estimate the total LNV cross section for each effective operator, assuming it is responsible for neutrino masses. Such searches can be complemented by looking at $e^-e^- \rightarrow W^-W^-$, which have been discussed in detail in the literature [54]. As discussed in Sec. 3.2.2, the different LNV operators couple to one or more gauge bosons via an appropriately closed fermion loop or direct coupling to the Higgs doublet field.

Charge and baryon number conservation dictate that the two quarks in $e^-e^- \rightarrow q\bar{q}q\bar{q}$ are down-type quarks, while the two antiquarks are up-type antiquarks. At the parton level, the scattering process is similar to $\beta\beta 0\nu$, which motivates exploiting simple variations of the diagrams in Fig. 3.3 in order to calculate the relevant amplitudes, as was done in Sec. 3.2.2. Here, the extensions are obvious: use crossing symmetry to rotate all lepton lines into the initial state and all quark lines to the final state taking special care to insert appropriate CKM matrix elements where needed. Due to the large characteristic

momentum transfer Q of the e^-e^- scattering, one must also “expand” the electroweak vertices and account for gauge boson propagation. With this in mind, the amplitude calculations can be carried over directly from the previous sections. Specific results are, however, quite distinct due to the higher center-of-mass energies involved. In the language of the underlying diagrams mediating this reaction, for diagrams characterized by TeV cutoff scales, diagram D_9 , if allowed at tree-level, will dominate the rates. As in the previous cases, for intermediate to high cutoff scales, general diagram dominance must be addressed on a case by case basis. It is important to appreciate that, since these are non-renormalizable effective interactions, cross-sections grow with center-of-mass energy. For this reason, I expect many of the low cutoff scale operators to yield observably large signals at the ILC.

Fig. 3.7 shows the $e^-e^- \rightarrow q\bar{q}q\bar{q}$ cross-section distribution, in femtobarns, at the ILC, calculated for all 129 of the analyzed LNV operators. Once again, the extracted value of the cutoff energy scale Λ_ν assuming constraints from neutrino masses are color-coded to indicate operators associated with a low ($\Lambda_\nu \lesssim 10$ TeV) or high ($\Lambda_\nu \gtrsim 10$ TeV) ultraviolet cutoff. Each bar is also labeled with the respective constituent operators, for convenience. Note that the vertical axis is truncated at fifteen operators (the left-most bin is over 60 operators high) to help clearly display relevant features of the plot. I also highlight the potential reach (defined as cross-section greater than the inverse of the integrated luminosity) of the ILC with a broken vertical line, assuming 100 fb^{-1} of integrated luminosity. This particular ILC luminosity value should be considered as a loose lower bound, introduced to give a feeling for the observable scales involved. It has

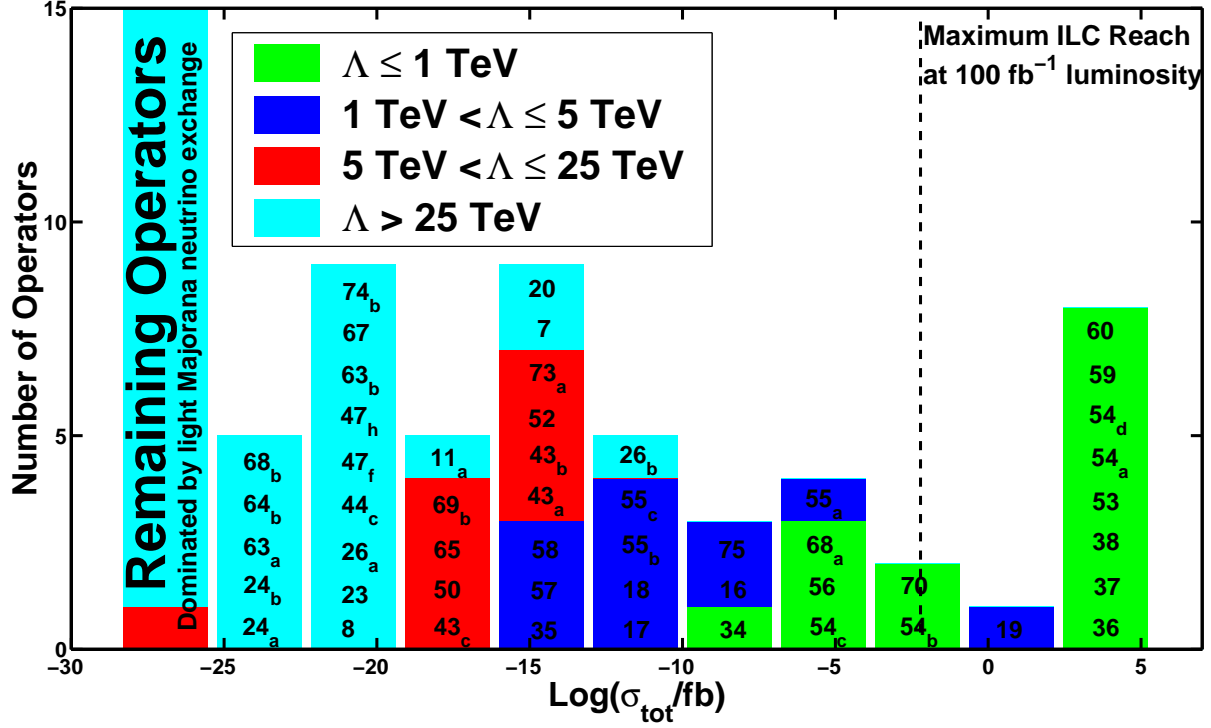


Figure 3.7. Distribution of total cross-section for the process $e^-e^- \rightarrow q\bar{q}q\bar{q}$ and no missing energy at an e^-e^- collider with 1 TeV of center-of-mass energy. Estimates were obtained assuming the scales Λ_ν derived in Sec. 3.1, as well as order one coupling constants. The histogram bars are labeled with operator names and color-coded by Λ_ν cutoff scale. Also shown (broken vertical line) is the reach of such an experiment assuming 100 fb^{-1} of integrated luminosity. The vertical axis is truncated to best display the relevant features of the plot.

recently been argued, for example, that a realistic machine should be able to outperform this estimate by over an order of magnitude [53].

A glance at Fig. 3.7 reveals that it generally adheres to the expected correlation of decreasing Λ_ν scales with increasing LNV rates, similar to what is observed for other LNV observable (*e.g.*, Fig. 3.4). The similarities between the different processes extend beyond mere trends to the specific ordering of the operators within each histogram. This

reflects the common underlying interactions that drive these processes. The operators on the far right of the plot, topping off the highest cross-sections, are exactly those operators with the largest m_{ee}^{eff} , now “split” into three different bars. The large bar just below 10^5 fb is composed of sub-TeV scale operators with tree-level diagram D_9 -like fermion content. Slightly smaller are the expectations for \mathcal{O}_{19} , again dominated by diagram D_9 , but characterized by a slightly larger Λ_ν scale (around one TeV). Moving down in cross-section, this is followed by the low cutoff scale operators $\mathcal{O}_{54b,c}$ and \mathcal{O}_{70} , dominated by a combination of diagrams D_6 and D_7 . On the opposite end of the plot I point out the large bar below 10^{-25} fb, composed mainly of operators associated to high cutoff scales ($\Lambda_\nu > 25$ TeV). The contributions of these operators are dominated by light Majorana neutrino exchange, but their histogram bar contain far fewer models than their $\beta\beta 0\nu$ counterpart, as many of the latter have been driven up due to new diagram D_4 and D_5 contributions. In general, the large center-of-mass energies tend to magnify differences between interaction rates that were not relevant in low-energy observables. This naively suggests that high energy probes have a higher potential for distinguishing different models.

There are eleven operators that lead to an observably large (as defined earlier) $e^-e^- \rightarrow q\bar{q}q\bar{q}$ cross-section at the ILC. Note that all of these were already “ruled out” by current $\beta\beta 0\nu$ searches. As discussed in Sec. 3.2.1, however, these bounds only effectively limit the couplings of the new physics to first generation of quarks and leptons, and hence, if such a scenario is realized in nature, one should still expect large contributions from decay modes that lead to second and third generation final state quarks. In fact, even one such heavy quark is enough to bypass the constraints from $\beta\beta 0\nu$ for several effective

operators. Such reasoning implies that constraints on the new physics flavor structure can be made quite strong at a linear collider via analyzes of the flavor of the final state quarks. By identifying and comparing the outgoing quark flavor one can extract individual limits on quark-lepton coupling constants within the operators. Additionally, kinematics can be used as a further operator probe. For example, one can potentially determine the dominant underlying LNV diagram (say D_6 , D_7 or D_9) by checking whether the various kinematic distributions are characteristic of W -boson exchange.

The ILC can cleanly select or discard some LNV scenarios. This characteristic is further enhanced by considerations of initial electron polarization. Planned linear colliders have the ability to produce partially polarized beams (80% polarization for e^- , 40% for e^+ [53, 55]). The power of a high energy polarized e^-e^- beam is in model identification and rejection. Of all operators that yield observably large cross-sections, the $e_L^-e_L^-$ mode can only probe \mathcal{O}_{53} , and therefore any positive LNV signal cleanly identifies this as the operator chosen by nature. In a similar way, the ILC running in its $e_L^-e_R^-$ mode can easily observe LNV from \mathcal{O}_{19} , \mathcal{O}_{54a} , \mathcal{O}_{54d} , \mathcal{O}_{59} and \mathcal{O}_{60} ; and to a lesser extent, operators \mathcal{O}_{54b} and \mathcal{O}_{70} , and possibly even \mathcal{O}_{54c} . Finally the $e_R^-e_R^-$ mode can probe operators \mathcal{O}_{36} , \mathcal{O}_{37} and \mathcal{O}_{38} . Within this framework, any LNV detected in one ILC polarization mode will generally not be seen in the others. This statement also applies to resonantly enhanced low scale operators that lie outside the observability window.

While e^-e^- collisions only probe effective operators that “talk” to first generation leptons, there are several lepton collider processes that allow one to explore other members of the charged lepton family. Future high energy muon colliders [56] could, in principle, also be used to study LNV. In this case, all of the preceding discussions regarding the

ILC are applicable. Electron linear collider facilities can also be used to study γe^- and $\gamma\gamma$ collisions [57]. γe^- collisions can be used to probe $\gamma e^- \rightarrow \ell_\alpha^+ + X$ (and hence the “ $e\alpha$ ” structure of different LNV operators), while $\gamma\gamma \rightarrow \ell_\alpha^\pm \ell_\alpha^\pm + X$ probes all the different α, β charged lepton flavors. For $\gamma\gamma$ collisions, for example, considering projected ILC-like collider parameters, one would expect the same operator distribution as Fig. 3.7, shifted down in cross-section by, roughly, a factor of $\alpha^2 \sim 10^{-4}$. Thus, a handful of operators should be testable at a future $\gamma\gamma$ collider assuming 100 fb^{-1} of integrated luminosity.

The preceding analyses carry over to the case of hadron colliders, such as the LHC, in a relatively straightforward way. The LHC, or Large Hadron Collider, is a proton–proton machine that will operate at a center-of-mass energy of 14 TeV and a characteristic integrated luminosity around 100 fb^{-1} [52] (in its high luminosity mode). The relevant LNV variants of Eq. (3.1) are $dd \rightarrow \ell_\alpha^- \ell_\beta^- uu$ and $uu \rightarrow \ell_\alpha^+ \ell_\beta^+ dd$ with no missing energy. Of course, at center-of-mass energies well above a TeV, the proton–proton collisions are dominated by the gluon content of the proton, so most interactions at the LHC will be initiated by gluon–gluon and gluon–quark scattering. The dominant LNV subprocesses are $qg \rightarrow \ell_\alpha^\pm \ell_\beta^\pm q\bar{q}q$ and $gg \rightarrow \ell_\alpha^\pm \ell_\beta^\pm q\bar{q}q\bar{q}$ and are illustrated in diagrams (a) and (b) of Fig. 3.8, respectively. These are characterized by similar final states as the quark–quark scattering reactions but, given that there is no explicit gauge boson field content in the LNV operators in question (Table 3.1), their amplitudes are proportional to unimportant order α_s and α_s^2 coefficients, respectively. The parton level diagram (c) shows the related process $gg \rightarrow \ell_\alpha \nu_\beta + q\bar{q}$. The rate for this process can be estimated, relative to its four jet cousins, by exchanging a final state phase space suppression for a single loop suppression. In all three diagrams depicted in Fig. 3.8, the LNV interaction regions

represented by large grey dots contain all of the diagrams discussed earlier, meaning that the operator amplitudes calculated for the ILC can be recycled in this analysis. While all three bare diagrams are characterized by rates of the same order of magnitude diagram (c) leads to missing transverse energy and potentially undetermined final-state lepton number, rendering it a less than optimal experimental search mode. Note that, in all of these cases, the external, and internal, fermions outside of the LNV interaction region can be of any flavor. Therefore, hadron collider experiments have, in principle, access to *all* LNV operator parameters. Cleanly identifying and constraining all said parameters should prove quite difficult for all but the most obvious signatures. The above statements regarding signals at the LHC are also applicable at the Tevatron with some minor, but important, modifications. The Tevatron's $p\bar{p}$ collisions are at a much lower center-of-mass energy, roughly 2 TeV, while the total expected integrated luminosity, less than 10 fb^{-1} per experiment, is orders of magnitude smaller. These factors lead to much lower amplitudes, reduced by approximately a factor of $(Q_{\text{Tevatron}}/Q_{\text{LHC}})^5 \approx 10^{-5}$.³ The smaller center-of-mass energy also limits the Tevatron's ability to directly produce new physics states. With this in mind I conclude that the Tevatron has little or no chance of discovering LNV (within this minimal framework).

A detailed set of predictions for the LHC would require a much more refined analysis, including the effects of parton structure functions, flux distributions, and backgrounds, and as such is beyond the scope of this general survey. I would, however, like to point out that some of the reactions outlined here are subject to large background rates. While SM

³Strictly speaking one must also account for the proton's structure functions at the Tevatron's energy scale. Unlike the LHC, where collisions are dominated by gluon-gluon interactions, proton collisions at the Tevatron are dominated by valence quark interactions. These considerations do not affect our conclusions.

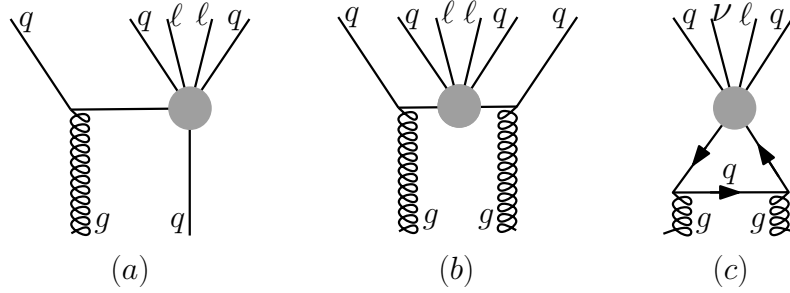


Figure 3.8. Parton level gluon–gluon and gluon–quark LNV interactions relevant at high energy hadron colliders. Each of these yields a same sign dilepton signal with jets and no missing energy. Notice that the final state flavor structure is completely arbitrary under the assumption of random order one coupling constants.

processes are lepton number conserving, many can fake the LNV signals in the complicated environment of a high energy hadronic interaction. The requirement of no missing final state energy is particularly hard to accommodate as some energy is always lost down the beampipe. As is typically done, one must rely on the less restrictive conservation of transverse momentum in order to constrain invisible states, such as neutrinos. SM same-sign dilepton production processes arising from, say, W -boson pair production, are serious potential sources of background. Furthermore, it is impossible to predict correlations among final state jets without selecting a particular operator and underlying model of new physics, making it difficult to impose general cuts to reduce other hadronic backgrounds. Of course, some of the low scale LNV operators yield large enough total cross-sections that even crude analyses may suffice to reveal their existence. I conclude by pointing out that a large amount of recent work has been dedicated to LNV searches at collider facilities [58]. Most of these approach the subject from the perspective of sub-TeV mass, mostly sterile Majorana neutrinos that mix with the active neutrinos and are thus related to light neutrino masses via the seesaw mechanism [7]. This amounts to one example that

leads to the dimension-five operator \mathcal{O}_1 , but where one assumes that the propagating degrees of freedom are twelve or thirteen orders of magnitude lighter than the ultraviolet cutoff scale Λ_ν .⁴ In this case, LNV interactions are dominated by diagram D_ν of Fig. 3.3 (where heavy (weak scale) neutrinos are also exchanged), and as such one should make use of specific kinematic cuts to reduce background rates. These cuts, however, may also remove LNV signals resulting from many of the scenarios explored here, particularly those whose rates are dominated by D_9 at tree-level. I urge experimentalists to account for this possibility while analyzing future data sets.

3.3. Neutrino mixing

Table 3.1 contains predictions for *all* the entries $m_{\alpha\beta}$, the Majorana neutrino mass matrix. These are computed in the weak basis where the weak interactions and the charged-lepton Yukawa couplings are diagonal, so that the eigenvalues of the neutrino mass matrix are the neutrino masses (bounded by oscillation experiments and, say, precision measurements of tritium beta-decay [23]), while its eigenvectors determine the neutrino mixing matrix, constrained mostly by oscillation experiments. Since different LNV effective operators predict different flavor-structures for the neutrino mass matrix, there is the possibility to constrain the different scenarios with existing oscillation data [16]. While I can only predict the values of $m_{\alpha\beta}$ within, at best, an order of magnitude, it is still possible to extract useful information from the derived large scale structure of the expressions. In particular I can test the hypothesis of whether λ values associated to different lepton flavors are allowed to be of the same order of magnitude. In order to

⁴This can be achieved in two different ways. Either the new physics is very weakly coupled, or the new physics – SM couplings are finely-tuned [29]. In order to observe right-handed neutrinos in colliders, the latter must be realized.

obtain more accurate predictions and further probe the fine details of lepton mixing one must succumb to specific models, beyond the scope and philosophy of this analysis.

The mass matrix for the three light Majorana neutrinos can be reconstructed from nine observables: three masses m_1, m_2, m_3 , taken to be real and positive; three (real) mixing angles $\theta_{12}, \theta_{23}, \theta_{13}$; and three CP-violating phases δ, ϕ_2, ϕ_3 . Here, δ is a so-called Dirac phase that is generally present in the system regardless of the neutrino's nature (Majorana or Dirac fermion), while ϕ_1, ϕ_2 are so-called Majorana phases, only present if the neutrinos are Majorana particles (which is the case of all scenarios under consideration here). Oscillation data determine with relatively good precision $\theta_{12}, \theta_{23}, \Delta m_{12}^2 \equiv m_2^2 - m_1^2$ and $|\Delta m_{13}^2| \equiv |m_3^2 - m_1^2|$. I define neutrino masses such that $m_1 < m_2$ and $\Delta m_{12}^2 < |\Delta m_{13}^2|$, so that the sign of Δm_{13}^2 remains as an observable which characterizes the neutrino mass hierarchy (“normal” for $\Delta m_{13}^2 > 0$, “inverted” for $\Delta m_{13}^2 < 0$). See, for example, [14] for details. As for the third mixing angle, $\sin^2 \theta_{13}$ is constrained to be less than 0.025 (0.058) at 2σ (4σ) from a three neutrino global oscillation analysis [16]. A considerable amount of uncertainty remains. In particular I have only upper bounds on the absolute neutrino mass scale, from kinematical measurements such as tritium beta decay [17, 18], plus cosmological observations [19, 20, 21, 22]. Finally, the three CP violating phases are completely unconstrained, and I have no information regarding the neutrino mass hierarchy.

The above experimental results allow for several different “textures” for $m_{\alpha\beta}$ in our weak basis of choice (see, for example, [59]). The purpose of this section is to discuss whether any of the textures predicted by the different LNV effective operators is “ruled out” by current observations. Most of the analyzed operators imply “anarchic” [24]

neutrino masses. This simply means that all elements of the neutrino mass matrix are uncorrelated and of the same order of magnitude. This hypothesis is known to “fit” the current data very well [24]. It will be further challenged by searches for θ_{13} (the anarchic hypothesis favors large θ_{13} values) and probes that may reveal if the neutrino masses are hierarchical or whether two or three of the masses are almost degenerate (anarchy naively predicts the former). If future data strongly points towards non-anarchic $m_{\alpha\beta}$, I will be forced to conclude that there is nontrivial “leptonic” structure in the dimensionless coefficients λ of most of the LNV operators considered here.

Many of the operators associated with a low neutrino-mass related cutoff scale ($\Lambda_\nu \leq 10$ TeV), on the other hand, naively predict more structured neutrino mass matrices.

Operators

$$\mathcal{O}_7, \mathcal{O}_8, \mathcal{O}_{19}, \mathcal{O}_{20}, \mathcal{O}_{34}, \mathcal{O}_{35}, \mathcal{O}_{54_{a,b,c,d}}, \mathcal{O}_{55_{a,b,c}}, \mathcal{O}_{56}, \mathcal{O}_{57}, \mathcal{O}_{58}, \mathcal{O}_{59}, \mathcal{O}_{60}, \mathcal{O}_{70}, \mathcal{O}_{75}, \quad (3.1)$$

which radiatively generate neutrino mass elements proportional to distinct charged lepton Yukawa coupling (y_e, y_μ, y_τ), yield mass matrices m such that

$$m \propto \begin{pmatrix} y_e & y_\mu & y_\tau \\ y_\mu & y_\mu & y_\tau \\ y_\tau & y_\tau & y_\tau \end{pmatrix}. \quad (3.2)$$

Additionally, models described at low energies by \mathcal{O}_{36} , \mathcal{O}_{37} and \mathcal{O}_{38} generate neutrino masses proportional to both associated charged Yukawa couplings, such that

$$m \propto \begin{pmatrix} y_e y_e & y_e y_\mu & y_e y_\tau \\ y_e y_\mu & y_\mu y_\mu & y_\mu y_\tau \\ y_e y_\tau & y_\mu y_\tau & y_\tau y_\tau \end{pmatrix}. \quad (3.3)$$

The strongly hierarchical nature of the charged lepton masses ($y_e \ll y_\mu \ll y_\tau$), implies that the $m_{\alpha\beta}$ elements of Eqs. (3.2) and (3.3) are expected to be hierarchical as well. In particular, the ee matrix element, m_{ee} , proportional to y_e or y_e^2 is, for all practical purposes, negligibly small¹ in both of these cases. On the other hand, it is well known that only a normal neutrino mass hierarchy is consistent with vanishing m_{ee} [60], so that both Eqs. (3.2) and (3.3) predict the neutrino mass ordering to be normal. In the absence of extra structure, scenarios characterized by the LNV operators listed in Eq. (3.1) plus \mathcal{O}_{36} , \mathcal{O}_{37} and \mathcal{O}_{38} will be ruled out if future data favor an inverted mass hierarchy, or if the neutrino masses end up quasi-degenerate (regardless of the hierarchy). As will become clear shortly, Eqs. (3.2) and (3.3) predict that the lightest neutrino mass (m_1 in this case) is small ($\lesssim \sqrt{\Delta m_{12}^2}$).

A more detailed analysis reveals that naive expectations from Eqs. (3.2) are already disfavored, while those from Eqs. (3.3) are virtually excluded. Assuming the normal hierarchy and very small m_{ee} , one can find a relation between the neutrino mass eigenstates and the oscillation parameters, thus reducing the number of free parameters in the mass matrix by one. Consider the diagonalization of the neutrino mass matrix defined by

¹Quantitatively, in the scenarios under investigation, m_{ee} values are, respectively, up to order one corrections, $y_e/y_\tau \sim 10^{-4}$ and $y_e^2/y_\tau^2 \sim 10^{-7}$ times the characteristic mass scale of the mass matrix.

$m_{\alpha\beta} = UM^DU^T$ with $M^D = \text{diag}(m_1, m_2e^{2i\phi_2}, m_3e^{2i\phi_3})$ and U the neutrino mixing matrix, expressed in the PDG parameterization. In this case,

$$m_{ee} = m_1 \cos^2 \theta_{12} \cos^2 \theta_{13} + m_2 \sin^2 \theta_{12} \cos^2 \theta_{13} e^{2i\phi_2} + m_3 \sin^2 \theta_{13} e^{2i(\phi_3 - \delta)}. \quad (3.4)$$

Setting $m_{ee} = 0$, one can solve for m_1 and one of the Majorana phases. Recalling that, for the normal mass hierarchy, $m_2 = \sqrt{m_1^2 + \Delta m_{12}^2}$ and $m_3 = \sqrt{m_1^2 + \Delta m_{13}^2}$, and assuming small θ_{13} and $\eta \equiv \sqrt{\Delta m_{12}^2 / \Delta m_{13}^2}$,

$$\begin{aligned} \frac{m_1}{\sqrt{\Delta m_{13}^2}} &\approx \eta \frac{\sin^2 \theta_S}{\cos^{1/2} 2\theta_S} - \theta_{13}^2 \frac{\cos^2 \theta_S}{\cos 2\theta_S} \cos[2(\phi_3 - \delta)], \\ \phi_2 &\approx \frac{\pi}{2} + \frac{1}{2} \arctan \left(\frac{4\theta_{13}^2 \sqrt{\cos 2\theta_S}}{\eta \sin^2 2\theta_S} \sin[2(\phi_3 - \delta)] \right). \end{aligned} \quad (3.5)$$

One can easily obtain approximate expressions for the other neutrino masses (m_2, m_3) and hence all elements $m_{\alpha\beta}$. Upon substituting the numeric best fit oscillation parameters to

avoid introducing a needlessly cumbersome expression, I get

$$\begin{aligned}
\frac{m_{\alpha\beta}}{\sqrt{\Delta m_{13}^2}} &= 0.5e^{i2\phi_3} \begin{pmatrix} 0 & 0 & 0 \\ 0 & 1 & 1 \\ 0 & 1 & 1 \end{pmatrix} + 0.71\theta_{13}e^{-i(\delta-2\phi_3)} \begin{pmatrix} 0 & 1 & 1 \\ 1 & 0 & 0 \\ 1 & 0 & 0 \end{pmatrix} \\
&+ 0.45\eta \begin{pmatrix} 0 & -1.3 & 1 \\ -1.3 & -1 & 0.61 \\ 1 & 0.61 & -0.36 \end{pmatrix} \\
&+ 0.91\theta_{13}^2 \cos[2(\delta - \phi_3)] \begin{pmatrix} 0 & 1 & -0.89 \\ 1 & 0.12 & 0.02 \\ -0.89 & 0.02 & -0.12 \end{pmatrix} \\
&+ 1.2i\theta_{13}^2 \sin[2(\phi_3 - \delta)] \begin{pmatrix} 0 & 1 & -0.67 \\ 1 & 1.2 & -0.83 \\ -0.67 & -0.83 & 0.56 \end{pmatrix}.
\end{aligned} \tag{3.6}$$

Eq. (3.7) suggests a clear hierarchy among the mixing matrix elements. The four, lower box-diagonal $\mu - \tau$ elements dominate, followed by the off-diagonal $e\mu$ and $e\mu$ entries, and finally the vanishingly small m_{ee} . Except for the vanishingly small m_{ee} , which was required *a priori*, all of the remaining properties follow directly from the experimentally determined mixing parameters. Among the dominant $\mu - \tau$ submatrix, Eq. (3.7) predicts that all entries are equal up to small order η and θ_{13} corrections. The magnitude, and sign, of these “breaking terms” can be tuned with the phases ϕ_3 and δ , and to a lesser extent

by varying η and θ_{13} within their allowed ranges. On the other hand, the relative sizes of $m_{e\mu}$ and $m_{e\tau}$ are expected to be similar but not identical, *i.e.*, $m_{e\mu} \sim m_{e\tau} \sim (m_{e\mu} - m_{e\tau})$.

While some of the gross features of Eq. (3.7) are shared by Eq. (3.2) and Eq. (3.3), a finer analysis reveals several disagreements. The major discrepancy lies in the required relations among the matrix elements. Eq. (3.2) predicts that all $m_{\alpha\tau}$ elements are equal, while Eq. (3.3) suggests $m_{e\tau} \ll m_{\mu\tau} \ll m_{\tau\tau}$. Both of these contradict, in different ways, the experimental constraint $m_{e\tau} \ll m_{\mu\tau} \approx m_{\tau\tau}$. Additionally, both Eq. (3.2) and Eq. (3.3) predict $m_{ee} \ll m_{\mu\mu} \ll m_{\tau\tau}$, while observations require $m_{ee} \ll m_{\mu\mu} \approx m_{\tau\tau}$. Similarly, both sets of operators suggest $m_{e\mu} \ll m_{e\tau}$ while, experimentally, they are constrained to be similar.

In order to quantify how much Eq. (3.2) and Eq. (3.3) (dis)agree with our current understanding of neutrino masses and lepton mixing, I numerically scanned the allowed mass matrix parameter space assuming the normal neutrino mass hierarchy and constraining $|m_{ee}| \leq y_e/y_\tau \times 1 \text{ eV} \approx 10^{-4} \text{ eV}$. It should be noted that, according to this relation, m_{ee} is allowed to deviate by nearly a factor of ten above naive expectations from mass matrix Eq. (3.2), thus accounting for the possible order of magnitude uncertainties in operator scales and coupling constants. This feature is only included for completeness, as one expects that such m_{ee} excursions from zero will generally have negligible effect on the mass matrix due to the robust nature of Eq. (3.7). Fig. 3.9, a scatter plot of mixing matrix elements, depicts the result of such a scan. Note that I plot the mass ratios with respect to assumed-to-be-dominant $m_{\tau\tau}$ element. The light grey regions of the plot were produced allowing all oscillation parameters to vary within their 95% confidence bounds

[16] and phases to vary within their entire physical range subject to the constraints discussed above. In the purple (dark) region, the phases and reactor mixing angle θ_{13} are allowed to vary while all other mixing parameters are held fixed at their best fit values. I depict the $\sin^2 \theta_{13}$ variation from zero to 0.06 (4σ upper bound [16]) by varying the purple shading from dark to light. It is easy to check that the numeric (Fig. 3.9) and analytic results (Eq. (3.7)) are consistent both qualitatively and quantitatively.

Fig. 3.9 also depicts the predictions from Eq. (3.2) and Eq. (3.3) with red (closed) and blue (open) dots, respectively. As expected, all the predictions from Eq. (3.3) fall near the origin in each panel and are safely excluded. Because expectations from Eq. (3.3) for all $m_{\alpha\beta}/m_{\tau\tau}$ are much smaller than one, I also include the dot coordinate values for both textures within the figure. In order to render the neutrino mass matrix predicted from \mathcal{O}_{36} , \mathcal{O}_{37} and \mathcal{O}_{38} consistent with experimental constraints on neutrino masses and lepton mixing, one is required to choose very hierarchical λ coefficients. In more detail, one needs to choose λ values so that all mixing matrix elements are enhanced relative to the dominant $m_{\tau\tau} \propto y_\tau y_\tau$ by numerical factors that range – for different entries – from 100 to 10^5 . A possible mechanism for achieving this is to suppress third generation couplings to new physics, thus driving up the ratio $m_{\alpha\beta}/m_{\tau\tau}$ along with the required cutoff scale Λ_ν . This procedure would have to be accompanied by a more modest reduction of the couplings of second generation fermions. Basically, I need to impose a flavor structure that “destroys” the naive flavor structure induced by the charged lepton Yukawa coupling hierarchy. I can safely conclude that \mathcal{O}_{36} , \mathcal{O}_{37} , and \mathcal{O}_{38} , which suggest that the neutrino mass matrix has the form Eq. (3.3), are strongly disfavored by current neutrino oscillation

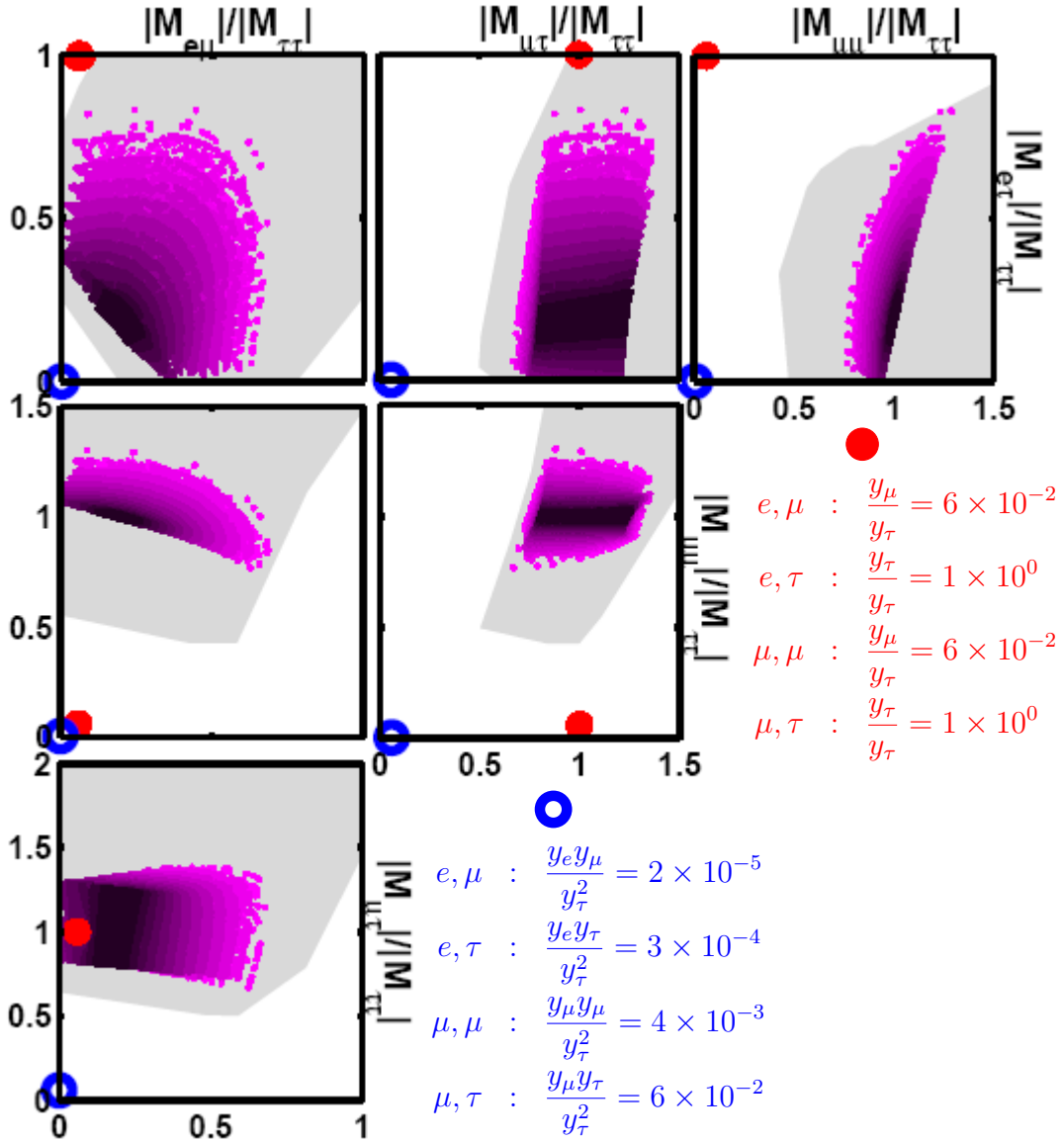


Figure 3.9. Scatter plots of the symmetric Majorana neutrino mass matrix elements normalized to $m_{\tau\tau}$. Each panel is produced assuming the normal mass hierarchy and parameter constraints insuring that $m_{ee} \leq 10^{-4}$ eV. The light grey region is calculated allowing all mixing parameters to vary within their respective 95% confidence intervals. In the purple (darker) regions, the solar and atmospheric parameters are held constant while all phases are scanned within their physical ranges and θ_{13} is varied between zero and its 4σ upper bound. The $\sin^2 \theta_{13}$ variation is illustrated by varying the shading from dark to light. Also indicated by red (closed) and blue (open) dots are the expectations derived from Eqs. (3.2) and (3.3), respectively, along with a listing of their associated coordinate values.

data and, if somehow realized in nature, must be accompanied by a very nontrivial flavor structure.

On the other hand, the operators listed in Eq. (3.1), which predict Eq. (3.2), are not quite as disfavored. In this case the hierarchies among different mass matrix elements are softer, and one can ask whether the red dots in Fig. 3.9 can move toward the experimentally allowed regions with order 1–10 relative shifts. Many of the predictions are already in agreement with experimental constraints, or at least close enough to be easily “nudged” toward acceptable levels with order one coefficients. The figure reveals that only $m_{\mu\mu}$ is predicted to be relatively too small. By enhancing it by a factor of order $y_\tau/y_\mu \sim 20$ one obtains moderately good agreement between Eq. (3.2) and experimental requirements. I therefore conclude that operators listed in Eq. (3.1) are at least marginally allowed by neutrino mixing phenomenology.

While essential for a complete understanding of neutrino masses and mixing, improved measurements of the already determined mixing angles and mass-squared differences will not help to further constrain/exclude any of the LNV scenarios in question. Considering our parameter flexibility, only future neutrino experiments that provide qualitatively new results can aid in this endeavor. In particular, the experimental determination of the neutrino mass hierarchy is essential in order to properly test the scenarios highlighted in this section, as they all predict, in the absence of very non-trivial flavor structure in the LNV sector, the normal hierarchy. Next-generation neutrino oscillation experiments are expected to provide non-trivial information regarding the neutrino mass hierarchy. Most rely on a neutrino/anti-neutrino oscillation asymmetry via Earth matter effects [14, 61], and depend heavily on a sufficiently large θ_{13} mixing angle. The possibility

that θ_{13} is vanishingly small, where the standard approach is ineffective, is addressed in [61] considering both oscillation and non-oscillation probes. In that case, one can hope to discern the neutrino mass spectrum in future neutrino factory [36]/ Superbeam [35] experiments coupled with improved constraints on the effective masses extracted from tritium beta decay [23] and cosmology [19, 20, 21, 22].² Note that these non-oscillation probes can be independently used to constrain LNV models, as they provide information regarding the the magnitude of the lightest mass eigenstate (m_1 [m_3] in the case of normal [inverted] hierarchy). For example, if either cosmological observations or tritium beta decay experiments see evidence for non-zero neutrino masses (in more detail, they constrain $\Sigma = \sum_i m_i$ and $m_{\nu_e}^2 = \sum_i m_i^2 |U_{ei}|^2$ respectively) such that $\Sigma \gg 0.05$ eV or $m_{\nu_e} \gg 0.01$ eV, one would conclude, assuming a normal mass hierarchy, that $m_1 \gg \sqrt{\Delta m_{12}^2}$. This would destroy the possibility of negligibly small m_{ee} , and hence disfavor the operators that lead to mass matrices of the type Eq. (3.2) and (3.3). Currently, Σ and m_{ν_e} are bounded to be below 0.94 eV and 2.0 eV, respectively, but the sensitivity to these observable is expected to significantly improve with next-generation experiments to 0.1 eV [62] and 0.2 eV [63], respectively.

3.4. Phenomenologically interesting operators: Sample Renormalizable Model

Having superficially surveyed a large set of LNV operators, I am now in a position to identify operators with “interesting” phenomenological features for further detailed study.

²One traditionally includes the effective $\beta\beta 0\nu$ mass m_{ee} given by Eq. (3.2) in a neutrino mass hierarchy analysis. However, as discussed in Sec. 3.2.1, m_{ee}^{eff} is a potentially convoluted process-dependent quantity that generally has little (directly) to do with neutrino masses. For this reason, $\beta\beta 0\nu$ constraints cannot be used to determine the neutrino mass spectrum from the point of this analysis.

One subset of potentially interesting operators is characterized by those that, when required to “explain” the observed neutrino masses, are accompanied by a low cutoff scale of, say, less than several TeV. Further requiring a small enough m_{ee}^{eff} in order to evade current $\beta\beta 0\nu$ constraints, this set contains only seven elements: $\mathcal{O}_{17}, \mathcal{O}_{18}, \mathcal{O}_{34}, \mathcal{O}_{35}, \mathcal{O}_{56}, \mathcal{O}_{57}, \mathcal{O}_{58}$. Of these, all but operators \mathcal{O}_{35} and \mathcal{O}_{58} (which lead to the zeroth-order neutrino mass matrix Eq. (3.2) and a suppressed m_{ee}) should provide a positive LNV signal in the next round of double-beta decay experiments, barring specific flavor symmetries or finely-tuned couplings. Furthermore, \mathcal{O}_{56} leads to a $\beta\beta 0\nu$ rate that is higher than what is naively dictated by the values of the neutrino masses. Finally, with the possible exception of \mathcal{O}_{56} which may mediate observable LNV processes at high energy colliders, none of the seven operators above are expected to mediate LNV violating phenomena (as defined here) at accessible rates.

An “orthogonal” subset consists of the higher dimensional operators already “excluded” by $\beta\beta 0\nu$. Not including those operators severely constrained by lepton mixing in Sec. 3.3, this list contains 11 elements: $\mathcal{O}_{16}, \mathcal{O}_{19}, \mathcal{O}_{53}, \mathcal{O}_{54a,b,c,d}, \mathcal{O}_{59}, \mathcal{O}_{60}, \mathcal{O}_{70}, \mathcal{O}_{75}$. Most of these are associated to cutoff scales of order the weak scale, which are likely to already be constrained by different searches for new degrees of freedom with masses around 100 GeV. Even if those are considered to be excluded, $\mathcal{O}_{16}, \mathcal{O}_{19}, \mathcal{O}_{75}$ are “safely” shielded from direct and indirect non-LNV searches,¹ while still mediating potentially observable LNV effects at colliders as long as the new physics does not couple, to zeroth order, to first generation quarks (in order to evade the $\beta\beta 0\nu$ constraints).

¹Generic new degrees of freedom at the weak scale are constrained by direct and indirect searches at high energy colliders (*e.g.*, resonances and effective four-fermion interactions, respectively), flavor-violating (*e.g.*, $\mu \rightarrow e\gamma$), and high precision experiments (*e.g.*, measurements of the anomalous muon magnetic moment).

Regardless of whether these different options for the LNV sector lead to observable LNV phenomena, the low extracted cutoff scale of *all* the operators highlighted above implies that new degrees of freedom should be produced and, with a little luck, observed at the LHC or, perhaps, the ILC. Furthermore, the TeV scale has already been identified as an interesting candidate scale for new physics for very different reasons, including the dark matter puzzle and the gauge hierarchy problem. The fact that, perhaps, the physics responsible for neutrino masses also “lives” at the TeV scale is rather appealing.

In order to study this new physics, as already emphasized earlier, ultraviolet complete manifestations of the physics that leads to the effective operators are required. Here I discuss one concrete example. Other examples (for different effective operators) were discussed in [15]. Given a specific LNV operator, it is a simple matter to write down equivalent renormalizable Lagrangians. I briefly illustrate this procedure by constructing a renormalizable model that will lead to the dimension-eleven operator \mathcal{O}_{56} . It is among the interesting LNV effective operators of the sample highlighted above, since it is currently unconstrained by $\beta\beta 0\nu$ searches regardless of the quark-flavor structure of the operator, while $m_{ee}^{\text{eff}} \gg m_{ee}$ for $\beta\beta 0\nu$. On the other hand, Λ_ν for \mathcal{O}_{56} is very low (below 500 GeV), so that the new degrees of freedom may already be constrained by, for example, Tevatron or LEP data. I will not worry about such constraints henceforth, but will only comment on possible phenomenological problems.

\mathcal{O}_{56} can be accommodated by a wide variety of models, as can be seen from its possible Lorentz structures. In terms of scalar/tensor helicity-violating bilinears $\Gamma_v = 1, \sigma_{\mu\nu}$, and

vector helicity-conserving bilinears $\Gamma_c = \gamma_\mu$, these are

$$\begin{aligned}
\mathcal{O}_{56} = & \{(L^i \Gamma_v Q^j)(d^c \Gamma_v d^c)(\bar{d}^c \Gamma_v \bar{e}^c), (L^i \Gamma_v Q^j)(d^c \Gamma_c \bar{d}^c)(d^c \Gamma_c \bar{e}^c), (L^i \Gamma_v d^c)(Q^j \Gamma_v d^c)(\bar{d}^c \Gamma_v \bar{e}^c), \\
& (L^i \Gamma_v d^c)(Q^j \Gamma_c \bar{d}^c)(d^c \Gamma_c \bar{e}^c), (L^i \Gamma_v d^c)(Q^j \Gamma_c \bar{e}^c)(d^c \Gamma_c \bar{d}^c), (L^i \Gamma_c \bar{d}^c)(Q^j \Gamma_v d^c)(d^c \Gamma_c \bar{e}^c), \\
& (L^i \Gamma_c \bar{e}^c)(Q^j \Gamma_c \bar{d}^c)(d^c \Gamma_v d^c), (L^i \Gamma_c \bar{e}^c)(Q^j \Gamma_v d^c)(d^c \Gamma_c \bar{d}^c), (L^i \Gamma_c \bar{e}^c)(Q^j \Gamma_c \bar{d}^c)(d^c \Gamma_v d^c)\} \\
& \times H^k H^l \epsilon_{ik} \epsilon_{jl}. \tag{3.1}
\end{aligned}$$

It is clear from the chiral field content that these operators depend on combination of helicity-conserving and helicity-violating interactions. In particular, it is impossible to form any of the operators in this long list with only the addition of vector boson states: new heavy scalar and/or tensor particles are probably required if \mathcal{O}_{56} is the proper tree-level manifestation of the LNV physics at low-energies.² Furthermore, the couplings of the new physics fields with one another must be constrained in order to “block” the presence of lower-dimensional tree-level effective operators. This usually implies the existence of new exact (broken) symmetries to forbid (suppress) particular interactions.

Certain Lorentz structures, those containing only Γ_v bilinears, can be realized assuming that the LNV ultraviolet sector contains only heavy *scalar* fields and I concentrate, for simplicity, on this possibility [64]. Simple scalar interactions that can lead to \mathcal{O}_{56} are shown in the diagram in Fig. 3.10. Specifically, these yield the effective operator Lorentz structure $(L^i Q^j)(d^c d^c)(\bar{e}^c \bar{d}^c) H^k H^l \epsilon_{ik} \epsilon_{jl}$ with the introduction of four charged scalar fields, $\phi_1, \phi_2, \phi_3, \phi_4$. The gauge structure is such that, under $(SU(3)_c, SU(2)_L, U(1)_Y)^3$, ϕ_1 transforms as a $(\bar{3}, 3, +1/3)$, ϕ_2 as $(\bar{3}, 1, -2/3)$, ϕ_3 as $(3, 1, -4/3)$, and ϕ_4 as $(\bar{3}, 1, -2/3)$. While

²Other possibilities include heavy vector-like fermions.

³In the case of $U(1)_Y$, ‘transforms as X ’ means ‘has hypercharge X ’.

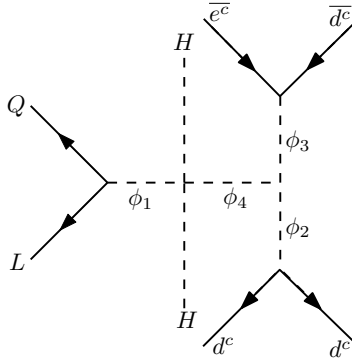


Figure 3.10. Sample scalar interactions that lead to the “interesting” effective operator \mathcal{O}_{56} with the Lorentz structure $(L^i Q^j)(d^c d^c)(\bar{e}^c \bar{d}^c)H^k H^l \epsilon_{ik} \epsilon_{jl}$.

ϕ_2 and ϕ_4 have identical gauge quantum numbers, they have different baryon number ($2/3$ versus $-1/3$). ϕ_1 has baryon number $-1/3$, while ϕ_3 has baryon number $1/3$. Lepton number cannot be consistently assigned as it is explicitly violated by two units.

ϕ_4 , which does not couple to any of the SM fermions, plays an essential role. It acts as a selective “insulator” that connects the various interaction terms in such a way as to only allow certain tree-level higher dimensional SM effective operators. All renormalizable theories that lead to only very high dimensional effective operators contain one or more of these “hidden sector” fields. Note that the new scalar fields should not acquire vacuum expectation values in order to avoid the presence of lower dimensional irrelevant operators that are likely to dominate low-energy phenomenology and – much more important – to prevent the spontaneous breaking of color or electromagnetic charge.

Given the scalar field content as well as its transformation properties under SM global and local symmetries, it is a simple matter to write down the minimal interaction Lagrangian density for the system. A candidate renormalizable Lagrangian is

$$\begin{aligned} \mathcal{L} = & \mathcal{L}^{(SM)} + \sum_i (|D_\mu \phi_i|^2 + M_i |\phi_i|^2) + y_1 QL\phi_1 + y_2 d^c d^c \phi_2 + y_3 e^c d^c \phi_3 + \lambda_{14} \bar{\phi}_1 \phi_4 HH \\ & + \lambda_{234} M \phi_2 \bar{\phi}_3 \phi_4 + h.c. . \end{aligned} \quad (3.2)$$

Each term in Eq. (3.2), including those involving covariant derivatives D_μ , is implicitly assumed to respect the gauge representations of the associated ϕ_i fields, as defined above. The Yukawa-type couplings y_i , as well as the λ_i scalar vertices are dimensionless, and assumed to be of order one, while I assume all scalar masses M_i to be of the same order of magnitude. In this case, $\Lambda \sim M_i$. In the λ_{234} term, an overall mass scale M has been “factored out” and is assumed to be of the same order as the M_i . Note that I neglect generation indices, which are implied. In the case $\lambda_{234} = 0$, lepton number is a classical global symmetry of Eq. (3.2), and one can view this three-scalar coupling as the source of lepton number violation. One may even envision a scenario where lepton number is spontaneously broken by the vacuum expectation value of some SM singlet ϕ_5 scalar field, $\langle \phi_5 \rangle = M$.

Provided all M_i are around 0.5 TeV, as required if this Lagrangian is to “explain” the observed light neutrino masses, LNV is certainly *not* the only (or even the main) consequence of this model. The y_1 and y_3 terms for example, will mediate $\mu \rightarrow e$ -conversion in nuclei at very dangerous levels if their flavor structure is generic. ϕ_2 can be resonantly produced in dd -collisions, while ϕ_1 and ϕ_3 qualify as scalar lepto-quarks, which are constrained by high energy collider experiments, including those at HERA [65], to

weigh more than a few hundred GeV [34]. For more details, I refer readers to, for example, the Particle Data Book [34] and references therein.

I will conclude this discussion by adding that several other effective operator can be realized in a very similar way. \mathcal{O}_{19} , for example, if it manifests itself with the Lorentz structure $(L^i Q^j)(d^c d^c)(\bar{e}^c \bar{u}^c)\epsilon_{ij}$, can be realized by a Lagrangian very similar to Eq. (3.2) where the d^c field in the y_3 -coupling interaction is replaced by a u^c field, and the ϕ_1 field is replaced by an $SU(2)_L$ singlet (it is a triplet in Eq. (3.2)). Of course, hypercharge assignments for the ϕ_i also need to be modified in a straight forward way. The associated non LNV phenomenology is similar, except for the fact that Λ_ν for \mathcal{O}_{19} (around 1 TeV) is larger than the one for \mathcal{O}_{56} and hence \mathcal{O}_{19} is less constrained by current experimental data. On the other hand, \mathcal{O}_{19} predicts potentially much larger rates for LNV observables at colliders (see Fig, 3.7).

Our definition of “interesting” is arbitrary and motivated only by the fact that the physics of the “interesting” operators highlighted earlier in this section will probably be explored at next-generation collider and high-precision experiments. One may argue that many operators which lead to the observable neutrino masses for high values of Λ_ν are interesting on their own right, either due to the theoretically pleasing properties of their associated potential ultraviolet completions, or by some observational peculiarity. There are many examples of the first type ranging from the different manifestations of the seesaw mechanism [7, 25, 26, 27] to the Zee model [66] and the minimal supersymmetric SM with R-parity violation [67]. Dedicated analysis of these cases have been widely pursued in the literature and will not be discussed here. I would also like to point out that some effective operators, like \mathcal{O}_7 and \mathcal{O}_8 , are, according to our criteria, very “uninteresting.”

Both \mathcal{O}_7 and \mathcal{O}_8 predict unobservably suppressed $\beta\beta 0\nu$ rates (both predict small m_{ee}) and equally hopeless collider prospects given that they are associated to very high cutoff scales, $\Lambda_\nu \approx 4 \times 10^2$ TeV and $\Lambda_\nu \approx 6 \times 10^3$ TeV, respectively. If either of these operators are responsible for the observed tiny neutrino masses, it is quite possible that I may never directly detect LNV. It is curious to consider possible means of indirect detection or other observable consequences of the different ultraviolet completions of such scenarios.⁴ It would also be interesting to ask whether either of these elusive models has any underlying theoretical motivation or whether they allow one to solve other outstanding problems in particle physics.

3.5. Conclusion

If neutrino masses are a consequence of lepton-number violating physics at a very high energy scale (higher than the scale of electroweak symmetry breaking), new physics effects – including the generation of neutrino Majorana masses – at low enough energies can be parameterized in terms of irrelevant operators whose coefficients are suppressed by inverse powers of an effective cutoff scale Λ . As discussed before, Λ is, roughly, the energy scale above which new degrees of freedom must be observed if the new ultraviolet physics is perturbative (if the new physics is very weakly coupled, the masses of the new degrees of freedom can be much smaller than Λ). I have explored a very large class of such scenarios through 129 irrelevant operators of energy dimension less than or equal to eleven that violate lepton number by 2 units. These are tabulated in first two columns of Table 3.1, along with a summary of our results.

⁴This is very similar to the case of \mathcal{O}_1 . The main redeeming feature of \mathcal{O}_1 , other than its simplicity, is the fact that many of its ultraviolet completions allow one to explain the matter–antimatter asymmetry of the universe [28].

Analyzing each effective operator individually, I estimated the predicted general form of the Majorana neutrino mass matrix. Our results are listed in the third column of Table 3.1. By comparing each such estimate with our current understanding of neutrino masses, I extracted the cutoff scale Λ_ν of each effective operator, assuming that it provides the dominant contribution to the observed neutrino masses. These results are listed in the fourth column of Table 3.1 assuming light neutrino masses equal to 0.05 eV (the square root of the atmospheric mass-squared difference), and are summarized as follows. Depending on the field content and dimension of the irrelevant operator, the “lepton number breaking scale” Λ_ν is predicted to be anywhere from the weak scale (~ 0.1 TeV) all the way up to 10^{12} TeV (see Fig. 3.2). This means that, depending on how lepton number is violated and communicated to the SM, the mass of the associated new degrees of freedom is predicted to be anywhere between 100 GeV and 10^{12} TeV, *even if all new physics couplings are order one*. I note that in the case of all variations of the seesaw mechanism (\mathcal{O}_1), neutrino physics constrains $\Lambda_\nu = 10^{12}$ TeV such that the new degrees of freedom are either unobservably heavy, extremely weakly coupled, or their couplings to the SM degrees of freedom are finely-tuned. It is fair to say that this behavior is not characteristic of all LNV ultraviolet physics. One sample ultraviolet theory that leads to dimension-eleven LNV effective operators was discussed in Sec. 3.4. Other examples can be found in [15], and include supersymmetry with trilinear R-parity violation and the Zee model.

Assuming that a particular operator is responsible for nonzero neutrino masses, it is straight forward to ask whether it leads to other observable consequences. Here, I concentrated on several LNV observables, and included future LNV searches at the LHC and

future lepton machines (like the ILC), along with their ability to directly produce (and hopefully observe) new physics states lighter than several hundred GeV. In column five of Table 3.1, I list the most favorable modes of experimental observation for each operator. The different relevant probes are: neutrinoless double-beta decay ($\beta\beta 0\nu$), neutrino oscillation and mixing (mix), direct searches for new particles at the LHC (LHC) and ILC (ILC), and virtual LNV effects at collider facilities (HElnv). I find it unlikely that other probes of LNV, including rare meson decays, should yield a positive signal in the foreseeable future. This conclusion is strongly based on the fact that, for all of our analysis, I assume that *all* new physics degrees of freedom are heavier than the weak scale. While the vast majority of operators is most sensitive to searches for neutrinoless double-beta decay, that is not true of all operators. Some lead to relatively suppressed rates for $\beta\beta 0\nu$ (mostly because they lead to mass matrices with a very small m_{ee}) even if they are associated to $\Lambda_\nu < 1$ TeV, indicating that, for these scenarios, we are more likely to observe the physics behind neutrino masses directly at colliders than to see a finite lifetime for $\beta\beta 0\nu$. Other scenarios naively lead to $\beta\beta 0\nu$ rates orders of magnitude higher than what is currently allowed by data. If these are responsible for the generation of neutrino masses, the new physics is constrained to be somewhat decoupled from first generation quarks (for example). In this case, there is hope that LNV phenomena at colliders, which are not restricted to first generation quarks, occur with non-negligible rates.

The sixth column of Table 3.1 lists the current “status” of the operator as either experimentally unconstrained (U), constrained (C), or disfavored (D). Such labels are assigned based only on the experimental probes reviewed in this work. By arbitrary convention, an ‘unconstrained’ operator can safely accommodate all existing data even

if one assumes *all* its flavor-dependent dimensionless coefficients to be of order one. A ‘constrained’ operator can accommodate all existing data after one allows some of the different flavor-dependent dimensionless coefficients to be suppressed with respect to the dominant ones by a factor of 100 or so (as described above). ‘Disfavored’ operators can only accommodate all data only if “tuned” much more severely than the ‘constrained’ ones, and are usually in trouble with more than one “type” of constraint. A glance at column six reveals that 11 out of the 129 operators are disfavored by current data. The most stringent constraints come from $\beta\beta 0\nu$, while all ‘disfavored’ operators are associated to cutoffs at or below 1 TeV. Three of the ‘disfavored’ operators, \mathcal{O}_{36} , \mathcal{O}_{37} , and \mathcal{O}_{38} , are also in disagreement with the neutrino oscillation data (see Sec. 3.3).

Our results illustrate that, as far as “explaining” neutrino masses, the model-building scene is wide open even if one postulates that neutrino masses arise as a consequence of lepton number violating, “heavy” physics. Significant progress will only be achieved once more experimental information becomes available. The observation that neutrinoless double-beta decay occurs with a nonzero rate will help point us in the right direction, but will certainly not reveal much about the mechanism behind neutrino masses. A more complete picture can only arise from combined information from several observables, including other LNV observables and the search for new physics at the electroweak scale. Other important experimental searches, not discussed here, include all lepton-number conserving “leptonic” probes, such as precision measurements of the anomalous magnetic moment of the muon, searches for leptonic electric dipole moments, searches for charged-lepton flavor violation (see [69] for a model independent discussion of this issue), and precision measurements of neutrino–nucleon and neutrino–lepton scattering.

CHAPTER 4

Neutrino Phenomenology of Very Low-Energy Seesaws

The seesaw mechanism [7] is an appealing way to generate the observed neutrino masses and lepton mixing matrix. The idea is simple. Add an arbitrary number of singlet fermion states to the SM matter content. The triviality of their quantum numbers allows them to have Majorana masses of magnitude M , as well as couple to the $SU(2)_L$ lepton and Higgs doublets. The latter vertices become Dirac mass terms of magnitude μ after electroweak symmetry breaking. The standard theoretical prejudice is that the Dirac masses are of order the charged fermion masses, while the Majorana masses are at some very high energy scale, $M \gg 100$ GeV. If this is indeed the case, the resulting propagating neutrino degrees of freedom separate into two quasi-decoupled groups: mostly active states with very small masses $m \sim \mu^2/M$ suppressed by the new physics scale, and mostly sterile states with very large masses M . In this scenario, the mostly right-handed states are not directly observable. Indeed, it is possible that if such a high-energy seesaw is realized in Nature, its only observable consequence is that the mostly active neutrinos have mass and mix.

Of course, there is no direct evidence that M – which I refer to as the seesaw scale – is large. Large M values are attractive for several reasons, including the fact that one may relate M to the grand unified scale. On the other hand, all M values are technically natural, given that when M vanishes the global symmetry structure of the Lagrangian is enhanced: $U(1)_{B-L}$ is a symmetry of the Lagrangian if $M = 0$, so that M is often

referred to as the lepton number breaking scale. This point was recently emphasized in [32]. Recent analyses have also revealed that there are several low-energy choices for the seesaw energy scale that allow one to address outstanding problems in particle physics and astrophysics. The main reason for this is that, unlike in the high-energy seesaw, in a low-energy seesaw the mostly right-handed states do not decouple but remain as kinematically accessible sterile neutrinos.

The data reported by the LSND short baseline neutrino oscillation experiment [70] can be explained by postulating the existence of light ($m \sim 1 - 10$ eV) sterile neutrino states. This result is currently being tested by the Fermilab MiniBooNE experiment [71] and, if confirmed, will lead the community to seriously contemplate the existence of light, SM singlet fermions. It was pointed out in [32] (see also [72]) that if $M \sim 1 - 10$ eV, the right-handed seesaw neutrinos can easily play the role of the LSND sterile neutrinos. There is also evidence for mixed sterile neutrinos at other energy scales: eV sterile neutrinos aid in heavy element nucleosynthesis in supernovae, keV sterile neutrinos can help explain the peculiar velocity of pulsars, and remain viable warm dark matter candidates. In the past several months, it has been shown that the seesaw right-handed neutrinos may play the role of all these astrophysically/cosmologically inspired sterile neutrinos [31, 73].

In this chapter, I consider the phenomenology of low-energy ($M \lesssim 1$ keV) seesaw scenarios, extending the analysis performed in [32] in several ways. In Sec. 4.1, I review the generation of neutrino mass via the seesaw mechanism and apply it to relatively light right-handed neutrino states. I pay special attention to the most general active–sterile seesaw mixing matrix, whose parameters are the main object of our study. In Sec. 4.2, I review the several different “evidences” for sterile neutrinos, and discuss whether these can be “fit”

by the low-energy seesaw. I concentrate on exploring solutions that can accommodate at the same time the LSND anomaly and the astrophysical processes outlined above, but also discuss different combinations of the seesaw parameters capable of explaining only the astrophysics-related observables. In Sec. 4.3, I examine other experimental probes that can be used to explore low-energy seesaws – regardless of their relationship to the LSND anomaly, pulsar kicks, and warm dark matter. I concentrate on the prospects of current/future tritium beta-decay and neutrinoless double-beta decay experiments. I conclude in Sec. 4.4 by summarizing our results, commenting on the plausibility of this scenario, and offering a general outlook for the future.

4.1. The Seesaw Mechanism and electron volt neutrino masses: preliminaries

In order to account for nonzero neutrino masses, I add to the SM particle content three $SU(3)_c \times SU(2)_L \times U(1)_Y$ gauge singlet fermion states N_i , conventionally referred to as right-handed neutrinos. While sterile under SM gauge interactions, right-handed neutrinos may still be charged under new, currently unknown gauge transformations. Such interactions, if at all present, are neglected in our analysis.

The most general renormalizable Lagrangian consistent with SM gauge invariance is

$$\mathcal{L}_\nu = \mathcal{L}_{\text{old}} - \lambda_{\alpha i} \bar{L}^\alpha H N^i - \sum_{i=1}^3 \frac{M_i}{2} \bar{N}^{ci} N^i + H.c., \quad (4.1)$$

where \mathcal{L}_{old} is the traditional SM Lagrangian, H is the Higgs weak doublet, L^α , $\alpha = e, \mu, \tau$, are lepton weak doublets, $\lambda_{\alpha i}$ are neutrino Yukawa couplings, and M_i are Majorana masses for the N_i . I choose, without loss of generality, the Majorana mass matrix M_R to be diagonal and its eigenvalues M_i to be real and positive. I also choose the charged

lepton Yukawa interactions and the charged weak current interactions diagonal so that all physical mixing elements are contained in the neutrino sector.

After electroweak symmetry breaking (when H develops a vacuum expectation value v), \mathcal{L}_ν will describe, aside from all other SM degrees of freedom, six neutral massive Weyl fermions — six neutrinos. The resulting mass terms can be expressed as:

$$\mathcal{L}_\nu \supset \frac{1}{2} \begin{pmatrix} \vec{\nu} & \vec{N}^c \end{pmatrix} \begin{pmatrix} 0 & \mu \\ \mu^T & M_R \end{pmatrix} \begin{pmatrix} \vec{\nu}^c \\ \vec{N} \end{pmatrix}, \quad (4.2)$$

where $\mu \equiv \lambda v$, and $\vec{\nu}$ and \vec{N} are vectors of the three active neutrinos (ν_e, ν_μ, ν_τ) and the three right-handed, sterile states, respectively. Each entry in the symmetric mass matrix of Eq (4.2) is itself a 3×3 matrix of mass parameters. Diagonalization of the mass matrix yields eigenstates with Majorana masses that mix the active–active states, related via the standard lepton mixing matrix V , and the active–sterile states. The physical neutrinos are thus linear combinations of all active and sterile states. Throughout I will work in the “seesaw limit,” defined by $\mu \ll M_R$. In this case, there are three mostly active light neutrinos and three mostly sterile heavy neutrinos where ‘mostly’ is determined by the induced mixing parameters.

In the seesaw limit, the diagonalization is simple. Assuming, for simplicity, that the mixing matrices are real:

$$\begin{aligned} \begin{pmatrix} 0 & \mu \\ \mu^T & M_R \end{pmatrix} &= \begin{pmatrix} 1 & \Theta \\ -\Theta^T & 1 \end{pmatrix} \begin{pmatrix} V & 0 \\ 0 & 1 \end{pmatrix} \begin{pmatrix} m & 0 \\ 0 & M_R \end{pmatrix} \begin{pmatrix} V^T & 0 \\ 0 & 1 \end{pmatrix} \\ &\times \begin{pmatrix} 1 & -\Theta \\ \Theta^T & 1 \end{pmatrix} + \mathcal{O}(\Theta^2), \end{aligned} \quad (4.3)$$

where m is the diagonal matrix of light neutrino masses and Θ is a matrix of active–sterile mixing angles found from the relations

$$\Theta M_R = \mu, \quad (4.4)$$

$$\Theta M_R \Theta^T = -V m V^T. \quad (4.5)$$

The elements of Θ are small ($\mathcal{O}(\mu/M_R)$), and the standard seesaw relation ($V m V^T = -\mu M_R^{-1} \mu^T$) is easily obtained by combining Eqs. (4.4) and Eqs. (4.5). On the other hand, using Eq. (4.5), I can relate the mixing parameters in Θ to the active–active mixing angles contained in V and the neutrino mass eigenvalues. In the case of observably light sterile neutrino masses, as considered in our analysis, this equation is very useful, as it places testable constraints on observable quantities. The general solution (first discussed in detail in [74]) of Eq. (4.5) is

$$\Theta = -V m^{1/2} O M_R^{-1/2}, \quad (4.6)$$

where O is an orthogonal matrix parameterized by three mixing angles $\phi_{12}, \phi_{13}, \phi_{23}$.¹ Physically, the mixing matrix O is a consequence of our freedom to choose the form of M_R . An illustrative example is found by considering the mass ordering of M_R in its diagonal form. The reordered matrix $M_R(m_i \leftrightarrow m_j)$ is equivalent to a $\pi/2$ rotation in the $i - j$ plane and therefore represents the same physics as the original matrix, as it should. In other words, $OM_R O^T$ is the physically relevant object, as opposed to O and M_R separately. This object, when constrained to be real, has six free parameters that I shall refer to as “heavy parameters:” $\phi_{12}, \phi_{13}, \phi_{23}, M_1, M_2, M_3$.

Using Eq. (4.6), the 6×6 unitary neutrino mixing matrix is

$$U = \begin{pmatrix} V & \Theta \\ -\Theta^T V & 1 \end{pmatrix}. \quad (4.7)$$

Note that, up to $\mathcal{O}(\Theta^2)$ corrections, V is unitary. U is entirely described in terms of the three light mixing angles, six mass eigenvalues and three angles ϕ_{ij} . Many combinations of these have been measured or constrained via oscillation searches, cosmology and astrophysics. In particular, the two active neutrino mass-squared differences and mixing angles have been measured [75, 76, 34], thus leaving free the six heavy parameters and the absolute scale of active neutrino masses.² With U , the corresponding neutrino mass values and the SM couplings I can calculate all observable quantities and compare them with data.

¹In general, O is a *complex* orthogonal matrix. Here, however, I will restrict our analysis to *real* neutrino mass matrices, unless otherwise noted.

²The active neutrino mass hierarchy, normal vs. inverted, is another (discrete) free parameter.

It is natural to wonder how well the seesaw approximation holds once one starts to deal with M_R values around 1 eV. From Eq. (4.4), it is clear that one can choose for the expansion parameter $\sqrt{m/M_R}$. In all scenarios considered here, $\sqrt{m/M_R} < 0.5$ (for $M \sim 1$ eV and $m \sim 0.3$ eV). In the worst case scenario, therefore, first order corrections are 55% of the leading order terms, while second order corrections are near 30%. Corrections to most observables of interest are much smaller than this because they are suppressed by larger right-handed neutrino masses. The first non-trivial correction to Eq. (4.6) occurs at second order and I find that, for the ambitions of this chapter, all approximations are under control. This simple argument has been verified numerically for the most worrisome cases.

Before concluding this section, I wish to add that operators that lead, after electroweak symmetry breaking, to Majorana masses for the left-handed neutrino states (M_L) are also allowed if one introduces $SU(2)_L$ Higgs boson triplets or nonrenormalizable operators to the SM Lagrangian. While I neglect these “active” Majorana masses, I caution the reader that the existence of such terms would alter our results significantly. In particular, assuming the seesaw approximation holds, Eq. (4.5) would read

$$VmV^T + \Theta M_R \Theta^T = M_L, \quad (4.8)$$

which leads to a relationship between Θ , m , and M_R different from Eq. (4.6). If this were the case, for example, it would no longer be true that the largest Θ value (in absolute value) is constrained to be smaller than $(m_{\max}/M_{R,\min})^{1/2}$, where m_{\max} is the largest element of m , while $M_{R,\min}$ is the smallest element of M_R . On the other hand, all objects on the left-hand side of Eq. (4.8) are observables. Hence, in the case of a low-energy

seesaw, one can expect, in principle, to be able to test whether there are contributions to the neutrino mass matrix that are unrelated to the presence of right-handed neutrinos. By measuring V , m , M_R , and Θ , one can establish whether M_L is consistent with zero.

4.2. Oscillation Phenomenology and Current Evidence for Low-Energy Seesaw

Here I examine a number of experimental and observational anomalies that may be explained by light sterile neutrinos. More specifically, I explore what these can teach us about the currently unknown parameters of the seesaw Lagrangian, described in detail in Sec. 4.1. In all cases I assume 3 mostly active and 3 mostly sterile neutrinos and, most of the time, will concentrate on a $3 + 2 + 1$ picture of neutrino mass eigenstates, that is, three mostly active sub-eV neutrinos, two mostly sterile eV neutrinos and one almost completely sterile keV neutrino. The hope is that the heavier state can account for warm dark matter (section 4.2.2) or pulsar kicks (Sec. 4.2.3), which both require at least one keV neutrino, while the other two mostly sterile states help “explain” the existing oscillation data where, for all practical purposes, the heaviest neutrino decouples and I are left with an effective $3 + 1$ or $3 + 2$ picture. I remind readers that a third possibility ($2+2^3$) is currently ruled out by solar and atmospheric data [77, 78, 79] and will be ignored. $3 + 1$ schemes that address the LSND anomaly are also disfavored by global analysis of short baseline oscillation experiments [77, 78, 79, 80] and, for this reason, I mostly concentrate on $3 + 2$ fits to the LSND anomaly [80].

³It would have been rather difficult to construct a $2+2$ neutrino mass hierarchy using the seesaw Lagrangian.

Our analysis method is as follows: For each experimental probe considered I perform a χ^2 “fit” of the mixing matrix U , given by Eq. (4.7), and neutrino masses to the “data”, and extract the region of parameter space that best explains the data. In most cases I allow the light mixing angles and mass squared differences to vary within their 1σ limits (according to [76]),⁴ the angles ϕ_i to vary unconstrained within their physical limits of $0 - 2\pi$, and the lightest active neutrino mass eigenvalue m_l to vary unconstrained between $0 - 0.5$ eV. The quotation marks around “fit” and “data” are meant to indicate that our methods are crude, in the sense that I am fitting to previously processed experimental data, assuming a diagonal correlation matrix with Gaussian uncertainties. In order to avoid the subtleties involved in such a “fit to a fit”, I hesitate to mention actual confidence intervals, but are compelled to do so for lack of a better measure of an allowed region. I sometimes present our best fit parameter points along with confidence intervals, but warn the reader to avoid strict interpretations of these numbers. While crude, our methodology of error analysis and fitting provides a very useful instrument for identifying whether (and how) the low-energy seesaw can accommodate a particular combination of data sets.

Before proceeding, it is useful to cement our notation. The neutrino masses will be ordered in ascending order of magnitude from m_1 to m_6 in the case of a normal active neutrino mass hierarchy ($m_2^2 - m_1^2 < m_3^2 - m_1^2$), while in the case of an inverted mass hierarchy they are ordered $m_3 < m_1 < m_2 < m_4 < m_5 < m_6$ (in this case $|m_3^2 - m_1^2| > m_2^2 - m_1^2$). The states with masses $m_{1,2,3}$ are mostly active, while those with masses $m_{4,5,6}$ are mostly sterile. Elements of the mixing matrix are referred to as $U_{\alpha i}$, where $\alpha = e, \mu, \tau, s_1, s_2, s_3$ (s 's are the right-handed neutrino degrees of freedom) and

⁴In the case of 3+1 “fits” (*cf.* Eqs. (4.10,4.11)), I kept the active neutrino parameters fixed at their best-fit values.

$i = 1, 2, 3, 4, 5, 6$. I also define $\Delta m_{ji}^2 = m_j^2 - m_i^2$ and will refer to the lightest active neutrino mass as m_l . In the case of normal (inverted) active neutrino mass hierarchy $m_l = m_1$ ($m_l = m_3$).

4.2.1. Short baseline oscillation constraints

Here I analyze the constraints imposed on the unknown mixing parameters by current neutrino oscillation data. I will assume that all solar, reactor, long-baseline and atmospheric data are properly fit with active–active oscillations, and that constraints on the other seesaw parameters will be provided mostly by short-baseline accelerator experiments. It is interesting to note that the inclusion of the angles ϕ_{ij} introduces enormous freedom into the system. Any one active–sterile mixing angle contained in Θ can always be set to zero by an appropriate choice of O . In fact, all but three elements may be set to zero simultaneously, with only a single non-zero element in each row and column. In this case, these are constrained to be around $\sqrt{m_l/M_{Ri}}$ where i is the column of the non-zero element. This is especially true when the mostly active neutrino masses are quasi-degenerate. An important “sum rule of thumb” is the following. For a given right-handed neutrino mass M_i , the active–sterile mixing angle squared is of order m/M_i , where m is a typical active neutrino mass. One can always choose parameters so that, for at most two values of $\alpha = e, \mu, \tau$, $U_{\alpha i}$ are abnormally small. In that case, however, the “other” $U_{\alpha i}$ is constrained to saturate the bound $|U_{\alpha i}|^2 \lesssim m_l/M_i$.

The most compelling evidence for light sterile neutrinos comes from the short baseline oscillation experiment by the Liquid Scintillator Neutrino Detector (LSND) collaboration at Los Alamos. Using a ~ 30 MeV $\bar{\nu}_\mu$ beam they observed a better than 3σ excess

of $\bar{\nu}_e$ -like events above their expected background at their detector some 30 m away from the production point [70]. This evidence of $\bar{\nu}_\mu \leftrightarrow \bar{\nu}_e$ oscillation requires a mass-squared difference greater than 1 eV², clearly incompatible with the small mass-squared differences observed between the active neutrinos. Several mechanisms, such as CPT-violation [81, 77], Lorentz invariance violation [82], quantum decoherence [83], sterile neutrino decay [84] and, of course, oscillation into sterile neutrinos have been proposed to explain this result. Here I concentrate on the last possibility.

In order to take into account all short baseline data I “fit” our mixing parameters and masses to the results of the 3 + 2 performed in [80], which are summarized in Table 4.1 [85]. Here I assume that the heaviest, mostly sterile state does not participate effectively in LSND oscillations. This is guaranteed to happen if $m_6 \gtrsim 10$ eV. On the other hand, $|U_{\alpha 6}|^2$ are partially constrained by our attempts to accommodate LSND data with seesaw sterile neutrinos, as will become clear in the next subsections.

I find that m_l , the lightest neutrino mass, is constrained to lie between (0.22–0.37) eV, with a “best fit” value of 0.29 eV. Thus the active neutrino mass spectrum is predicted

Table 4.1. Parameter values used in our analysis. These were extracted from a fit to all short baseline neutrino oscillation experiments including LSND within the 3 + 2 scenario [80, 85]. 1σ indicates a rough estimate of the 1 sigma allowed range for the different parameters.

	U_{e4}	$U_{\mu 4}$	U_{e5}	$U_{e\mu 5}$	Δm_{41}^2 (eV ²)	Δm_{51}^2 (eV ²)
Central Value	0.121	0.204	0.036	0.224	0.92	22
1σ	0.015	0.027	0.034	0.018	0.08	2.4

to be quasi-degenerate. A sample 6×6 neutrino mixing matrix that fits all data is

$$U_{3+2} = \begin{pmatrix} 0.8301 & 0.5571 & 0.001365 & 0.1193 & -0.009399 & -0.006513 \\ -0.3946 & 0.5866 & 0.7072 & 0.2016 & 0.2262 & 0.0003363 \\ 0.3932 & -0.5879 & 0.7070 & 0.4760 & -0.0949 & 0.001470 \\ -0.2067 & 0.09514 & -0.4792 & 1 & 0 & 0 \\ 0.1343 & -0.1832 & -0.09284 & 0 & 1 & 0 \\ 0.004963 & 0.004295 & -0.001268 & 0 & 0 & 1 \end{pmatrix}, \quad (4.9)$$

while the associated masses are $m_1 \simeq m_2 \simeq m_3 = 0.28$ eV, $m_4 = 1.0$ eV, $m_5 = 4.7$ eV, and $m_6 = 6.4$ keV. Note that the matrix in Eq. (4.9) is only approximately unitary, up to corrections of order 25%. This result agrees qualitative with those obtained in [32]. The neutrino masses and mixings obtained in this “fit” are depicted in Fig. 4.1. I will use the results of “fits” similar to this one throughout the chapter.

One can also aim at a (currently disfavored) $3 + 1$ LSND fit.⁵ In this case, much lower m_l values are also allowed, extending well into the hierarchical spectrum range. In this case, all m_l values above 0.01 eV and 0.03 eV are allowed, assuming an inverted and normal mass hierarchy, respectively. This is to be compared with the results found in [32], where only trivial choices for O were considered. Examples that “fit” all oscillation data include, for an inverted active mass hierarchy: $m_1 \simeq m_2 = 0.066$ eV, $m_3 = 0.043$ eV,

⁵This is easily accomplished by requiring $m_5 \gtrsim 10$ eV.

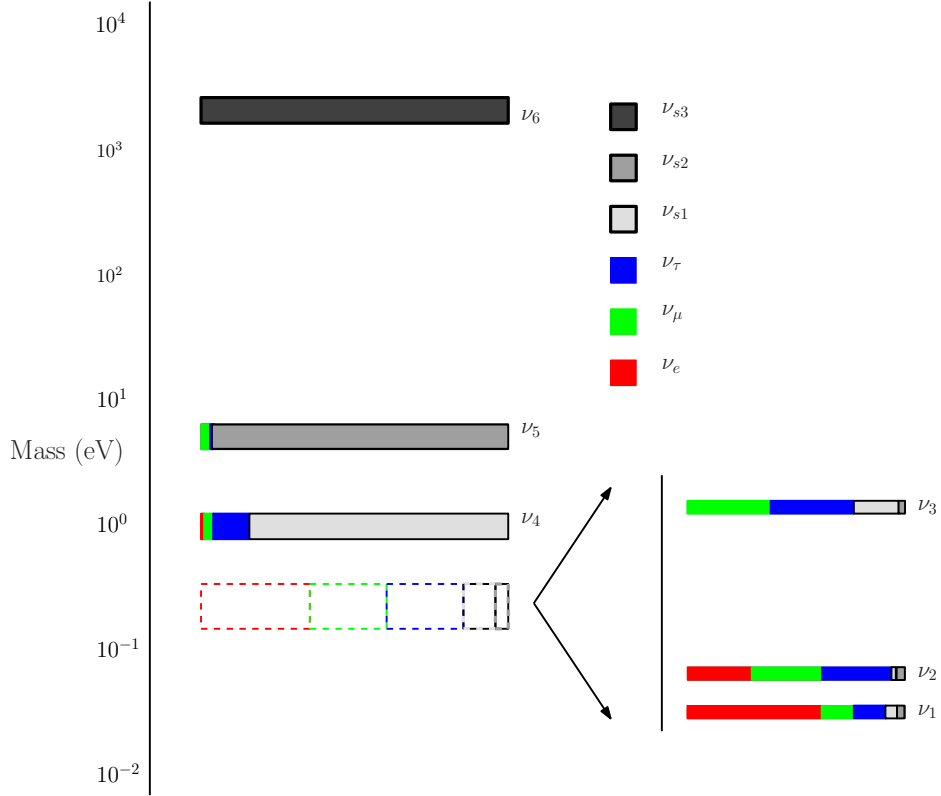


Figure 4.1. Neutrino mass eigenstate spectrum, along with the flavor composition of each state. This case accommodates all neutrino oscillation data, constraints from r-process nucleosynthesis in supernovae, and may help explain anomalous pulsar kicks (see text for details). While I choose to depict a normal hierarchy for the active neutrino states, an inverted active neutrino mass hierarchy would have yielded exactly the same physics (as far as the observables considered are concerned).

$m_4 = 0.96$ eV, $m_5 = 5$ keV, and $m_6 = 10$ GeV, together with

$$U_{3+1}^{\text{inverted}} = \begin{pmatrix} 0.8305 & 0.5571 & 0 & 0.1359 & -0.00009142 & -0.000002198 \\ -0.3939 & 0.5872 & 0.7071 & 0.2046 & 0.00005000 & 0.000001202 \\ 0.3939 & -0.5872 & 0.7071 & -0.04421 & -0.003236 & -0.0000001857 \\ -0.01486 & -0.2218 & -0.1134 & 1 & 0 & 0 \\ 0.001370 & -0.001878 & 0.002253 & 0 & 1 & 0 \\ 0.000002372 & 0.0000004094 & -0.0000007187 & 0 & 0 & 1 \end{pmatrix}. \quad (4.10)$$

For a normal mass hierarchy, I find that $m_1 = 0.055$ eV, $m_2 = 0.056$ eV, $m_3 = 0.0744$ eV, $m_4 = 0.96$ eV, $m_5 = 5$ keV, $m_6 = 10$ GeV, and

$$U_{3+1}^{\text{normal}} = \begin{pmatrix} 0.8305 & 0.5571 & 0 & 0.1173 & -0.002100 & 0.000001418 \\ -0.3939 & 0.5872 & 0.7071 & 0.2176 & 0.0004625 & -0.000001364 \\ 0.3939 & -0.5872 & 0.7071 & 0.09802 & 0.002804 & 0.000001283 \\ -0.05028 & -0.1355 & -0.2231 & 1 & 0 & 0 \\ 0.0008214 & 0.002545 & -0.002310 & 0 & 1 & 0 \\ -0.000002220 & 0.0000007646 & 0.00000005663 & 0 & 0 & 1 \end{pmatrix}, \quad (4.11)$$

“fit” all oscillation data quite well.

Note that a null result from MiniBooNE is bound to place significant limits on the seesaw energy scale. If all right-handed neutrino masses are similar, the effective mixing angle that governs $\nu_\mu \rightarrow \nu_e$ transitions is $\sin^2 2\theta_{\text{MiniBooNE}} \lesssim 4m^2/M^2$. Hence, a null result at MiniBooNE would rule out a seesaw energy scale M lighter than 6 eV, assuming all active neutrino masses m are around 0.1 eV [71]. This limit is sensitive to the lightest neutrino mass m_l and can be somewhat relaxed (similar to how I obtain a good 3+2 to all neutrino data) by postulating a (mild) hierarchy of right-handed neutrino masses and by assuming that sterile-electron and sterile-muon neutrino mixing is suppressed with respect to naive expectations for the lightest mostly sterile state(s). For larger values of m_l , M values around 10 eV are already constrained by $\nu_\mu \rightarrow \nu_e$ searches at the NuTeV [86] and NOMAD [87] experiments, and $\nu_\mu \rightarrow \nu_\tau$ searches at CHORUS [88].

4.2.2. Cosmological and Astrophysical Constraints, Warm Dark Matter

Very light sterile neutrinos that mix with the active neutrinos are constrained by several cosmological and astrophysical observables. The “seesaw” right-handed neutrinos are no exception. Given that active–sterile mixing angles $|U_{\alpha i}|^2 \lesssim m_l/m_i$ ($\alpha = e, \mu, \tau, i = 4, 5, 6$), it turns out that for “standard cosmology,” the right-handed neutrinos thermalize with the early universe thermal bath of SM particles, as long as the reheat temperature is higher than their Majorana masses. For the low seesaw energy scales I am interested in, this is a problem. For the values of M_R under consideration here, thermal right-handed neutrinos easily overclose the universe. Smaller m_l values ($m_l \lesssim 10^{-5}$ eV) lead to the possibility that right-handed neutrinos are the dark matter, as recently discussed in the literature [31, 73]. I comment on this and other possibilities shortly.

Fig. 4.2 depicts the region of the $|U_{e6}|^2 \times m_6$ -plane in which the contribution of the heaviest neutrino ν_6 to Ω (the normalized energy density of the universe, ρ/ρ_c) is larger than 0.3 (dark region). The same constraint roughly applies for all $\alpha = e, \mu, \tau$ and $i = 4, 5, 6$. The dashed diagonal lines correspond to $|U_{\alpha 6}|^2 = m_l/m_6$, for different values of m_l . All lines lie deep within the dark $\Omega_s > 0.3$ region.

For smaller values of M_R , the situation is also constrained. For M_R values below tens of eV, thermal sterile neutrinos contribute to the amount of hot dark matter in the universe [90, 21, 22, 20, 91]. Right-handed neutrinos will thermalize as long as $m_i \sin^2 \theta_{i\alpha} \gtrsim 5 \times 10^{-4}$ eV [92, 93]. In low energy seesaws, this roughly translate into $m \gtrsim 10^{-3}$ eV, where m is the active neutrino mass scale. For the cases of interest here

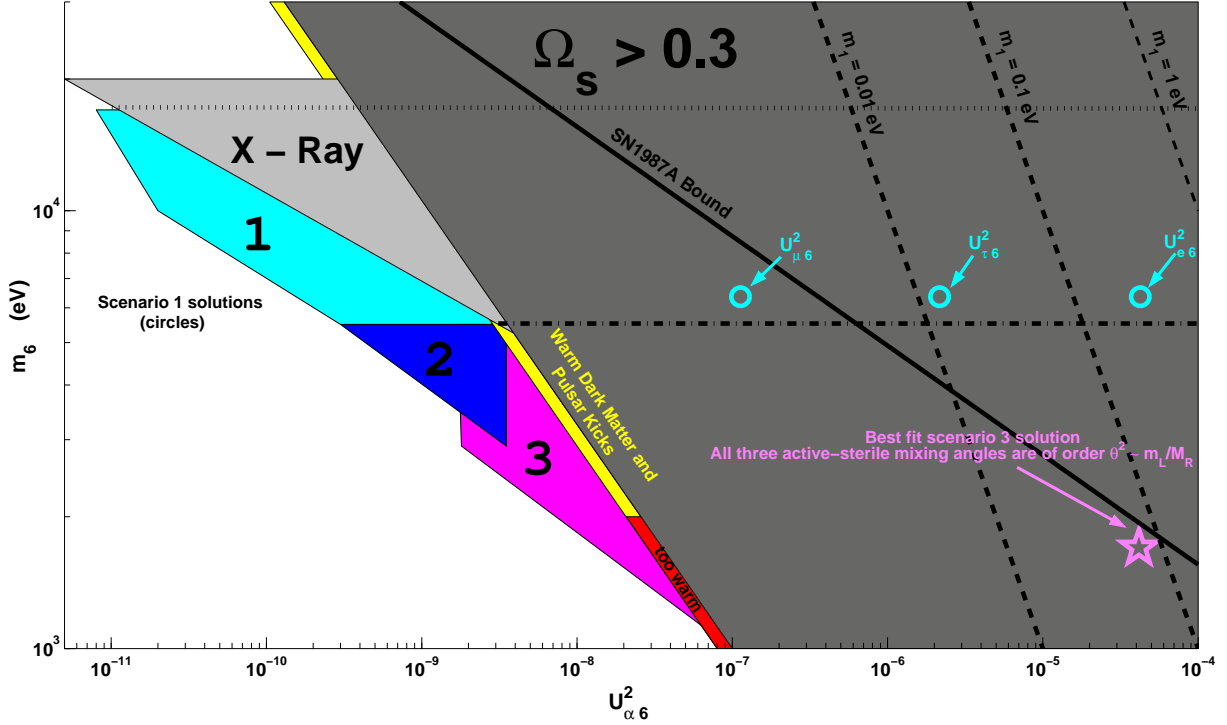


Figure 4.2. Adapted from [89]. Cosmological and astrophysical constraints on the $|U_{\alpha 6}|^2 \times m_6$ -plane. In the large dark grey region, the density of a thermal ν_6 population is $\Omega_s > 0.3$, while the light grey ‘X-ray’ region is disfavored by X-ray observations. The regions labeled 1,2,3 are preferred if one is to explain anomalous pulsar kicks with active–sterile oscillations inside supernovae. Regions 1 and 3 qualitatively extend inside the $\Omega_s > 0.3$ part of the plane as indicated by the horizontal dotted and dash-dotted lines, respectively. The regions ‘Warm Dark Matter’ and ‘Too Warm Dark Matter’ are meant to represent the region of parameter space where thermal ν_6 qualifies as a good (or bad) warm dark matter candidate. The region above the solid diagonal line is disfavored by the observation of electron (anti)neutrinos from SN1987A. The diagonal dashed lines correspond to $U_{e6}^2 = m_l/m_6$, for different values of m_l . Also shown is our ‘best fit’ sterile solution for different pulsar kick scenarios, assuming the 3 + 2 LSND fit for the lighter states. The regions one and three best fit values are represented by circles and a star respectively. See text for details.

$m \gtrsim \sqrt{\Delta m_{21}^2} \sim 10^{-2}$ eV, in which case m_i values above somewhere between¹ 0.2–2 eV are ruled out [90, 94, 21, 22, 20, 91]. Note that in our “best fit” 3+2 solution to the LSND data, the sum of all active neutrino masses violates slightly some of these constraints. This problem can be easily evaded if I choose m_l values close to the lower end of the “allowed region”. Other “mild” non-standard cosmology effects (see, for example, [95]) are also known to alleviate the hot dark matter bound on neutrino masses. Note that any sterile neutrino solution to the LSND anomaly faces a similar problem, which must be resolved with non-standard cosmology.

Big-bang nucleosynthesis also proves to be a large obstacle when it comes to the existence of light sterile neutrinos in thermal equilibrium in the early Universe (at temperatures above several MeV). In the absence of “non-standard” assumptions, big-bang nucleosynthesis constrains the existence of new thermal relativistic degrees of freedom (see, for example, [91, 96]).

One way to avoid the bounds described above (see also, for example, [97]) is to consider that the reheating temperature T_r of the universe is very low. This way, right-handed neutrinos, in spite of their “large” mixing angles, never reach thermal equilibrium in the early universe and neither overclose the universe nor contribute to the amount of hot dark matter. Quantitatively, $T_r \lesssim 5$ MeV is sufficient to avoid eV-mass (or heavier) sterile neutrinos that are allowed to explain the LSND anomaly [98]. Unless otherwise noted, this is the assumption I make here. Other possibilities include adding new neutrino interactions

¹The upper bound on the sum of neutrino masses from cosmology depends on several assumptions that go into analyzing the different cosmological observations. These include the issue of defining the values of the concordance cosmological model and deciding which data sets to include in the fit.

to lighter scalars, so that neutrinos remain in thermal equilibrium until they are non-relativistic [95]. According to [95], this can even be accomplished for light neutrinos, as long as the neutrino–scalar field coupling is finely tuned (see, however, [91]). Yet another possibility is to consider that the lepton asymmetry of the universe is large. The authors of [99] have recently studied this issue in detail, and concluded that a lepton asymmetry of order 10^{-4} is required in order to allow the existence of LSND sterile neutrinos to be in agreement with data from large-scale structure and big-bang nucleosynthesis (see also [97]).

Under these circumstances, it is interesting to consider whether light seesaw right-handed neutrinos still qualify as good warm dark matter. This could happen if their production in the early universe was non-thermal. One concern surrounding warm dark matter is whether it is ruled out by large scale structure surveys. Here, I will not add to this discussion but refer readers to the recent literature on the subject [100]. A brief summary of the situation is as follows: constraints on warm dark matter can be translated into a lower bound on the mostly sterile neutrino mass. The lower bound has been computed by different groups, and lies somewhere between 3 and 14 keV [100]. Different lower bounds depend on several issues, including which subset of Lyman alpha-forest data is taken into account.

Another constraint on potential dark matter sterile neutrinos comes from the observation of X-rays originating in galactic clusters. Such regions of the universe should be overdense with warm dark matter heavy neutrinos, which can be directly observed via their radiative decay $\nu_6 \rightarrow \nu_i + \gamma$ [101]. Bounds from X-ray observations have been summarized very recently in [102]. Combining the results of [102] and Fig. 4.2, I find that

for lightest neutrino masses larger than 10^{-2} eV, such bounds can only be avoided for $m_i \lesssim 100$ eV, where large scale structure constraints on warm/hot dark matter are severe. This qualitative analysis indicates that seesaw sterile neutrinos cannot, simultaneously, fit the LSND data and serve as cold dark matter.

On the astrophysics side, the most severe constraint on light, sterile neutrinos is provided by the observation of electron (anti)neutrinos coming from SN1987A. The current analysis consists of comparing the model-dependent neutrino flux at the surface of the neutrinosphere with that detected on Earth. Large sterile neutrino mixing and mass would result in modification/depletion of the detected neutrino signal (for a recent detailed discussion, see [103]). Although only twenty neutrinos were observed in this event, one can still place bounds on sterile-active neutrino mixing. As far as “LSND” sterile neutrinos are concerned, these bounds are still weaker than those obtained by the null short baseline oscillation experiments [104] and therefore already accounted for in our analysis. Heavier right-handed neutrinos can, however, be excluded by SN1987A neutrino data. Fig. 4.2 depicts the region of parameter space excluded by SN1987A data (region to the right of solid, diagonal line). This bound is defined by $m_i \sqrt{2} \sqrt{U_{\alpha i}} > 0.22$ keV [105, 98]. See also [93]. According to Fig. 4.2, supernova bounds force the seesaw scale to be below a few keV for m_l values above 0.01 eV.

4.2.3. Pulsar Kicks

Pulsars are born from the gravitational collapse of the iron core of a massive star. These core collapse supernova are an excellent source of neutrinos, producing all (active) flavors copiously (see [106] for a detailed review). Current observations point to the fact that

some pulsars move with peculiar velocities much greater than those expected from an asymmetric supernova explosion mechanism. Quantitatively, current three dimensional models yield velocities up to 200 km/s [107] while pulsars moving at speeds as high as 1600 km/s have been observed. I note, however, that some two-dimensional hydrodynamic studies [108] indicate that natural anisotropies generated during supernova explosions can, in fact, yield large neutron star velocities consistent with observations. However, more simulations seem to be required in order to validate this claim. Here, I will operate under the hypothesis that new physics, usually in the form of new neutrino physics, is responsible for the large pulsar kicks.

Since roughly 99% of the approximately 10^{53} ergs of energy released in a core collapse supernova is in the form of neutrinos, it is reasonable that neutrino physics provides a solution to this anomaly. At these rates a small (1–3)% asymmetry in neutrino emission can account for the observed large pulsar velocities. Neutrinos are always *produced* asymmetrically in the polarized medium of the proto-neutron star, due to the left-handed nature of their interactions. Unfortunately, asymmetric production cannot solve this problem because the associated medium densities are such that neutrinos undergo multiple scattering within the star’s interior, eventually diffusing out of an effective surface, called the *neutrinosphere*, with all initial asymmetries washed away. Several distinct mechanisms have been formulated to sidestep this fact. Specifically, the existence of large neutrino magnetic moments has been explored in [109], and can be tested in next generation neutrino scattering experiments [110, 111, 112, 113]. Proposed solutions also exist which utilize

standard three flavor neutrino oscillations, where ν_μ and ν_τ appearing between their neutrinosphere and the larger ν_e neutrinosphere can stream unhindered out of the star [114]. This solution is, however, currently disfavored by terrestrial oscillation experiments.

I concentrate on the case of oscillations into sterile neutrinos, which can proceed in various ways, depending on the mass and coupling of the relevant neutrinos as well as the properties of the collapsing star, including its density and magnetic field. Following [89], I separate and analyze these within three distinct categories. Each one requires the existence of a keV-scale sterile neutrino with very small couplings to the active flavors, of the order $10^{-4} - 10^{-5}$, especially if light sterile neutrinos are thermally produced in the early universe. Under these circumstances, if seesaw neutrinos are to play the role of the sterile neutrinos responsible for pulsar kicks, $|U_{\alpha i}|^2 \lesssim m/m_i$ ($i = 4, 5, 6$) must lie in the 10^{-9} range for $m_i \sim 10^4$ eV. This implies $m \sim 10^{-5}$ eV and is only compatible with a hierarchical active neutrino mass spectrum and very light m_i , as identified in [31, 73].

Here, instead, I will concentrate on identifying solutions that will address pulsar kicks and the LSND anomaly. According to the discussion in the previous subsection, the mostly sterile neutrino masses m_4 and m_5 are constrained to be less than 10 eV so that a 3+2 solution to the LSND anomaly can be obtained from the seesaw Lagrangian. The heaviest neutrino mass m_6 is unconstrained, so I am free to vary it as needed in order to attack the pulsar peculiar velocity issue.² Naively, the fraction of ν_α ($\alpha = e, \mu, \tau$) in ν_6 is expected to be of the order $U_{\alpha 6} \sim \sqrt{0.3 \text{ eV}/3 \times 10^3 \text{ eV}} = 10^{-2}$, much too large to satisfy the pulsar kick plus cosmology constraints summarized in Fig. 4.2. On the other hand, once the $\Omega_S < 0.3$ constraint is removed, the ‘pulsar kicks’ allowed region of the plane

²I can neglect the lighter sterile neutrinos (ν_4 and ν_5) as they should not alter the kicking mechanism significantly due to their small mass and non-resonant production.

is significantly enlarged, as qualitatively indicated by the horizontal lines in Fig. 4.2. In this case, which I must consider anyway if I am to have agreement between LSND and searches for hot dark matter, one can envision explaining pulsar kicks and the LSND data simultaneously. Note that once heavy sterile neutrinos are “removed” (so that they do not overclose the universe), constraints from X-ray observations (see Fig. 4.2) are also removed.

In scenario 1, the pulsar kick is produced via an active–sterile MSW resonance in the core of the proto-neutron star at large densities, greater than 10^{14} g/cm³, and magnetic fields, near 10^{16} G [115]. The effective neutrino matter potential in material polarized by a strong magnetic field contains a term proportional to $\vec{k} \cdot \vec{B}/|\vec{k}|$ [116, 117], where \vec{k} is the neutrino’s three-momentum and \vec{B} is the local magnetic field vector. Clearly the MSW resonance occurs at a radius that depends on $\vec{k} \cdot \vec{B}/|\vec{k}|$, the relative orientation of the neutrino momentum and magnetic field. Sterile neutrinos produced at smaller radii (higher temperatures) carry greater average momentum than those produced at larger radii (lower temperatures), yielding an asymmetric momentum distribution of emitted neutrinos. This asymmetry is capable of producing the observed pulsar kicks, in the direction of the magnetic field, when the mass and coupling of the sterile state is near 8 keV and above 1.5×10^{-5} , respectively [89]. I found the “best fit” to the LSND data (using ν_4 and ν_5) and pulsar kicks (using ν_6) and $m_6 > 5$ keV. The $|U_{\alpha 6}|^2$ and m_6 “best fit” values are depicted in Fig. 4.2. This solution is strongly disfavored by the observation of neutrinos from SN1987A. The fact that $|U_{e6}|$ is much larger than the other two active–sterile mixing angles is due to the fact that $|U_{e4}|$ and $|U_{e5}|$ are constrained by LSND data to be much smaller than naive expectations (see Eq. (4.9)). In order to reduce $|U_{e6}|$, one

would have to either reduce m_l by an order of magnitude – which renders the 3+2 fit to oscillation data very poor – or increase m_6 , which would only push $|U_{e6}|$ deeper into the region of parameter space ruled out by SN1987A. One can however, find 3+1 solutions to LSND data where ν_5 could pose as the sterile neutrino that explains why pulsar peculiar velocities are so large (see Eqs. (4.10,4.11)).

Scenario 2 also relies on a direction-dependent MSW resonance, this time occurring outside the core where the matter density and temperature are much lower. Here, both the active and sterile neutrinos are free to stream out of the star. The departing active flavors still have a small interaction cross-section, $\sigma \sim G_F^2 E_\nu^2$, and can therefore deposit energy and momentum into the star’s gravitationally bound envelope proportional to the matter it transverses. Via the direction-dependent resonance, neutrinos moving in the direction of the magnetic field remain active longer, deposit more momentum, and thus kick the star forward. The observations can be explained in this case with a smaller sterile neutrino mass and larger active–sterile coupling near 4 keV and 4.5×10^{-5} respectively [89]. In the case of our LSND “fit” to the data, I can constrain one of $|U_{\mu 6}|^2$ or $|U_{\tau 6}|^2$ to lie inside region 2. The other $|U_{\alpha 6}|^2$ ($\alpha = e, \tau$ or e, μ), however, are constrained to be large, thus violating the SN1987A bound in much the same way as the scenario 1 best fit results. Another possibility is to choose all $|U_{\alpha 6}|^2$ of the same order of magnitude. I do not explicitly consider these points as they reside in the region of parameter space where region 2 and 3 overlap, and behave in the same way as the point described below, under scenario 3.

Scenario 3 proceeds through off-resonance production of the sterile neutrino in the proto-neutron star core [118]. The amplitude for sterile neutrino production by a weak

process is proportional to $U_{\alpha 6}^m$, the effective mixing angle between the heavy mass eigenstate and the flavor eigenstate. Initially, this quantity is very small due to matter effects in the dense core. The effective potential in the star’s interior is quickly driven to zero in the presence of sterile neutrino production by a negative feedback mechanism. If this occurs in a time less than the diffusion time-scale for the active neutrinos, approximately (3 – 10) s, the mixing angle will reach its vacuum value [119]. The sterile neutrinos will then be produced and emitted asymmetrically and thus kick the pulsar to large velocities. Lower limits on the vacuum mass and mixing values are derived by requiring that the off-resonance time scale (inversely proportional to $m_6^4 \sin^2 2\theta_{\alpha 6}$) for the evolution of the matter potential to zero be less than about ten seconds. This places the sterile mass and mixing at approximately 1 keV and above 5×10^{-5} , respectively. Since all three active flavors are present in equal abundances, and all contribute to the effective matter potential, the mixing angle in question is not any particular $U_{\alpha 6}$. Rather it is the angle, θ_6 associated with the projection of ν_6 onto the space spanned by ν_e , ν_μ and ν_τ , that is $\theta_6^2 \equiv U_{e6}^2 + U_{\mu 6}^2 + U_{\tau 6}^2$. From Eq. (4.6) I see that $\theta_6 = \sqrt{m_l/m_6}$ up to corrections due to the non-unitarity of V and active neutrino mass differences. This is independent of mixing angles, and therefore cannot be tuned to be small. Our “best fit” region-3 solution is depicted in Fig. 4.2 by a star. It turns out that $U_{\alpha 6}$ have very similar values for $\alpha = e, \mu, \tau$. In order to evade the SN1987A constraint, I were forced to pick m_l values close to lower bound of our 3+2 LSND “fit” ($m_l = 0.22$ eV), so that $|U_{e4}|$, $|U_{\mu 4}|$, and $|U_{\mu 5}|$ are close to the low-end of the allowed range in Table 4.1.

4.2.4. Supernova Nucleosynthesis

Core collapse supernova are believed to produce the observed heavy element ($A \geq 100$) abundance through the r-process, or rapid neutron capture process. Here I briefly review this mechanism (see [120] for a comprehensive review), as well as its facilitation by the addition of active–sterile neutrino oscillations [121]. This scenario begins in the neutrino driven wind; that is, the wind of ejected nucleons driven by neutrinos radiated from the cooling proto-neutron star. The maintenance of equilibrium among neutrons, protons, and electron (anti)neutrinos in neutrino capture processes leads to a neutrino–rich environment. As the wind propagates, it cools enough for all free protons to bind into α particles. In the ideal r-process picture, as the wind cools further these α particles bind into intermediate size seed nuclei which later undergo neutron capture to form the observed heavy r-process elements.

This ideal scenario is dampened by the large number of electron neutrinos present at the stage of α particle formation. These will capture on the free neutrons, converting them to protons, which in turn will fuse to make more α particles. The end result is a very small free neutron to α particle ratio, conditions unfavorable for r-process element formation. This is known as the α effect and must be circumvented to produce the correct distribution of heavy elements. A clear solution to this problem is to reduce the number of electron neutrinos present at this stage, which can be accomplished by resonant $\nu_e \rightarrow \nu_s$ conversion³ [121].

³In this mechanism the effective matter potential, which depends on the number of electrons, positrons and neutrinos, varies wildly as a function of distance from the core. Along this radial direction there are three relevant MSW resonant conversions that must be tracked and understood: $\nu_e \rightarrow \nu_s$, $\bar{\nu}_e \rightarrow \bar{\nu}_s$ and $\bar{\nu}_s \rightarrow \bar{\nu}_e$. See [121] for more information.

The sterile neutrino solution to the r-process mechanism is modeled and fit to the data in reference [122] including the effects of relevant nuclear physics and additional neutrino oscillations in the star’s envelope. The analysis is expanded in [123] with the inclusion of fission cycling of the produced heavy elements. The analysis indicates the need for an eV-scale sterile neutrino with an allowed parameter space much larger than that constrained by LSND. By itself, the requirement of successful r-process in supernovae only weakly constrains the light neutrino mass scale to be greater than 10^{-2} eV and 10^{-3} eV for a 1 eV and 10 eV sterile neutrino, respectively. With regard to the LSND results, it has been demonstrated that the $3 + 1$ oscillation scenario fits within this parameter space [123]. Considering that the best fit mass-squared difference and mixing angles for the fourth mass eigenstate, which makes up most of the lightest sterile neutrino, is very similar between the $3 + 1$ and $3 + 2$ case [85], it is reasonable to conclude that $\nu_e \leftrightarrow \nu_{s4}$ resonant conversion will also fit within this scenario. Even oscillations into the heavier ν_{s5} state can potentially solve this anomaly if the neutrino driven wind expansion time-scale is sufficiently small, ≤ 0.1 sec. To conclude this section I note that, although the sterile neutrino solution to the supernova nucleosynthesis problem fits well within our seesaw framework, it adds no additional constraints, and therefore does not increase the predictability of our scenario.

4.3. Other Probes of the Seesaw Energy Scale

Here I survey other existing and future probes of light sterile neutrinos. As opposed to the previous cases, these probes are perfectly consistent by themselves. That is, extra heavy neutrinos are not required to solve problems within the system. However, their

addition can lead to large modifications to the outcome of such experiments, thus rendering the eV-scale seesaw scenario testable. Specifically, I consider bounds from tritium beta-decay and neutrinoless double-beta decay. Observations in all of these areas have already yielded useful constraints on sterile neutrinos, and the situation is expected to improve in the next few years.

4.3.1. Tritium Beta-Decay

The endpoint of the electron energy spectrum in the beta-decay of tritium is a powerful probe of nonzero neutrino masses. This results from the decay kinematics of the system which is necessarily modified by the presence of a massive neutrino. The nonzero neutrino mass effect can be understood almost entirely from the analysis of the phase space distribution of the emitted electrons, and is therefore quite model independent. Existing beta decay experiments extract limits on an effective electron neutrino mass $m_{\nu_e}^2 = \sum_i |U_{ei}|^2 m_i^2$ [23], provided that the neutrino masses are smaller than the detector energy resolution. Currently the most stringent bounds on $m_{\nu_e}^2$ are $(2.3)^2 \text{ eV}^2$ at 95% confidence from the Mainz experiment [17] and $(2.5)^2 \text{ eV}^2$ at 95% confidence from the Troitsk experiment [18]. In the next few years the Katrin experiment should exceed these limits by nearly two orders of magnitude, probing down to $(0.2)^2 \text{ eV}^2$ at the 90% confidence level [63]. One might naively compute this effective mass for the “best fit” mixing parameters obtained in the previous section. In this case, I expect a keV seesaw neutrino to contribute to $m_{\nu_e}^2$ by a huge amount $\delta m_{\nu_e}^2 = U_{e6}^2 m_6^2 \sim \frac{m_l}{m_6} m_6^2 = m_l m_6$ [32] so that it would be excluded by the current precision measures of tritium beta-decay for $m_l \gtrsim 10^{-3} \text{ eV}$. This is clearly an incorrect treatment of the physics. As pointed out in, for example, [124], the existence of

a heavy neutrino state would produce a kink in the electron energy spectrum of size $|U_{ei}|^2$ at an energy $E_0 - m_i$ as well as a suppression of events at the endpoint of order $1 - |U_{ei}|^2$. Here U_{ei} ($i = 4, 5, 6$) is the mixing between the electron neutrino flavor eigenstate and the heavy mass eigenstate, while $E_0 = 18.6$ keV is the endpoint energy of tritium beta-decay.

Fig. 4.3 depicts $1 - S/S_0$, where S is the β -ray energy spectrum obtained assuming three mostly active, degenerate neutrinos with mass $m = 0.1$ eV and one mostly sterile neutrino ν_i with various masses m_i and mixing angle $U_{ei}^2 = m/m_i$, while S_0 is the spectrum associated with massless neutrinos. One can readily observe “kinks” in the spectrum above m_i . For β -energies above $E_0 - m_i$, the impact of the sterile state is to “remove” around $1 - |U_{ei}|^2$ of the β -rays from spectrum. This is most significant between $E_0 - m_i$ and E_0 minus the mass of the active neutrinos. For energies below $E_0 - m_i$, the spectrum agrees with that obtained from the emission of one effective neutrino with mass-squared $m_{\nu_e}^2$.

I estimate the sensitivity of future tritium beta-decay experiments to the emission of one heavy state by considering the ratio between the number of electrons with energies above $E_0 - \Delta E$ in the case of one heavy massive neutrino ν_i and in the case of massless neutrinos

$$R(U_{ei}, M_R) = \frac{|U_{ei}|^2 \int_{E_0 - \Delta E}^{E_0} dE \frac{dN}{dE}(m_i) + (1 - |U_{ei}|^2) \int_{E_0 - \Delta E}^{E_0} dE \frac{dN}{dE}(0)}{\int_{E_0 - \Delta E}^{E_0} dE \frac{dN}{dE}(0)}, \quad (4.12)$$

where dN/dE is the energy distribution of β -rays, which depends on the neutrino mass m_i . This expression can be easily generalized for more than one heavy neutrino. The advantage of using the ratio above is that potential systematic uncertainties and normalization effects can be safely ignored. An experiment is sensitive to a massive neutrino state if it can

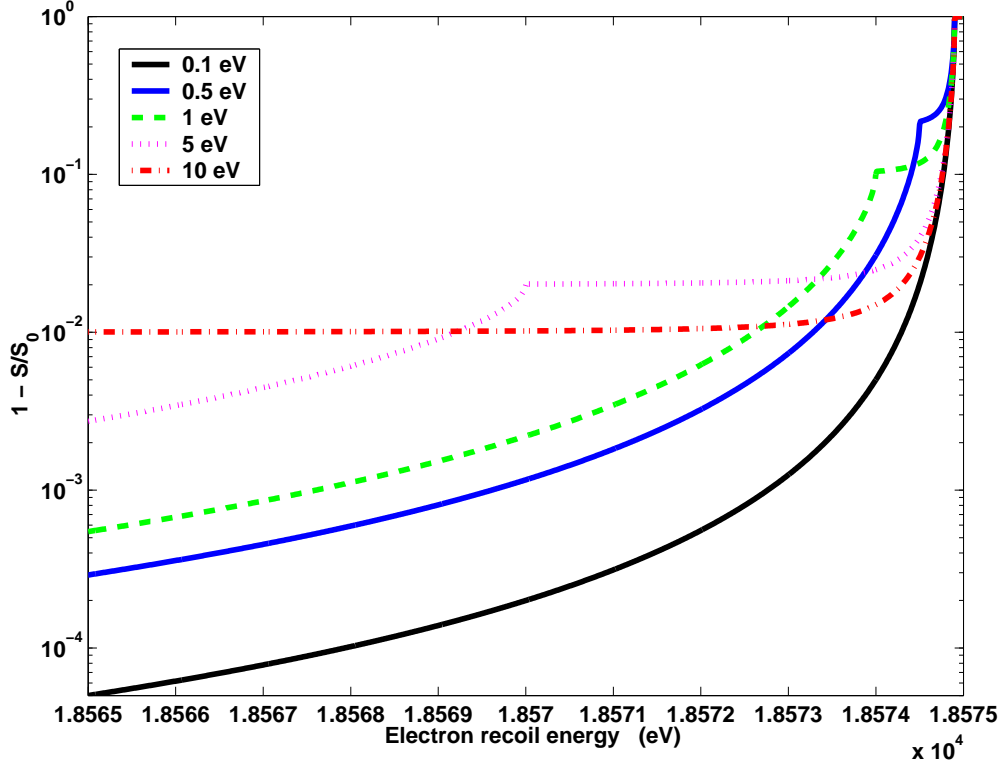


Figure 4.3. $1 - S/S_0$ as a function of the β -ray energy, where S is the β -ray energy spectrum obtained assuming three mostly active, degenerate neutrinos with mass $m = 0.1$ eV and one mostly sterile neutrino ν_i with $m_i = 0.1, 0.5, 1, 5,$ and 10 eV. The mixing angle is given by $U_{ei}^2 = m/m_i$. S_0 is the spectrum associated with massless neutrinos. See text for details.

distinguish R from unity, a determination that should be limited by statistics due to the very low β -ray flux in the high-energy tail of the electron spectrum.

In order to compute R , I use an analytic expression for Eq. (4.12), which exists provided that one neglects nucleon recoil in the decay. Fig. 4.4 depicts constant R -contours in the $|U_{ei}| \times m_i$ plane. Contours were computed for $\Delta E = 25$ eV, in order to allow one to easily compare our results with the sensitivity estimates of the Katrin experiment. After data-taking, Katrin is expected to measure R at the 0.1%–1% level (lightest grey region). Its sensitivity is expected to be $\sqrt{m_{\nu_e}^2} > 0.2$ eV at the 90% confidence level. This can be

extracted from the plot by concentrating on the $U_{ei} = 1$ line. Note that while the expected energy resolution for Katrin is of order 1 eV, the expected number of signal events above $E_0 - 1$ eV is minuscule (both in absolute terms and compared with expected number of background events), so that most of the sensitivity to nonzero neutrino masses comes from analyzing the shape of the electron spectrum in the last tens of electron-volts. A larger “window” would suffer from increased systematic uncertainties, so that $\Delta E \sim 25$ eV is representative of Katrin’s optimal reach [63].

The shape of the constant R contours is easy to understand. As already discussed, for $m_i > \Delta E$, the effect of the right-handed neutrinos is to reduce the spectrum in an energy independent way by $1 - |U_{ei}|^2$, while for $m_i < \Delta E$, states with the same effective mass-squared $m_i^2 |U_{ei}|^2$ produce the same effect in tritium beta-decay so that the diagonal lines coincide with lines of constant $m_i^2 |U_{ei}|^2$.

A more sensitive approach would be to “bin” the last tens of eV of the “data” into 1 eV bins, and fit the distribution to a massless neutrino hypothesis. For the values of the parameters in which I am interested, I find that one 25 eV bin yields roughly the same sensitivity to nonzero neutrino masses as twenty five 1 eV bins for large masses and small mixing angles. For smaller masses and larger mixing angles, a “binned” analysis should be sensitive to effects which are localized in individual bins (such as “kinks”). Another recent estimate of the sensitivity of tritium beta-decay experiments to heavy, sterile neutrinos can be found in [93]. Our results agree qualitatively.

Fig. 4.4 also depicts the loose upper bound for $U_{ei} = \sqrt{m_l/m_i}$ as a function m_i , for $m_l = 0.32$ eV and $m_l = 0.01$ eV. For $m_l \gtrsim 0.1$ eV, Katrin should be sensitive to $M_R \lesssim 1$ keV while for $m_l \gtrsim 0.01$ eV (the solar mass scale) Katrin should be sensitive to

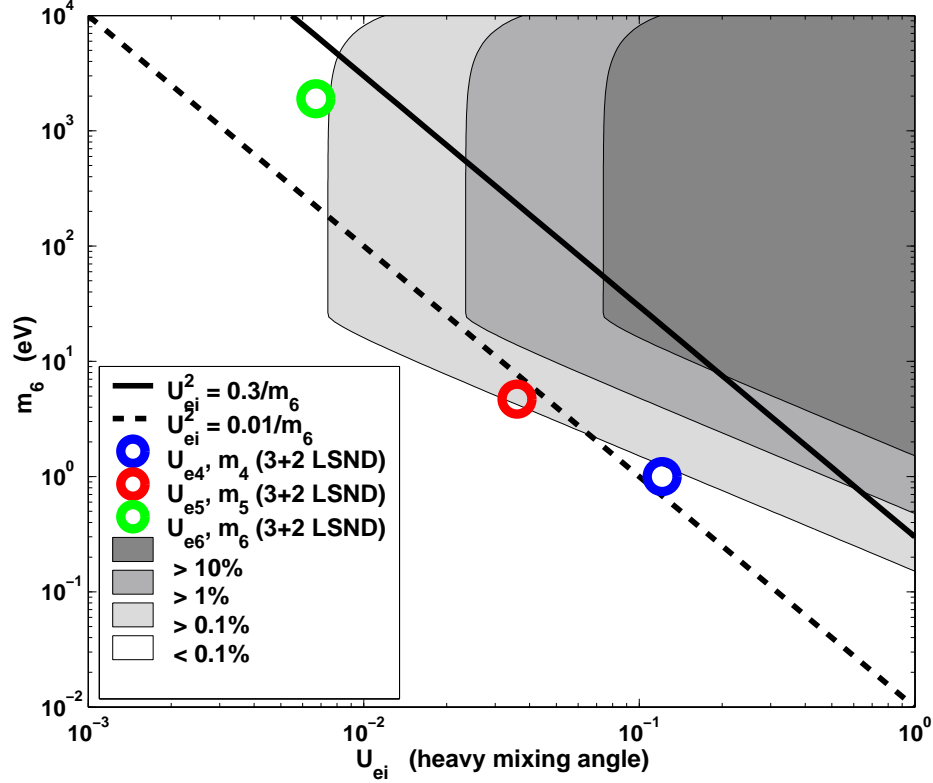


Figure 4.4. Contour plot of constant R , as defined by Eq. (4.12), assuming an energy window $\Delta E = 25$ eV. The solid (dashed) line corresponds to $\sqrt{m_l/m_i}$, a naive upper bound for $|U_{ei}|$, for $m_l = 0.3$ eV (0.01 eV). The circles correspond to U_{ei} for the three mostly sterile states obtained by our “fit” to other neutrino data, Eq. (4.9). See text for details.

$M_R \gtrsim 10$ eV and $M_R \lesssim 100$ eV, where here I assume that all right-handed neutrino masses are of order M_R . In the case of seesaw parameters that fit the LSND data with a 3+2 neutrino spectrum (see Eq. (4.9)), expectations are high as far as observing a kinematical neutrino mass effect at Katrin, in spite of the fact that the fit to LSND data requires U_{e4} and U_{e5} to be “abnormally” low. Fig. 4.4 depicts U_{ei} and m_i values for the heavy neutrinos (open circles). The contribution of the heaviest of the two LSND-related sterile neutrinos is of order the Katrin sensitivity, while the active contribution itself, which leads

to $m_{\nu_e}^2 = \sum_{i=1,2,3} |U_{ei}^2 m_i^2| \sim m_l^2$ is already within the Katrin sensitivity range, given that large $m_l > 0.22$ eV values are required by our 3+2 LSND “fit”. The effect of ν_6 is small if m_6 is larger than 1 keV (required if one takes the “pulsar kicks” hint into account), but would be very significant if m_6 were less than 1 keV.

4.3.2. Neutrinoless Double-Beta Decay

If the neutrinos are Majorana fermions – as predicted in the case of interest here – lepton number is no longer a conserved quantity. The best experimental probe of lepton number violation is the rate for neutrinoless double-beta decay. This process, which violates lepton number by two units, is currently the subject of intense search [125, 40]. If neutrino masses are the only source of lepton number violation, the decay width for neutrinoless double-beta decay is

$$\Gamma_{0\nu\beta\beta} \propto \left| \sum_i U_{ei}^2 \frac{m_i}{Q^2 + m_i^2} \mathcal{M}(m_i^2, Q^2) \right|^2, \quad (4.13)$$

where \mathcal{M} is the relevant nuclear matrix element and $Q^2 \sim 50^2$ MeV² is the relevant momentum transfer. In the limit of very small neutrino masses ($m_i^2 \ll Q^2$), $\Gamma_{0\nu\beta\beta}$ is proportional to an effective neutrino mass $|m_{ee}|$,

$$m_{ee} = \sum_i^n U_{ei}^2 m_i. \quad (4.14)$$

The sum is over all light neutrino mass eigenstates. In the case of a low-energy seesaw, when all m_i , $i = 1, \dots, 6$ are much smaller than Q^2 , it is easy to see that m_{ee} vanishes [32]. The reason for this is that, in the weak basis I are working on (diagonal charged-lepton and charged weak-current), m_{ee} is the ee -element of the neutrino mass matrix, as defined

in Eq. (4.2). One can trivially check that, by assumption, not only does m_{ee} vanish, but so do all other $m_{\alpha\beta}$, $\alpha, \beta = e, \mu, \tau$. Note that this result does not depend on the fact that I have been assuming all elements of the neutrino mass matrix to be real [126].

For heavy ν_i neutrinos, $U_{ei}^2 m_i$ no longer captures the dependency of $\Gamma_{0\nu\beta\beta}$ on the exchange of ν_i . For $m_i^2 \gg Q^2$, instead, the dependency on neutrino exchange is proportional to U_{ei}^2/m_i . If this is the case, the overall contribution (including all heavy and light states) is no longer proportional to m_{ee} but, instead, can be qualitatively expressed as a function of an effective m_{ee}^{eff} ,

$$m_{ee}^{\text{eff}} \equiv Q^2 \sum_i \frac{U_{ei}^2 m_i}{Q^2 + m_i^2}. \quad (4.15)$$

The approximation $\Gamma_{0\nu\beta\beta} \propto |m_{ee}^{\text{eff}}|$ is good as long as one can neglect the dependency of \mathcal{M} on m_i and is not expected to be a great approximation when $m_i^2 \sim Q^2$. Nonetheless, m_{ee}^{eff} still qualitatively captures the behavior of $\Gamma_{0\nu\beta\beta}$ as a function of the sterile neutrino masses and studying its behavior is sufficient for our ambitions in this discussion.

Fig. 4.5 depicts m_{ee}^{eff} for our “best fit” 3+2 LSND solution (see Sec.4.2.1), as a function of the unconstrained m_6 . As advertised, m_{ee}^{eff} vanishes for $m_6^2 \ll Q^2$. The figure also depicts the “active only” value of $m_{ee}^{\text{active}} = \sum_{i=1,2,3} U_{ei}^2 m_i$. Even in the limit $m_6^2 \gg Q^2$, there is still partial cancellation between the mostly active and mostly sterile “LSND” states. This is a feature of the Lagrangian I am exploring here, and is not in general observed in other scenarios with light sterile neutrinos tailor-made to solve the LSND anomaly.

Currently, the most stringent limits on this effective mass comes from the Heidelberg-Moscow experiment [127] where they find $m_{ee} < 0.91$ eV at 99% confidence. In the near future, experiments aim to reach down to m_{ee} values close to 10^{-2} eV [125, 40]. A signal

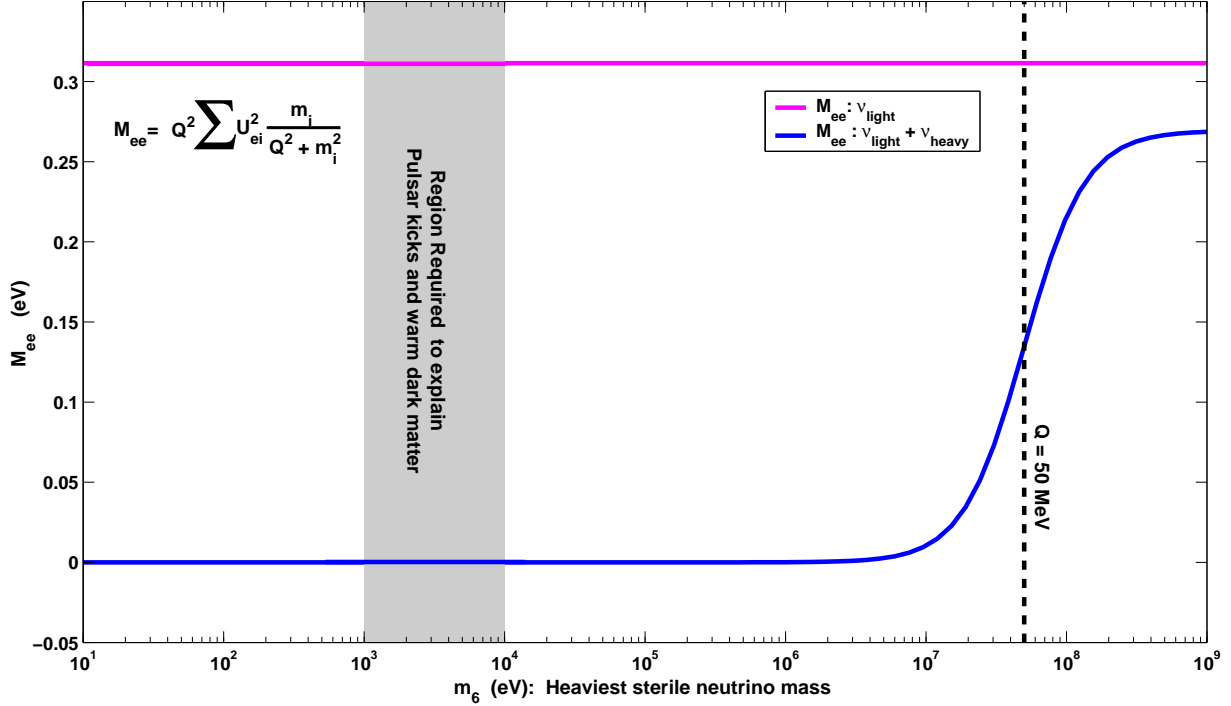


Figure 4.5. Effective m_{ee} for neutrinoless double-beta decay as a function of m_6 , the heaviest right-handed neutrino mass, assuming the existence of only light, active, neutrinos (magenta curve), with a degenerate mass spectra, and for our “best fit” 3 + 2 LSND sterile neutrino solution (blue curve). See text for details. Also indicated is the parameter region preferred by astrophysical hints of sterile neutrinos. I assume $Q = 50$ MeV. In the case of a low-energy seesaw, m_{ee} vanishes as long as $m_6 \ll Q$.

would rule out a seesaw scale below tens of MeV. On the other hand, if I were to conclude that the neutrino masses are quasi-degenerate (through, say, a signal in tritium beta-decay) and if the LSND 3+2 solution were experimentally confirmed, a vanishing result for m_{ee} could be considered strong evidence for a very small seesaw scale. On the other hand, if this were the case (m_{ee} zero, large active neutrino masses), it would also be very reasonable to conclude that neutrinos are Dirac fermions. Distinguishing between the two possibilities would prove very challenging indeed. It is curious (but unfortunate) that in a

low energy seesaw model the neutrinos are Majorana fermions, but all “standard” lepton-number violating observables vanish, given that their rates are all effectively proportional to $m_{\alpha\beta}$!

4.4. Conclusions

The “New Standard Model” (equal to the “old” Standard Model plus the addition of three gauge singlet Weyl fermions) is, arguably, the simplest extension of the SM capable of accommodating neutrino masses. This Lagrangian contains a new dimension-full parameter: the right-handed neutrino mass scale M , which must be determined experimentally. Unlike the Higgs mass-squared parameter, all M values are technically natural given that the global symmetry of the Lagrangian is enhanced in the limit $M \rightarrow 0$.

Very large M values are *theoretically* very intriguing, and have received most of the attention of the particle physics community. There are several strong hints that new phenomena are expected at the electroweak breaking scale $\sim 10^3$ GeV, the grand unified scale $\sim 10^{15-16}$ GeV, and the Planck scale $\sim 10^{18-19}$ GeV, and it is tempting to associate M to one of these energy scales. Furthermore, large M values provide an elegant mechanism for generating the matter antimatter asymmetry of the Universe [68]. Of course, large M values are experimentally very frustrating. It may ultimately prove impossible to experimentally verify whether the New Standard Model is really the correct way to describe Nature.

Here, I explore the opposite end of the M spectrum, $M \lesssim 1$ keV. Such values are *phenomenologically* very intriguing, given that small M values imply the existence of light sterile neutrinos that mix significantly with the active neutrinos and can potentially be

directly observed. Furthermore, there are several experimental and astrophysical phenomena that are best understood if one postulates the existence of light, moderately mixed sterile neutrinos. I find that by requiring all three right-handed neutrino masses to be less than a few keV I can simultaneously explain all neutrino oscillation data, including those from LSND, explain the large peculiar velocities of pulsars, and accommodate the production of heavy elements in supernova environments. Our fit also provides constraints for the “active” neutrino oscillation parameters, most strongly to the lightest active neutrino mass. All successful parameter choices that accommodate the LSND data require m_l to be “large” ($m_l \gtrsim 0.1$ eV), and the “best fit” requires all active neutrino masses to be quasi-degenerate. It is important to emphasize that the presence of light sterile neutrinos that mix relatively strongly with the active neutrinos is only in agreement with cosmological data (especially large scale structure and big-bang nucleosynthesis) if non-standard cosmological ingredients are present.

Fig. 4.1 depicts such a scenario. This six neutrino mass spectrum (including mixing angles) fits all neutrino oscillation data (including those from LSND), provides a sterile neutrino solution to the pulsar kick puzzle, and contains all the necessary ingredients for heavy element nucleosynthesis in supernovae. The heaviest of the neutrinos does not qualify as thermal warm dark matter (in the absence of new cosmological ingredients, its presence would overclose the Universe). Note that even if it were non-thermally produced, constraints from the observation of X-rays from the center of the galaxy would rule out ν_6 as a good dark matter candidate. Lighter ν_6 masses will evade X-ray constraints, but would render ν_6 too “hot,” and hence not a good dark matter candidate.

On the negative side, low M values are, theoretically, rather puzzling. In order to obtain the observed light neutrino masses, neutrino Yukawa couplings are required to be much smaller than the electron Yukawa coupling, and it is tempting to believe that such small numbers are proof that a more satisfying understanding of fermion masses must exist. Furthermore, thermal leptogenesis is no longer an option (see, however, [128]). Finally, the fact that M is naively unrelated to other mass scales can also be perceived as disheartening, but, in our opinion, should be interpreted as evidence that there is more to the lepton sector than meets the eye.

Regardless of one's preference for a high or low seesaw energy scale, and independent of whether the data from LSND and the astronomical observables discussed above have anything to do with sterile neutrinos, our main point is that the determination of M is an *experimental* issue. In the near/intermediate future, low energy seesaw scales will be probed by several experiments, most importantly measurements of the end-point of tritium beta-decay, the MiniBooNE experiment, searches for neutrinoless double-beta decay and, if we get lucky, the detection of neutrinos from a nearby supernova explosion. I find, for example, that *Katrin* should be sensitive to seesaw energy scales below tens of keV if all right-handed neutrino masses are similar, while null results from MiniBooNE would severely constrain right-handed neutrino masses below several eV. I conclude by pointing out that larger (but still “small”) values of M are much harder to constrain. For GeV sterile neutrinos, typical active–sterile mixing angles are $U_{\alpha i}^2 \lesssim 10^{-10}$, probably too small to observe in particle physics processes. It is frustrating (and, I hope, ultimately false) that we seem to be unable to experimentally distinguish $M \sim 1$ GeV from $M \sim 10^{14}$ GeV...

References

- [1] A. de Gouvea and J. Jenkins, Phys. Rev. D **77**, 013008 (2008) [arXiv:0708.1344 [hep-ph]].
- [2] A. de Gouvêa, J. Jenkins and N. Vasudevan, Phys. Rev. D **75**, 013003 (2007) [arXiv:hep-ph/0608147];
- [3] A. de Gouvêa, J. Jenkins, arXiv:0804.3627 [hep-ph]
- [4] For a review of the gauge hierarchy problem and some possible solutions R. Mahbubani (thesis), “Beyond the Standard Model: The Pragmatic approach to the gauge hierarchy problem,”
- [5] P. Langacker, Phys. Rept. **72**, 185 (1981).
- [6] M. Trodden and S. M. Carroll, arXiv:astro-ph/0401547.
- [7] P. Minkowski, Phys. Lett. B **67**, 421 (1977); M. Gell-Mann, P. Ramond and R. Slansky in *Supergravity*, eds. D. Freedman and P. Van Nieuwenhuizen (North Holland, Amsterdam, 1979), p. 315; T. Yanagida in *Proceedings of the Workshop on Unified Theory and Baryon Number in the Universe*, eds. O. Sawada and A. Sugamoto (KEK, Tsukuba, Japan, 1979); S.L. Glashow, *1979 Cargèse Lectures in Physics — Quarks and Leptons*, eds. M. Lévy *et al.* (Plenum, New York, 1980), p. 707. See also R.N. Mohapatra and G. Senjanović, Phys. Rev. Lett. **44**, 912 (1980) and J. Schechter and J.W.F. Valle, Phys. Rev. D **22**, 2227 (1980).
- [8] A. de Gouvea, A. Friedland and H. Murayama, Phys. Lett. B **490**, 125 (2000) [arXiv:hep-ph/0002064].
- [9] A. de Gouvea, B. Kayser and R. N. Mohapatra, Phys. Rev. D **67**, 053004 (2003) [arXiv:hep-ph/0211394].
- [10] P. Langacker and J. Wang, Phys. Rev. D **58**, 093004 (1998) [arXiv:hep-ph/9802383].
- [11] S. T. Petcov and M. Piai, Phys. Lett. B **533**, 94 (2002) [arXiv:hep-ph/0112074].

- [12] H. Fritzsch and J. Plankl, Phys. Rev. D **35**, 1732 (1987).
- [13] E. Jenkins and A. V. Manohar, arXiv:0706.4313 [hep-ph].
- [14] See, for example, M. C. Gonzalez-Garcia and M. Maltoni, arXiv:0704.1800 [hep-ph]; A. Strumia and F. Vissani, arXiv:hep-ph/0606054; R. N. Mohapatra *et al.*, arXiv:hep-ph/0510213; A. de Gouvêa, Mod. Phys. Lett. A **19**, 2799 (2004) [arXiv:hep-ph/0503086]; A. de Gouvêa, arXiv:hep-ph/0411274.
- [15] K. S. Babu and C. N. Leung, Nucl. Phys. B **619**, 667 (2001) [arXiv:hep-ph/0106054].
- [16] M. Maltoni, T. Schwetz, M. A. Tortola and J. W. F. Valle, New J. Phys. **6**, 122 (2004) [arXiv:hep-ph/0405172].
- [17] C. Kraus *et al.*, Eur. Phys. J. C **40**, 447 (2005) [arXiv:hep-ex/0412056].
- [18] V. M. Lobashev *et al.*, Nucl. Phys. Proc. Suppl. **91**, 280 (2001).
- [19] For recent estimates see and comprehensive review, see J. Lesgourgues and S. Pastor, Phys. Rept. **429**, 307 (2006) [arXiv:astro-ph/0603494].
- [20] G. L. Fogli *et al.*, arXiv:hep-ph/0608060.
- [21] U. Seljak, A. Slosar and P. McDonald, JCAP **0610**, 014 (2006).
- [22] S. Hannestad and G. G. Raffelt, astro-ph/0607101.
- [23] For a recent detailed discussion see Y. Farzan and A. Yu. Smirnov, Phys. Lett. B **557**, 224 (2003) [arXiv:hep-ph/0211341].
- [24] L.J. Hall, H. Murayama and N. Weiner, Phys. Rev. Lett. **84**, 2572 (2000) [arXiv:hep-ph/9911341]; A. de Gouvêa and H. Murayama, Phys. Lett. B **573**, 94 (2003) [arXiv:hep-ph/0301050].
- [25] E. Ma, Phys. Rev. Lett. **81**, 1171 (1998) [arXiv:hep-ph/9805219]; B. Bajc and G. Senjanovic, arXiv:hep-ph/0612029.
- [26] R. N. Mohapatra and G. Senjanovic, Phys. Rev. D **23**, 165 (1981); G. B. Gelmini and M. Roncadelli, Phys. Lett. B **99**, 411 (1981).
- [27] R. Foot, H. Lew, X. G. He and G. C. Joshi, Z. Phys. C **44**, 441 (1989).

- [28] M. Fukugita and T. Yanagida, Phys. Lett. B **174**, 45 (1986). For a recent review, see W. Buchmuller, R. D. Peccei and T. Yanagida, Ann. Rev. Nucl. Part. Sci. **55**, 311 (2005) [arXiv:hep-ph/0502169].
- [29] A. Pilaftsis, Z. Phys. C **55**, 275 (1992); J. Bernabéu, A. Santamaria, J. Vidal, A. Mendez and J.W.F. Valle, Phys. Lett. B **187**, 303 (1987); W. Buchmuller and D. Wyler, Phys. Lett. B **249**, 458 (1990); W. Buchmuller and C. Greub, Nucl. Phys. B **363**, 345 (1991); A. Datta and A. Pilaftsis, Phys. Lett. B **278**, 162 (1992); G. Ingelman and J. Rathsman, Z. Phys. C **60**, 243 (1993); C.A. Heusch and P. Minkowski, Nucl. Phys. B **416**, 3 (1994). For recent discussions see J. Kersten and A. Yu. Smirnov, arXiv:0705.3221 [hep-ph]; A. de Gouvêa, arXiv:0706.1732 [hep-ph].
- [30] D. Gorbunov and M. Shaposhnikov, arXiv:0705.1729 [hep-ph].
- [31] T. Asaka, S. Blanchet and M. Shaposhnikov, Phys. Lett. B **631**, 151 (2005);
- [32] A. de Gouvêa, Phys. Rev. D **72**, 033005 (2005).
- [33] A. Atre, V. Barger and T. Han, Phys. Rev. D **71**, 113014 (2005) [arXiv:hep-ph/0502163].
- [34] W. M. Yao *et al.* [Particle Data Group], J. Phys. G **33**, 1 (2006).
- [35] W. T. Weng *et al.*, J. Phys. G **29**, 1735 (2003); Y. Oyama, arXiv:hep-ex/0512041; M. G. Albrow *et al.*, arXiv:hep-ex/0509019.
- [36] See, for example, C. H. Albright *et al.* [Neutrino Factory/Muon Collider Collaboration], arXiv:physics/0411123; S. Geer, Phys. Rev. D **57**, 6989 (1998) [Erratum-ibid. D **59**, 039903 (1999)] [arXiv:hep-ph/9712290].
- [37] P. Zucchelli, Phys. Lett. B **532**, 166 (2002);
- [38] J. Maalampi and N. Romanenko, Phys. Lett. B **474**, 347 (2000) [arXiv:hep-ph/9909416].
- [39] See, for example, M. Doi, T. Kotani and E. Takasugi, Prog. Theor. Phys. Suppl. **83**, 1 (1985); A. S. Barabash, JINST **1**, P07002 (2006) [arXiv:hep-ex/0602037].
- [40] S.R. Elliott and P. Vogel, Ann. Rev. Nucl. Part. Sci. **52**, 115 (2002); [arXiv:hep-ph/0202264];

- [41] For a recent assessment, see V. A. Rodin, A. Faessler, F. Simkovic and P. Vogel, Nucl. Phys. A **766**, 107 (2006) [arXiv:nucl-th/0503063]. Erratum arXiv:0706.4304 [nucl-th].
- [42] H. V. Klapdor-Kleingrothaus, I. V. Krivosheina, A. Dietz and O. Chkvorets, Phys. Lett. B **586**, 198 (2004) [arXiv:hep-ph/0404088].
- [43] H. V. Klapdor-Kleingrothaus *et al.*, Eur. Phys. J. A **12**, 147 (2001) [arXiv:hep-ph/0103062].
- [44] C. E. Aalseth *et al.* [IGEX Collaboration], Phys. Rev. D **65**, 092007 (2002) [arXiv:hep-ex/0202026].
- [45] S. M. Bilenky, C. Giunti, J. A. Grifols and E. Masso, Phys. Rept. **379**, 69 (2003) [arXiv:hep-ph/0211462]; C. Aalseth *et al.*, arXiv:hep-ph/0412300.
- [46] M. Flanz, W. Rodejohann and K. Zuber, Phys. Lett. B **473**, 324 (2000) [Erratum-*ibid.* B **480**, 418 (2000)] [arXiv:hep-ph/9911298].
- [47] A. G. Akeroyd *et al.* [SuperKEKB Physics Working Group], arXiv:hep-ex/0406071; I. I. Bigi and A. I. Sanda, arXiv:hep-ph/0401003.
- [48] See, for example, J. Drees, Int. J. Mod. Phys. A **17**, 3259 (2002) [arXiv:hep-ex/0110077].
- [49] See, for example, M. Breidenbach, IEEE Trans. Nucl. Sci. **33**, 46 (1986).
- [50] A. Abbaneo *et al.* [LEP Electroweak Working Group, SLD Electroweak and Heavy Flavor Groups], arXiv:hep-ex/0312023. See also M. Carena, A. de Gouvêa, A. Freitas and M. Schmitt, Phys. Rev. D **68**, 113007 (2003) [arXiv:hep-ph/0308053].
- [51] S. Bar-Shalom, N. G. Deshpande, G. Eilam, J. Jiang and A. Soni, Phys. Lett. B **643**, 342 (2006) [arXiv:hep-ph/0608309].
- [52] See, for example, G. Rolandi, Int. J. Mod. Phys. A **21**, 1654 (2006).
- [53] See, for example, M. Alabau Pons, P. Bambade, O. Dadoun, R. Appleby and A. Faus-Golfe, arXiv:physics/0609043; R. D. Heuer, Nucl. Phys. Proc. Suppl. **154**, 131 (2006). See also <http://www.linearcollider.org/cms/>.
- [54] D. London, G. Belanger and J. N. Ng, Phys. Lett. B **188**, 155 (1987).

- [55] K. Moffeit, M. Woods, P. Schuler, K. Moenig and P. Bambade, SLAC-TN-05-045, LCC-0159, IPBI-TN-2005-2.
- [56] C. M. Ankenbrandt *et al.*, Phys. Rev. ST Accel. Beams **2**, 081001 (1999) [arXiv:physics/9901022]; M. M. Alsharoa *et al.* [Muon Collider/Neutrino Factory Collaboration], Phys. Rev. ST Accel. Beams **6**, 081001 (2003) [arXiv:hep-ex/0207031]. See also http://www.fnal.gov/projects/muon_collider/.
- [57] See, for example, V. I. Telnov, Acta Phys. Polon. B **37**, 1049 (2006) [arXiv:physics/0604108]; E. Accomando *et al.* [CLIC Physics Working Group], arXiv:hep-ph/0412251.
- [58] See, for example, F. del Aguila, J. A. Aguilar-Saavedra and R. Pittau, arXiv:hep-ph/0703261; A. Datta, M. Guchait and A. Pilaftsis, Phys. Rev. D **50**, 3195 (1994) [arXiv:hep-ph/9311257]; F. M. L. de Almeida, Y. D. A. Coutinho, J. A. Martins Simões, A. J. Ramalho, S. Wolck and M. A. B. do Vale, Phys. Rev. D **75**, 075002 (2007) [arXiv:hep-ph/0703094]; T. Han and B. Zhang, Phys. Rev. Lett. **97**, 171804 (2006) [arXiv:hep-ph/0604064]; O. Panella, M. Cannoni, C. Carimalo and Y. N. Srivastava, Phys. Rev. D **65**, 035005 (2002) [arXiv:hep-ph/0107308].; A. Ali, A. V. Borisov and N. B. Zamorin, Eur. Phys. J. C **21**, 123 (2001) [arXiv:hep-ph/0104123]; A. Ali, A. V. Borisov and N. B. Zamorin, arXiv:hep-ph/0112043.
- [59] M. Frigerio and A. Yu. Smirnov, Phys. Rev. D **67**, 013007 (2003) [arXiv:hep-ph/0207366]; Nucl. Phys. B **640**, 233 (2002) [arXiv:hep-ph/0202247]; A. Merle and W. Rodejohann, Phys. Rev. D **73**, 073012 (2006) [arXiv:hep-ph/0603111].
- [60] See, for example, S. M. Bilenky, C. Giunti, C. W. Kim and S. T. Petcov, Phys. Rev. D **54**, 4432 (1996) [arXiv:hep-ph/9604364].
- [61] A. de Gouvêa and W. Winter, Phys. Rev. D **73**, 033003 (2006) [arXiv:hep-ph/0509359]; A. de Gouvêa and J. Jenkins, arXiv:hep-ph/0507021; A. de Gouvêa, J. Jenkins and B. Kayser, Phys. Rev. D **71**, 113009 (2005) [arXiv:hep-ph/0503079].
- [62] See, for example, J. Lesgourgues and S. Pastor in [**19**, **20**, **21**, **22**]; K. N. Abazajian and S. Dodelson, Phys. Rev. Lett. **91**, 041301 (2003) [arXiv:astro-ph/0212216].
- [63] A. Osipowicz *et al.* [KATRIN Collaboration], arXiv:hep-ex/0109033. See also <http://www-ik.fzk.de/~katrin/index.html>.
- [64] For a scenario that also pursues lepton-number violation from new exotic scalar fields, see G. K. Leontaris, K. Tamvakis and J. D. Vergados, Phys. Lett. B **162**, 153 (1985).

- [65] See, for example, C. Adloff *et al.* [H1 Collaboration], *Eur. Phys. J. C* **11**, 447 (1999) [Erratum-ibid. *C* **14**, 553 (2000)] [arXiv:hep-ex/9907002].
- [66] A. Zee, *Nucl. Phys. B* **264**, 99 (1986).
- [67] For overviews, see R. Barbier *et al.*, *Phys. Rept.* **420**, 1 (2005) [arXiv:hep-ph/0406039]; H. K. Dreiner, arXiv:hep-ph/9707435.
- [68] For a recent review, see W. Buchmuller, R.D. Peccei and T. Yanagida, *Ann. Rev. Nucl. Part. Sci.* **55**, 311 (2005).
- [69] D. Black, T. Han, H. J. He and M. Sher, *Phys. Rev. D* **66**, 053002 (2002) [arXiv:hep-ph/0206056].
- [70] A. Aguilar *et al.* [LSND Collaboration], *Phys. Rev. D* **64**, 112007 (2001).
- [71] A. Bazarko [MiniBooNE Collaboration], *Nucl. Phys. Proc. Suppl.* **91**, 210 (2001).
- [72] W. Krolikowski, *Acta Phys. Polon. B* **35**, 2241 (2004).
- [73] T. Asaka, A. Kusenko and M. Shaposhnikov, *Phys. Lett. B* **638**, 401 (2006).
- [74] J.A. Casas and A. Ibarra, *Nucl. Phys. B* **618**, 171 (2001).
- [75] A. Strumia and F. Vissani, hep-ph/0606054; R.N. Mohapatra and A.Yu. Smirnov, hep-ph/0603118; R.N. Mohapatra *et al.*, hep-ph/0510213; A. de Gouvêa, hep-ph/0411274. A. de Gouvêa, *Mod. Phys. Lett. A* **19**, 2799 (2004).
- [76] M. Maltoni, T. Schwetz, M. A. Tortola and J. W. F. Valle, *New J. Phys.* **6**, 122 (2004).
- [77] A. Strumia, *Phys. Lett. B* **539**, 91 (2002).
- [78] M. Maltoni, T. Schwetz, M. A. Tortola and J. W. F. Valle, *Nucl. Phys. B* **643**, 321 (2002).
- [79] M. Maltoni, T. Schwetz, M. A. Tortola and J. W. F. Valle, hep-ph/0305312.
- [80] M. Sorel, J. M. Conrad and M. Shaevitz, *Phys. Rev. D* **70**, 073004 (2004).
- [81] H. Murayama and T. Yanagida, *Phys. Lett. B* **520**, 263 (2001); G. Barenboim, L. Borisso, J.D. Lykken and A.Yu. Smirnov, *JHEP* **0210**, 001 (2002); M. C. Gonzalez-Garcia, M. Maltoni and T. Schwetz, *Phys. Rev. D* **68**, 053007 (2003).

- [82] V. A. Kostelecky and M. Mewes, Phys. Rev. D **70**, 076002 (2004); V. A. Kostelecky and M. Mewes, Phys. Rev. D **69**, 016005 (2004); L. B. Auerbach *et al.* [LSND Collaboration], Phys. Rev. D **72**, 076004 (2005); A. de Gouvêa and Y. Grossman, hep-ph/0602237; T. Katori, A. Kostelecky and R. Tayloe, hep-ph/0606154.
- [83] G. Barenboim and N. E. Mavromatos, JHEP **0501**, 034 (2005).
- [84] S. Palomares-Ruiz, S. Pascoli and T. Schwetz, JHEP **0509**, 048 (2005).
- [85] M. Sorel, private communication.
- [86] S. Avvakumov *et al.*, Phys. Rev. Lett. **89**, 011804 (2002).
- [87] P. Astier *et al.* [NOMAD Collaboration], Phys. Lett. B **570**, 19 (2003)
- [88] E. Eskut *et al.* [CHORUS Collaboration], Phys. Lett. B **434**, 205 (1998); Phys. Lett. B **424**, 202 (1998).
- [89] A. Kusenko, Int. J. Mod. Phys. D **13**, 2065 (2004).
- [90] D.N. Spergel *et al.*, astro-ph/0603449.
- [91] M. Cirelli and A. Strumia, astro-ph/0607086.
- [92] K. Enqvist, K. Kainulainen and M. J. Thomson, Nucl. Phys. B **373**, 498 (1992); X. Shi, D. N. Schramm and B. D. Fields, Phys. Rev. D **48**, 2563 (1993).
- [93] A.Yu. Smirnov and R.Z. Funchal, Phys. Rev. D **74**, 013001 (2006).
- [94] S. Dodelson, A. Melchiorri and A. Slosar, Phys. Rev. Lett. **97**, 04301 (2006).
- [95] See, for example, J.F. Beacom, N.F. Bell and S. Dodelson, Phys. Rev. Lett. **93**, 121302 (2004).
- [96] See, for example, V. Barger, J. P. Kneller, H. S. Lee, D. Marfatia and G. Steigman, Phys. Lett. B **566**, 8 (2003).
- [97] K. Abazajian, N. F. Bell, G. M. Fuller and Y. Y. Y. Wong, Phys. Rev. D **72**, 063004 (2005).
- [98] G. Gelmini, S. Palomares-Ruiz and S. Pascoli, Phys. Rev. Lett. **93**, 081302 (2004).
- [99] For a recent analysis, see Y. Z. Chu and M. Cirelli, Phys. Rev. D **74**, 085015 (2006).

- [100] For very recent discussions, see K. Abazajian, Phys. Rev. D **73**, 063513 (2006); U. Seljak, A. Makarov, P. McDonald and H. Trac, astro-ph/0602430; K. Abazajian and S.M. Koushiappas, Phys. Rev. D **74**, 023527 (2006); M. Viel, J. Lesgourgues, M.G. Haehnelt, S. Matarrese and A. Riotto, astro-ph/0605706.
- [101] K. Abazajian, G. M. Fuller and W. H. Tucker, Astrophys. J. **562**, 593 (2001). Recent discussions can be found in K. Abazajian and S.M. Koushiappas in [100]; C.R. Watson, J.F. Beacom, H. Yuksel and T.P. Walker, astro-ph/0605424.
- [102] A. Kusenko, astro-ph/0608096.
- [103] M. Cirelli, G. Marandella, A. Strumia and F. Vissani, Nucl. Phys. B **708**, 215 (2005).
- [104] M. Sorel and J. M. Conrad, Phys. Rev. D **66**, 033009 (2002).
- [105] K. Kainulainen, J. Maalampi and J. T. Peltoniemi, Nucl. Phys. B **358**, 435 (1991).
- [106] H. A. Bethe, Rev. Mod. Phys. **62**, 801 (1990).
- [107] Z. Arzoumanian, D. F. Chernoffs and J. M. Cordes, Astrophys. J. **568**, 289 (2002).
- [108] L. Scheck, T. Plewa, H. T. Janka, K. Kifonidis and E. Mueller, Phys. Rev. Lett. **92**, 011103 (2004). L. Scheck, K. Kifonidis, H. T. Janka and E. Mueller, astro-ph/0601302.
- [109] M. B. Voloshin, Phys. Lett. B **209**, 360 (1988).
- [110] A. de Gouvêa and J. Jenkins, Phys. Rev. D **74**, 033004 (2006).
- [111] T. Adams *et al.* (J Jenkins), arXiv:0803.0354 [hep-ph]
- [112] Z. Daraktchieva *et al.* [MUNU Collaboration], Phys. Lett. B **615**, 153 (2005).
- [113] H. B. Li *et al.* [TEXONO Collaboration], Phys. Rev. Lett. **90**, 131802 (2003).
- [114] A. Kusenko and G. Segre, Phys. Rev. Lett. **77**, 4872 (1996).
- [115] M. Barkovich, J. C. D'Olivo and R. Montemayor, hep-ph/0503113.
- [116] H. Nunokawa, V. B. Semikoz, A.Yu. Smirnov and J.W.F. Valle, Nucl. Phys. B **501**, 17 (1997).
- [117] S. Esposito and G. Capone, Z. Phys. C **70**, 55 (1996).

- [118] G. M. Fuller, A. Kusenko, I. Mocioiu and S. Pascoli, *Phys. Rev. D* **68**, 103002 (2003).
- [119] K. Abazajian, G. M. Fuller and M. Patel, *Phys. Rev. D* **64**, 023501 (2001).
- [120] S. Wanajo, T. Kajino, G. J. Mathews and K. Otsuki, astro-ph/0102261.
- [121] G. C. McLaughlin, J. M. Fetter, A. B. Balantekin and G. M. Fuller, *Phys. Rev. C* **59**, 2873 (1999).
- [122] J. Fetter, G. C. McLaughlin, A. B. Balantekin and G. M. Fuller, *Astropart. Phys.* **18**, 433 (2003).
- [123] J. Beun, G. C. McLaughlin, R. Surman and W. R. Hix, hep-ph/0602012.
- [124] Y. Farzan, O.L.G. Peres and A.Yu. Smirnov, *Nucl. Phys. B* **612**, 59 (2001).
- [125] F. T. Avignone, *Nucl. Phys. Proc. Suppl.* **143**, 233 (2005).
- [126] B. Kayser, *Phys. Rev. D* **30**, 1023 (1984).
- [127] A.M. Bakalyarov, A.Y. Balysh, S.T. Belyaev, V.I. Lebedev and S.V. Zhukov [C03-06-23.1 Collaboration], *Phys. Part. Nucl. Lett.* **2**, 77 (2005) [*Pisma Fiz. Elem. Chast. Atom. Yadra* **2**, 21 (2005)].
- [128] M. Shaposhnikov and I. Tkachev, *Phys. Lett. B* **639**, 414 (2006).

APPENDIX A

Standard Model of Particle Physics

The Standard Model (SM) is a local Lorentz invariant quantum field theory defined by its gauge symmetry, field content and symmetry breaking scale. The gauge symmetry is

$$SU(3)_C \times SU(2)_L \times U(1)_Y. \quad (\text{A.1})$$

Each group has its own distinct gauge coupling and is necessarily associated with spin one gauge boson fields transforming under the adjoint group representations. These are the eight gluons (G), three weak isobosons (W), and single hypercharge boson (B), respectively. The fermion field content, along with its associated quantum numbers, is listed in Table A. Here, i is a flavor label that runs over the three known generations. In other words, there are at least three copies of each fermion generation identical in interactions, which are only mass scale. Additionally, there is a single complex Lorentz scalar, the Higgs boson H, with quantum numbers $(\mathbf{1}, \mathbf{2}, -1/2)$.

From here it is a simple matter to write down the most general Lagrangian incorporating these principles. This consists of three parts; the gauge sector

$$\mathcal{L}_{Gauge} = v \sum_i \bar{L}_i \gamma_\mu D^\mu L_i + \bar{Q}_i \gamma_\mu D^\mu Q_i + \bar{e}_i \gamma_\mu D^\mu e_i + \bar{d}_i \gamma_\mu D^\mu d_i + \bar{u}_i \gamma_\mu D^\mu u_i + |D^\mu H|^2, \quad (\text{A.2})$$

Field	$SU(3)_c$	$SU(2)_L$	$U(1)_y$
L_i	1	2	$-\frac{1}{2}$
\overline{e}_i	1	1	1
Q_i	3	2	$\frac{1}{6}$
\overline{u}_i	$\overline{3}$	1	$-\frac{2}{3}$
\overline{d}_i	$\overline{3}$	1	$\frac{1}{3}$

Table A.1. Summary table of the Standard Model fermion field content along with their associated gauge quantum numbers. The fields are written in terms of their chiral left handed projections which may be conjugated to yield the right handed projections. The boldface entries describe the representation of the field under the nonabelian symmetry groups.

the Yukawa sector

$$\mathcal{L}_{Yukawa} = y_\ell^{ij} \overline{L}_i H e_j + y_d^{ij} \overline{Q}_i H d_j + y_u^{ij} \overline{Q}_i H^\dagger u_j + h.c.^1, \quad (\text{A.3})$$

and the Higgs sector

$$\mathcal{L}_{Higgs} = \mu^2 H^\dagger H + \eta (H^\dagger H)^2. \quad (\text{A.4})$$

Here, $D_\mu = \partial_\mu - ig_s G_\mu \lambda - ig W_\mu \tau - ig' B_\mu Y$ is the covariant derivative containing the gauge fields with the matrices λ and τ , the generators of $SU(3)_c$ and $SU(2)_L$ in the appropriate representation. Notice that all fermions and gauge bosons are strictly massless in this theory. This follows from the chiral nature of the fermions where the left and right handed fields transform differently under $SU(2)_L \times U(1)_Y$ thus forbidding the required $\overline{\psi}_L \psi_R$ mass term.

¹The simple multiplicative notation employed here is schematic. Since all terms are weak isosinglets it is clear that some spinor products between doublets are nontrivial involving the antisymmetric tensor $\epsilon_{\alpha\beta}$.

The standard treatment now postulates that the $\mu^2 < 0$ in Eq. (A.4) so that H acquires a vacuum expectation value (vev). This breaks electroweak symmetry

$$SU(2)_L \times U(1)_Y \rightarrow U(1)_Q \quad (\text{A.5})$$

at the energy scale characterized by v . Once done, only one abelian gauge symmetry remains to mediate electromagnetic interactions. Upon expanding the SM Lagrangian about v , one finds that the charged fermions (now under Q) have acquired masses as well as three of the electroweak gauge bosons. These extra longitudinal degrees of freedom arise from the Goldstone Higgs bosons “eaten” by the gauge fields. One can easily rewrite the Lagrangian terms expanded about the new vacuum and in the basis of definite gauge boson mass, but this is not needed for what follows. For completeness, I do point out that orthogonal linear combinations of W_1 and W_2 combine to form the massive W^\pm bosons, and similarly, combinations of W_3 and B combine to form the massive Z and (photon) A bosons. The $SO(2)$ transformation that facilitates the rotation to this mass basis is defined by θ_w , the weak mixing angle. One should also notice that the massless photon is now the field associated with the remaining unbroken symmetry.

From the point of view of this thesis, the most important feature of the SM Lagrangian is its accidental symmetries. The gauge and Higgs sectors contain a huge global symmetry $SU(3)_f^5$ corresponding to the freedom to rotate each of the five field families in generation space. The Yukawa terms substantially break this but still leave some residual symmetries. In particular, I find that if I assign identical $U(1)$ charges, called baryon number (B), to Q_i , u_i and d_i while holding the rest of the field content neutral, B is conserved. Similarly, I see that Lepton number (L) is conserved provided that I assign identical charges to

both L_i and e_i with the remaining content neutral². This is not the whole story, as both B and L are broken by nonperturbative instanton effects. At the end of the day, only one non-anomalous symmetry remains, conserving the quantity $B - L$, $U(1)_{B-L}$. It is important to understand that this symmetry is completely accidental within the SM and that any additional new physics is likely to break it. This implies that searches for B and L violation are ideal laboratories for studying physics BSM. The search for Lepton Number Violation (LNV) is the major unifying theme of this work, as it is intimately related to the Majorana nature of neutrinos.

²Of course, in the SM with no means of generating neutrino mass, a separately conserved lepton number may be assigned to each lepton family. This is broken by the observed neutrino mixing phenomena induced by BSM physics

APPENDIX B

Extended $SU(2)$ neutrino mixing matrix notation

Neutrino mixing and all of its invariance may be expressed as products of three distinct matrix classes in addition to the identity \mathbf{I} ¹. Two are defined in terms of continuous variables. These are real orthogonal rotations in the $a - b$ plane $\mathbf{R}^{\mathbf{ab}}(\theta)$ and single phase rotations $\mathbf{P}^{\mathbf{a}}(\phi)$ defined by

$$\mathbf{R}^{\mathbf{ab}}(\theta) \equiv \begin{cases} [\mathbf{R}^{\mathbf{ab}}(\theta)]_{aa} = [\mathbf{R}^{\mathbf{ab}}(\theta)]_{bb} = \cos \theta \\ [\mathbf{R}^{\mathbf{ab}}(\theta)]_{ab} = -[\mathbf{R}^{\mathbf{ab}}(\theta)]_{ba} = -\sin \theta \\ [\mathbf{R}^{\mathbf{ab}}(\theta)]_{ij} = \delta_{ij} \quad (ij \neq a, b) \end{cases} \quad (\text{B.1})$$

and

$$[\mathbf{P}^{\mathbf{a}}(\phi)]_{ij} = \delta_{ij} e^{i\phi\delta_{ia}}, \quad (\text{B.2})$$

respectively. The discrete transformation

$$\mathbf{A}^{\mathbf{ab}} = \mathbf{A}^{\mathbf{ba}} = \frac{1}{2} \mathbf{R}^{\mathbf{ab}}\left(\frac{\pi}{2}\right) \{ \mathbf{P}^{\mathbf{b}}(\pi) - \mathbf{P}^{\mathbf{a}}(\pi) \} \quad (\text{B.3})$$

completes the set. It is a simple matter to write an arbitrary mixing matrix with such components. For example, the complex rotation matrix typically assigned to the 1 – 3 plane in

¹It is also true that one may use the full $SU(n)$ algebra to parameterize n neutrino mixing in a more elegant way than in my extended $SU(2)$ parameterization. These algebras are well known, but their use would require new commutator relations for each separate case, which is not conducive to my global approach.

standard three neutrino mixing analysis is $\tilde{\mathbf{R}}^{\mathbf{ab}}(\theta, \delta) = \mathbf{P}^{\mathbf{a}}(-\delta)\mathbf{P}^{\mathbf{b}}(\delta)\mathbf{R}^{\mathbf{ab}}(\theta)\mathbf{P}^{\mathbf{a}}(\delta)\mathbf{P}^{\mathbf{b}}(-\delta)$. Additionally, discrete permutations of ab vector elements are accomplished with $\mathbf{S}^{\mathbf{ab}} = \mathbf{R}^{\mathbf{ab}}(\pi/2)\mathbf{P}^{\mathbf{b}}(\pi)$. Manipulations of these matrices utilize their commutation relations defined by

$$[\mathbf{R}^{\mathbf{ab}}(\theta), \mathbf{R}^{\mathbf{bc}}(\theta')] = \sin \theta (1 - \cos \theta') \mathbf{A}^{\mathbf{ab}} + \sin \theta' (1 - \cos \theta) \mathbf{A}^{\mathbf{bc}} \quad (\text{B.4})$$

$$+ \frac{1}{2} \sin \theta \sin \theta' \left\{ \mathbf{R}^{\mathbf{ac}}(-\frac{\pi}{2}) - \mathbf{R}^{\mathbf{ac}}(\frac{\pi}{2}) \right\}$$

$$[\mathbf{R}^{\mathbf{ab}}(\theta), \mathbf{P}^{\mathbf{a}}(\phi)] = \sin \theta (e^{i\phi} - 1) \mathbf{A}^{\mathbf{ab}} \quad (\text{B.5})$$

$$[\mathbf{R}^{\mathbf{ab}}(\theta), \mathbf{A}^{\mathbf{ab}}] = -\sin \theta \{ \mathbf{P}^{\mathbf{b}}(\pi) - \mathbf{P}^{\mathbf{a}}(\pi) \} \quad (\text{B.6})$$

$$[\mathbf{R}^{\mathbf{ab}}(\theta), \mathbf{A}^{\mathbf{ac}}] = \sin \theta \mathbf{A}^{\mathbf{bc}} + \frac{1}{2} (\cos \theta - 1) \left\{ \mathbf{R}^{\mathbf{ac}}(-\frac{\pi}{2}) - \mathbf{R}^{\mathbf{ac}}(\frac{\pi}{2}) \right\} \quad (\text{B.7})$$

$$[\mathbf{A}^{\mathbf{ab}}, \mathbf{P}^{\mathbf{a}}(\phi)] = \frac{1}{2} (e^{i\phi} - 1) \left\{ \mathbf{R}^{\mathbf{ab}}(-\frac{\pi}{2}) - \mathbf{R}^{\mathbf{ab}}(\frac{\pi}{2}) \right\} \quad (\text{B.8})$$

$$[\mathbf{A}^{\mathbf{ab}}, \mathbf{A}^{\mathbf{ac}}] = \frac{1}{2} \left\{ \mathbf{R}^{\mathbf{bc}}(-\frac{\pi}{2}) - \mathbf{R}^{\mathbf{bc}}(\frac{\pi}{2}) \right\}. \quad (\text{B.9})$$

All other commutators vanish. This matrix set closes upon itself facilitating a simple platform to perform manipulations. In that spirit, the following identities are easy to

prove and useful in calculations:

$$\mathbf{P}^{\mathbf{a}}(\phi)\mathbf{P}^{\mathbf{a}}(-\phi) = I \quad (\text{B.10})$$

$$\mathbf{R}^{\mathbf{ab}}(\theta)\mathbf{R}^{\mathbf{ab}}(-\theta) = \mathbf{R}^{\mathbf{ab}}(\theta)\mathbf{R}^{\mathbf{ba}}(\theta) = I \quad (\text{B.11})$$

$$\mathbf{R}^{\mathbf{ab}}(\theta + \theta') = \mathbf{R}^{\mathbf{ab}}(\theta)\mathbf{R}^{\mathbf{ab}}(\theta') \quad (\text{B.12})$$

$$\mathbf{P}^{\mathbf{a}}(\phi + \phi') = \mathbf{P}^{\mathbf{a}}(\phi)\mathbf{P}^{\mathbf{a}}(\phi') \quad (\text{B.13})$$

$$\mathbf{P}^{\mathbf{a}}(\pi)\mathbf{P}^{\mathbf{b}}(\pi) = \mathbf{R}^{\mathbf{ab}}(\pi) \quad (\text{B.14})$$

$$\mathbf{P}^{\mathbf{b}}(\pi)\mathbf{R}^{\mathbf{ab}}(\theta) = \mathbf{R}^{\mathbf{ab}}(-\theta)\mathbf{P}^{\mathbf{b}}(\pi) \quad (\text{B.15})$$

$$\mathbf{R}^{\mathbf{ab}}(\theta)\mathbf{P}^{\mathbf{a}}(\phi) - \mathbf{P}^{\mathbf{b}}(\phi)\mathbf{R}^{\mathbf{ab}}(\theta) = \cos\theta (e^{i\phi} - 1) \mathbf{A}^{\mathbf{ab}} \quad (\text{B.16})$$

$$\mathbf{A}^{\mathbf{ab}}\mathbf{P}^{\mathbf{a}}(\phi) = \mathbf{P}^{\mathbf{b}}(\phi)\mathbf{A}^{\mathbf{ab}} \quad (\text{B.17})$$

$$\mathbf{R}^{\mathbf{ab}}(\theta)\mathbf{R}^{\mathbf{ca}}\left(\frac{\pi}{2}\right) = \mathbf{R}^{\mathbf{ca}}\left(\frac{\pi}{2}\right)\mathbf{R}^{\mathbf{cb}}(\theta). \quad (\text{B.18})$$